



FRIEDRICH-SCHILLER-
UNIVERSITÄT
JENA

Chemisch-Geowissenschaftliche Fakultät

MASTERARBEIT

Characterization of the
1-Hydroxy-2-methyl-2-(*E*)-butenyl-
4-diphosphate Reductase (HDR)
from *Picea abies* and *Populus* × *canescens*

vorgelegt von

Piera Wiesinger
geboren am 25. Mai 1996
in Freising

durchgeführt am Max-Planck-Institut für Chemische Ökologie



Jena, 15.04.2021

GutachterIn: Dr. Axel Schmidt

Jun.-Prof. Dr. Julie A. Z. Zedler

“The day is coming when a single carrot, freshly observed, will set off a revolution.”

-

Paul Cézanne

Selbstständigkeitserklärung

Ich versichere hiermit, dass ich die von mir eingereichte Abschlussarbeit selbstständig verfasst und keine anderen als die angegebenen Quellen und Hilfsmittel benutzt, sowie Zitate und gedankliche Übernahmen kenntlich gemacht habe.

Ort, Datum

Unterschrift

Acknowledgements

I would like to thank everyone who has supported me during this work:

Axel Schmidt for his contagious enthusiasm about terpenes, plants and the HDR and for giving me the opportunity to work on this project. It was captivating from the beginning. Thank you for the supervision and that your door was always open for every question I had.

Jun.-Prof. Julie Zedler for reviewing my thesis.

Professor Jonathan Gershenzon for giving me the opportunity to do my Master Thesis in the Biochemistry group.

Toni Krause, for sharing his project with me, giving suggestions for every answer I had and for bringing up new ideas.

The CONDEF group, especially Marion Stäger and Diego González-Cabanelas for the support in the lab and Kristina Kshatriya for revising my thesis.

Michael Reichelt for always very quickly fixing the LC, when some problem appeared.

The Biochemistry group for the hearty atmosphere. Every day it was a pleasure to work surrounded by all you. Thanks for the nice talks in the lunch breaks and during the day!

Johanna Rettner, my Master student colleague, for inspiring talks.

Ines Kuhlmann for the uncomplicated lend out of the glove box and Daniel Veit for helping to install the box.

Lena Schaefer, Ann-Katrin Gerullis and my family for revising my thesis.

I want to thank my family, my mother Annalisa, my father Klaus and my sister Teresa for always supporting me during my studies, especially during hard times.

To you, Lars, I say thank you for your ideas and support and for the music.

Abstract – Deutsch

Isoprenoide bilden die größte Klasse der Naturstoffe. Sie haben alle ein Kohlenstoffgerüst (C_{x5}), welches aus den isomeren C_5 -Grundbausteinen Isopentenylidiphosphat (IDP) und Dimethylallyldiphosphat (DMADP) aufgebaut ist. In den Chloroplasten der Pflanzen wird die Reaktion zu IDP und DMADP durch die 1-Hydroxy-2-methyl-2-(*E*)-butenyl-4-diphosphat Reduktase (HDR), dem letzten Enzym des Methylerythritolphosphat (MEP) Biosynthesewegs, katalysiert. Obwohl die HDR eine zentrale Rolle spielt, da sie die Grundbausteine für die Isoprenoid-Biosynthese zur Verfügung stellt, wurde die pflanzliche HDR, im Gegensatz zur bakteriellen HDR, wenig erforscht. Die Proteinstruktur der HDR von *Escherichia coli* wurde durch Röntgenstrukturanalyse aufgeklärt. Diese HDR besitzt ein $[4Fe-4S]^{2+}$ -Cluster im katalytischen Zentrum, welches sauerstoffsensitiv ist. Die im Rahmen dieser Masterarbeit ausgewertete Literatur und aufgestellte Alignments deuten darauf hin, dass auch die pflanzliche HDR ein solches Cluster aufweist.

In dieser Masterarbeit wurden die HDR-Enzyme der gemeinen Fichte, *Picea abies*, und der Graupappel, *Populus × canescens*, als rekombinante Proteine nach heterologer Expression in *E. coli*, charakterisiert. Die beiden Pflanzenarten unterscheiden sich in der Zusammensetzung ihrer Isoprenoide: *P. canescens* emittiert hohe Menge an Isopren, während *P. abies* viele Mono-, Sesqui- und Diterpene bildet. In der Graupappel ist ein *HDR* Gen (*PcHDR*), exprimiert, in der Fichte hingegen zwei *HDR* Gene (*PaHDR1* und *PaHDR2*). Die Enzymaktivität der rekombinanten *PcHDR*, *PaHDR1* und *PaHDR2* wurde untersucht, sowie das jeweils katalysierte Verhältnis von IDP zu DMADP. Dazu wurden die drei HDR ohne Transitpeptide (-T) heterolog in *E. coli* exprimiert. Die anschließende Aufreinigung und Enzym-Assays erfolgten in einer *Glove Box* unter Stickstoffatmosphäre. Der Versuchsaufbau und die Durchführung in der *Glove Box* wurden in dieser Arbeit etabliert. Nach Optimierung der Reaktionsbedingungen, wurden enzymkinetische Messungen durchgeführt. Sowohl *PcHDR-T*, als auch *PaHDR2-T* weisen eine Michaelis-Menten-Konstante K_M von $\sim 21 \mu M$ und eine katalytische Effizienz (k_{cat}/K_M) von $\sim 1.4 \mu M^{-1} min^{-1}$ auf. Die Verhältnisse der Produkte IDP/DMADP liegen jeweils bei $\sim 9:1$ und bei $\sim 6:1$. Dagegen weist *PaHDR1-T* einen K_M von $\sim 16 \mu M$ und eine katalytische Effizienz von $\sim 0.5 \mu M^{-1} min^{-1}$ auf. Das Produktverhältnis liegt bei $\sim 21:1$. Im Zusammenhang mit weiteren zukünftigen Untersuchungen *in planta*, leisten die Ergebnisse dieser Arbeit einen Beitrag zum besseren Verständnis der Regulation der Isoprenoid-Biosynthese.

Abstract – English

Isoprenoids form the largest class of natural products. They are all composed of a carbon skeleton made up of the C₅-isomers named isopentenyl diphosphate (IDP) and dimethylallyl diphosphate (DMADP). Inside the chloroplasts of plants the reaction to IDP and DMADP is catalyzed by the final enzyme of the methylerythritol phosphate (MEP) biosynthesis pathway, namely 1-Hydroxy-2-methyl-2-(*E*)-butenyl-4-diphosphate reductase (HDR).

Even though the HDR plays a crucial role, as it provides the substrates for the isoprenoid biosynthesis, little research has been carried out on its function in plants; meanwhile, bacterial HDR has been investigated intensively. The protein structure of the HDR from *Escherichia coli* has been solved by crystallization. This HDR holds an [4Fe-4S]²⁺ cluster in its catalytic center, which is sensitive to oxygen. The literature and alignments evaluated for this thesis suggest that HDR from plants also incorporates an iron-sulfur cluster.

In this thesis, the HDRs from Norway spruce (*Picea abies*) and grey poplar (*Populus × canescens*) have been characterized as recombinant enzymes after heterologous expression in *E. coli*. The two species differ in their isoprenoid production, as *P. canescens* emits high amounts of isoprene, whereas *P. abies* produces a number of mono-, sesqui- and di-terpenes. In grey poplar one *HDR* gene, named *PcHDR*, is expressed, whereas two distinct *HDR* genes, named *PaHDR1* and *PaHDR2*, are expressed in Norway spruce. The enzyme activity of the recombinant *PcHDR*, *PaHDR1* and *PaHDR2* as well as the catalysed IDP/DMADP ratio have been analysed. In order to do so, truncated versions of those three putative *HDR* genes, lacking a transit peptide (-T), were expressed in *E. coli*. Purification and enzyme assays were carried out in a nitrogen atmosphere. To this end, an experimental setup in a glove box and the appropriate procedure were established in this thesis. After optimizing the reaction conditions, enzyme kinetic studies were carried out. *PcHDR-T* and *PaHDR2-T* both have a Michaelis-Menten constant (K_M) of ~21 μM, a catalytic efficiency (k_{cat}/K_M) of ~1.4 μM⁻¹min⁻¹ and catalyses an IDP/DMADP ratio of ~9:1 and ~6:1 respectively. In contrast, *PaHDR1-T* has a K_M of ~16 μM, a catalytic efficiency of ~0.5 μM⁻¹min⁻¹ and a ratio of 21:1.

Together with further investigation *in planta*, this thesis makes a contribution to gaining a better understanding of the regulation of the isoprenoid biosynthesis.

List of content

List of Abbreviations	V
List of Figures	VII
List of Tables	IX
1 Introduction	1
1.1 Isoprenoids in plants	1
1.1.1 Function of isoprenoids in plants	1
1.1.2 Biosynthesis of isoprenoids	2
1.1.3 Isoprene emission and terpenoid composition of <i>Populus × canescens</i> and <i>Picea abies</i>	4
1.2 The methylerythritol phosphate (MEP) pathway	6
1.3 The 1-hydroxy-2-methyl-2-(E)-butenyl 4-diphosphate reductase (HDR) in plants	8
1.4 Reaction of the HDR	9
1.4.1 The iron-sulfur cluster.....	9
1.4.2 The reaction mechanism	11
1.4.3 The IDP/DMADP ratio	12
1.5 Starting point of the project	13
1.6 Aim of this work	14
2 Material and Methods	15
2.1 Materials	15
2.1.1 Chemicals, reagents, media and buffers.....	15
2.1.1.1 Chemicals.....	15
2.1.1.2 Antibiotics	15
2.1.1.3 LB (lysogeny broth) medium.....	15
2.1.1.4 Buffers for protein purification and enzyme assays.....	15

2.1.1.5	Reagents for sodium dodecyl sulfate polyacrylamide gel electrophoresis (SDS-PAGE).....	16
2.1.2	Bacterial strains.....	16
2.1.3	Primer, plasmids and constructs	17
2.1.3.1	Primer	17
2.1.3.2	Plasmids.....	18
2.1.3.3	Putative HDR constructs	19
2.1.4	Plant material	19
2.1.5	Equipment.....	19
2.1.5.1	General equipment.....	19
2.1.5.2	Glove box.....	19
2.1.6	Software and databases.....	20
2.2	Methods.....	21
2.2.1	Ribonucleic acid (RNA) extraction	21
2.2.2	Reverse transcription to cDNA.....	21
2.2.3	Gateway cloning	22
2.2.3.1	PCR with attB sites	22
2.2.3.2	BP and LR reaction.....	23
2.2.4	Agarose gel electrophoresis	23
2.2.5	Gel extraction with Zymoclean Gel DNA Recovery Kit.....	23
2.2.6	Measuring RNA and DNA concentration.....	24
2.2.7	Sequencing.....	24
2.2.8	Culturing of bacteria	25
2.2.9	Plasmid preparation	25
2.2.10	Transformation of <i>E. coli</i>	25
2.2.11	Heterologous Expression of HDR	25
2.2.11.1	Pre-culture.....	25

2.2.11.2	Induction culture	25
2.2.12	Anaerobic extraction and purification of recombinant protein	26
2.2.12.1	Harvesting and Sonication	26
2.2.12.2	Purification via GST-tag	26
2.2.13	Sodium dodecyl sulfate polyacrylamide gel electrophoresis (SDS-PAGE)	26
2.2.14	Determination of protein concentration	26
2.2.15	Anaerobic enzyme assays	27
2.2.16	Calibration curve for DMADP, IDP and HMBDP quantification	27
2.2.17	Analytical methods	28
2.2.17.1	Quantification of HMBDP and IDP+DMADP with XBridge BEH Amide column 28	
2.2.17.2	Separation of DMADP and IDP with Astec® Cyclobond® I 2000 column	29
3	Results and Discussion.....	31
3.1	The genetic and molecular level of putative 1-hydroxy-2-methyl-2-(E)-butenyl 4-diphosphate reductases (HDRs)	31
3.1.1	Evolutionary aspects	31
3.1.2	Sequencing results.....	33
3.1.3	Conserved amino acids and motifs – predictions on the iron-sulfur-cluster and binding pocket.....	35
3.1.4	The transit peptide.....	38
3.2	Establishing the experimental setup.....	39
3.2.1	Setup of the glove box	39
3.2.2	Establishing the protocol.....	41
3.3	Enzymatic characterization	44
3.3.1	Purification of HDR constructs.....	44
3.3.2	Calibration curve.....	46
3.3.3	Activity profile of <i>PcHDR</i> +T and <i>PaHDR2</i> -T2.....	46
3.3.4	Optimization of reaction conditions for <i>PaHDRs</i> and <i>PcHDR</i>	47

3.3.4.1	pH optimization	48
3.3.4.2	Temperature optimization.....	49
3.3.5	Kinetic studies on the HDR – determination of K_M and k_{cat}	50
3.4	Determination of IDP/DMADP ratio	55
4	Conclusion and Outlook	57
5	Literature	59
6	Appendix	i
6.1	Alignments.....	i
6.2	Transit peptides.....	vii
6.3	Plasmid maps	vii
6.4	Sequences.....	ix
6.4.1	<i>Populus × canescens</i> HDR DNA and amino acid sequences.....	ix
6.4.1.1	<i>PcHDR-T</i>	ix
6.4.1.2	<i>PcHDR+T</i>	x
6.4.2	<i>Picea abies</i> HDR DNA and amino acid sequences	xi
6.4.2.1	<i>PaHDR1</i>	xi
6.4.2.2	<i>PaHDR2</i>	xii
6.5	3D-Models Infos	xiii
6.6	Loss of enzyme activity and activity in FT and W1 fractions	xiv
6.7	Michaelis-Menten plots	xiv

List of Abbreviations

°C	degree celsius
μ	micro
ATP	adenosine triphosphate
BSA	Bovine Serum Albumin
cDNA	complementary desoxyribonucleic acid
CHES	2-(cyclohexylamino)ethanesulfonic acid
CTP	cytidine triphosphate
ddH ₂ O	double distilled water
DMADP	dimethylallyl diphosphate
dNTP	desoxynucleotide triphosphates
DP	declustering potential
DTT	dithiothreitol
DXP	1-deoxyxylulose 5-phosphate
DXS	deoxyxylulose phosphate synthase
EPR	electron paramagnetic resonance
Fd	ferredoxin
FID	flame ionization detector
FNR	ferredoxin-NADP ⁺ reductase
FS	fluorescence sequencing
g	gram
GAP	glyceraldehyde-3-phosphate
GbHDR	<i>Ginkgo biloba</i> HDR
GC	gas chromatography
GST-tag	glutathione S-transferase tagged
HDR	1-Hydroxy-2-methyl-2-(E)-butenyl-4-diphosphate reductase
HDS	1-hydroxy-2-methyl-2-(E)-butenyl 4-diphosphate synthase
HEPES	4-(2-hydroxyethyl)-1-piperazineethanesulfonic acid
HILIC	hydrophilic interaction liquid chromatography
HMBDP	1-hydroxy-2-methyl-2-(E)-butenyl 4-diphosphate
HPLC-ESI-MS	high performance liquid chromatography electrospray ionization mass spectrometry
HSAB	hard and soft (Lewis) acid and bases
IDI	isopentenyl diphosphate isomerase
IDP	isopentenyl diphosphate
kb	kilobase
k _{cat}	catalytic constant

kDa	kilodalton
K_M	Michaelis-Menten constant
l	liter
LB	lysogeny broth
LC-MS	liquid chromatography mass spectrometry
LC-MS/MS	liquid-chromatography tandem mass spectrometry
m	milli
M	molar
MEcDP	2-C-methyl-D-erythritol-2,4-cyclodiphosphate
MEP	methylerythritol phosphate
MES	2-(N-morpholino)ethanesulfonic acid
min	minutes
MOPSO	3-(N-morpholino)-2-hydroxypropane sulphonic acid
MVA	mevalonate
MW	molecular weight
n	nano
N	amino
NADP	nicotinamide adenine dinucleotide phosphate
NCD	amino-terminal conserved domain
NMR	nuclear magnetic resonance
N-terminal	amino terminal
OD	optical density
ON	over night
<i>Pa</i> HDR	<i>Picea abies</i> HDR
<i>Pc</i> HDR	<i>Populus x canescens</i> HDR
psi	pounds per square inch
RNA	ribonucleic acid
rpm	rotations per minute
RT	room temperature
RT-qPCR	real-time quantitative polymerase chain reaction
SDS-PAGE	sodium dodecyl sulfate polyacrylamide gel electrophoresis
sec	second
SOC medium	Super Optimal broth with Catabolite repression medium
TBE	Tris Borate Ethylenediaminetetraacetic acid
UV/VIS	ultraviolet/visible
v	volume
V	volt
w	weight

List of Figures

Figure 1: Reaction catalysed by the 1-Hydroxy-2-methyl-2-(<i>E</i>)-butenyl-4-diphosphate reductase (HDR)	2
Figure 2: Scheme of the isoprenoid biosynthesis.....	3
Figure 3: <i>P. canescens</i> wildtype (3 months old) and <i>P. abies</i> wildtype (12 months old), grown at the MPI for Chemical Ecology, Jena.....	4
Figure 4: Scheme of the MEP pathway.....	7
Figure 5: 3D-modell from <i>E. coli</i> HDR based on X-ray crystallographic data (PDB Database set: 3KE8), a) entire protein, b) zoomed in [4Fe-4S] ²⁺ cluster	9
Figure 6: Scheme from Chaignon et al. (2020) of the mechanism proposed for the reaction catalyzed by the HDR from <i>E. coli</i>	11
Figure 7: Relative normalized expression of the HDR1 and HDR2 from a) <i>P. canescens</i> and b) <i>P. abies</i> in different tissues.....	13
Figure 8: Phylogenetic tree of putative HDR genes from <i>Arabidopsis thaliana</i> (AT), <i>Populus trichocarpa</i> (Potri), <i>Ginkgo biloba</i> (Ginkgo), <i>Picea sitchensis</i> , <i>Picea abies</i> (MA and GQ), <i>Pinus taeda</i> and <i>Pinus densiflora</i>	31
Figure 9: Alignment of HDR peptide sequences from <i>P. abies</i> , <i>P. canescens</i> and <i>P. trichocarpa</i>	34
Figure 10: 3D models of the HDRs from <i>E. coli</i> , <i>Populus × canescens</i> and <i>Picea abies</i> (models made by SWISS-MODEL Expasy)	36
Figure 11: In silico docking model of ferredoxin (Fd) and ferredoxin-NADP ⁺ reductase (FNR) with HDR from <i>Mentha × piperita</i> (adapted figure from Johnson et al., 2017).....	37
Figure 12: Experimental setup in the glove box	39
Figure 13: Chromatograms of controls for a) <i>Pc</i> HDR-T, b) <i>Pc</i> HDR+T, c) <i>Pa</i> HDR1-T, d) <i>Pa</i> HDR2-T and e) <i>Pa</i> HD2-T2	43
Figure 14: SDS-PAGE of <i>Pc</i> HDR-T+GST-tag (~74 kDa) and <i>Pc</i> HDR+T+GST-tag (~78 kDa)	44
Figure 15: SDS-PAGE of <i>Pa</i> HDR1-T+GST-tag (~74 kDa).....	44

Figure 16: SDS-PAGE of <i>Pa</i> HDR2-T+GST-tag (~74 kDa) and <i>Pa</i> HDR2-T2+GST-tag (~77 kDa).....	45
Figure 17: Calibration curve for HMBDP and IDP+DMADP	46
Figure 18: Assay to proof activity of <i>Pc</i> HDR+T and <i>Pa</i> HDR2-T2	47
Figure 19: Activity profile of a) <i>Pc</i> HDR-T, b) <i>Pa</i> HDR1-T and c) <i>Pa</i> HDR2-T at different pH values (MES/HEPES/CHES buffer).....	48
Figure 20: Activity profile of a) <i>Pc</i> HDR-T, b) <i>Pa</i> HDR1-T and c) <i>Pa</i> HDR2-T at different temperatures	50
Figure 21: Measurements for the determination of the initial velocities of product formation by a) <i>Pc</i> HDR-T, b) <i>Pa</i> HDR1-T and c) <i>Pa</i> HDR2-T at different substrate concentrations	51
Figure 22: Lineweaver-Burk plots to determine K_M , v_{max} and k_{cat} of a) <i>Pc</i> HDR-T, b) <i>Pa</i> HDR1-T and c) <i>Pa</i> HDR2-T	52
Figure 23: Lineweaver-Burk plot to compare K_M and v_{max} of <i>Pc</i> HDR-T, <i>Pa</i> HDR1-T and <i>Pa</i> HDR2-T	53
Figure 24: IDP/DMADP ratios synthesized by <i>Pc</i> HDR-T, <i>Pa</i> HDR1-T and <i>Pa</i> HDR2-T .	55
Figure 25: Alignment of peptide sequences from different organisms with MegAlign Pro ClustalW algorithm (GONNET)	vi
Figure 26: pDEST TM 15 plasmid map	vii
Figure 27: pDONR TM 201 and pDONR TM 207 plasmid map	viii
Figure 28: Loss of enzyme activity after one day of storage and present activity in Flow through and Wash 1 fraction	xiv
Figure 29: Michaelis-Menten Plot to determine K_M , v_{max} and k_{cat} of a) <i>Pc</i> HDR-T, b) <i>Pa</i> HDR1-T and c) <i>Pa</i> HDR2-T	xiv

List of Tables

Table 1: In vitro ratio of IDP/DMADP produced by the HDR from different organisms	12
Table 2: MOPSO Buffer, pH 7.8.....	15
Table 3: MES/HEPES/CHES Buffer, pH variable.....	16
Table 4: <i>E. coli</i> strains.....	17
Table 5: Primer for sequencing	17
Table 6: Primer for Gateway cloning.....	18
Table 7: Plasmids for Gateway cloning	18
Table 8: Titles of putative HDR constructs and corresponding template genes	19
Table 9: Software and databases	20
Table 10: Components for reverse transcription.....	21
Table 11: Components for attB-PCR	22
Table 12: Program for attB-PCR.....	23
Table 13: Components for PCR for sequencing.....	24
Table 14: Program for PCR for sequencing.....	24
Table 15: Components of anaerobic enzyme assays.....	27
Table 16: Solvent gradient profile for separation of MEP-pathway metabolites with XBridge BEH Amide XP Column.....	29
Table 17: Solvent gradient profile for separation of DMADP and IDP with Astec® Cyclobond® I 2000 column.....	29
Table 18: Characteristic biochemical values of HDRs from different organisms	54
Table 19: In vitro ratio of IDP/DMADP produced by the HDR from various organisms..	56
Table 20: Predictions about the transit peptide of <i>PcHDR</i> , <i>PaHDR1</i> and <i>PaHDR2</i> from ChloroP.....	vii
Table 21: Data about accuracy and quality of 3D-model predictions of <i>PcHDR</i> , <i>PaHDR1</i> and <i>PaHDR2</i> by SWISS-MODEL Expasy.....	xiii
Table 22: Comparison of 3D-model predictions of <i>PcHDR</i> , <i>PaHDR1</i> and <i>PaHDR2</i> to template 3szu (PDB title) by SWISS-MODEL Expasy.....	xiii

1 Introduction

1.1 Isoprenoids in plants

1.1.1 Function of isoprenoids in plants

Isoprenoids constitute the largest class of natural products. More than 80,000 different isoprenoids are biosynthesised in nature (Christianson, 2017), about 30,000 of them by plants (Opitz et al., 2014). How can nature produce such an enormous variety of molecules in an efficient manner? Two isomeric C₅ building blocks go through several condensation steps and subsequent chemical modifications are carried out. This thesis investigates the biosynthesis of the two building blocks in the chloroplasts of grey poplar (*Populus × canescens*) and Norway spruce (*Picea abies*).

What are isoprenoids? Isoprenoids are all metabolites derived from the C₅ structure isoprene (see Figure 2) (Ruzicka, 1953). The huge variety of chemical structures of isoprenoids reflects their function and mode of action. Some isoprenoids are considered to belong to the primary metabolism if they are part of growth or cell cycle control, photosynthesis or respiration (Estévez et al., 2001; Chen et al., 2011). Isoprenoids, which are classified as secondary metabolites, play important roles, for example, in the protection of the plant's life and integrity, if they are defence molecules, toxic to a pathogen or herbivore or acting as repellents (Gershenzon and Dudareva, 2007; Boncan et al., 2020). They can also act as signalling molecules, often in volatile form. This includes, in case of a pest attack, attraction of helper organisms or warning signals for their neighbouring plants to activate their defences, or in case of reproduction, attraction of pollinators (Pichersky and Gershenzon, 2002). This means they can be part of intraspecies as well as interspecies communication. Not only single components, but also a mixture of isoprenoids is used by plants, which may result in a more specific mode of action (Gershenzon and Dudareva, 2007). Lastly, isoprenoids can also protect the plant against abiotic stress such as heat, solar radiation or drought (Vickers et al., 2009; Boncan et al., 2020; Jalil and Ansari 2020).

1.1.2 Biosynthesis of isoprenoids

How is the huge variety of molecules synthesized? All isoprenoids are synthesized from the two isomeric C₅-units isopentenyl diphosphate (IDP) and dimethylallyl diphosphate (DMADP) (Figure 1 and Figure 2) (Schrader and Bohlmann, 2015). There are two known pathways which produce DMADP and IDP. The mevalonate (MVA) and the methylerythritol phosphate (MEP) pathway. The MVA pathway is present in animals, fungi, archaea, some bacteria and the cytosol of plants. The product of this pathway is solely IDP. The MEP pathway is present in most prokaryotes, in the eukaryotic apicomplexa and in the plastids of plants (Frank and Groll, 2017). In contrast to the MVA pathway, the products of the MEP pathway are both DMADP and IDP. They reaction is catalyzed by the final enzyme of the pathway – the 1-Hydroxy-2-methyl-2-(*E*)-butenyl-4-diphosphate reductase (HDR) (EC 1.17.7.4 KEGG database, IUPAC nomenclature: (2*E*)-4-hydroxy-3-methylbut-2-en-1-yl diphosphate reductase). The reaction catalysed by the HDR is shown in Figure 1.

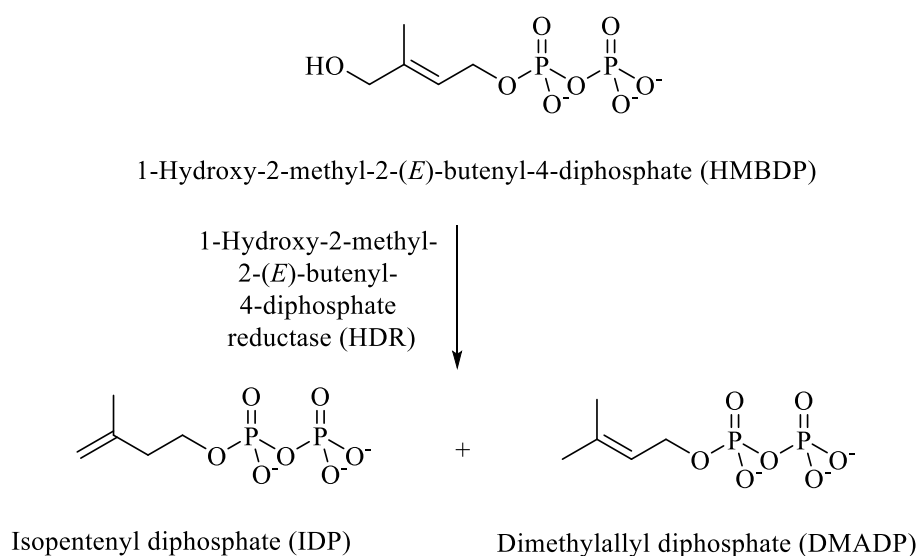


Figure 1: Reaction catalysed by the 1-Hydroxy-2-methyl-2-(*E*)-butenyl-4-diphosphate reductase (HDR)

In plants, the isopentenyl diphosphate isomerase (IDI) is present both in chloroplasts and the cytosol to catalyze the conversion of IDP to DMADP and vice versa (Phillips et al., 2008). Starting from these two building blocks, chains of different C₅-length are formed via a head-to-tail-condensation of one DMADP unit and one to several IDP units by isoprenyl diphosphate synthases (Schmidt and Gershenzon, 2007). The resulting chains are then further modified by terpene synthases, which among others carry out cyclizations, hydroxylations, oxidations and reductions (Schrader and Bohlmann, 2015). Terpenoids, which are a subgroup of isoprenoids, are commonly classified based on their chain length. They are named mono- (C₁₀), sesqui- (C₁₅), di- (C₂₀), sester- (C₂₅), tri- (C₃₀), tetra- (C₄₀) and polyterpenes (C_n). A scheme for the biosynthetic pathway is presented in Figure 2.

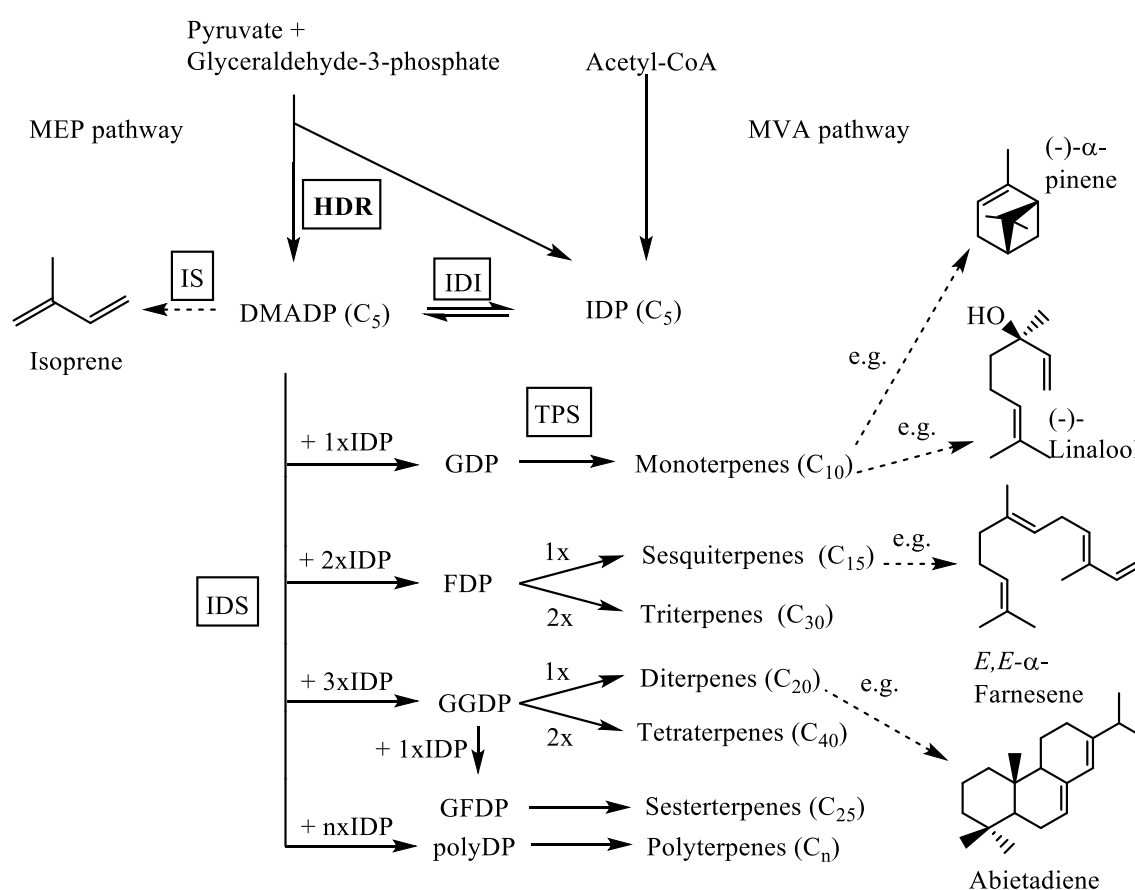


Figure 2: Scheme of the isoprenoid biosynthesis (scheme adapted from (Schmidt and Gershenzon, 2007; Krause et al., 2020)) enzymes have a frame, MEP (methylerythritol phosphate), MVA (mevalonate), HDR (1-hydroxy-2-methyl-2-(*E*)-butenyl 4-diphosphate reductase), IS (isoprene synthase), DMADP (dimethylallyl diphosphate), IDP (isopentenyl diphosphate), IDI (isopentenyl diphosphate isomerase), IDS (isoprenyl diphosphate synthase), GDP (geranyl diphosphate), FDP (farnesyl diphosphate), GGDP (geranylgeranyl diphosphate), GFDP (geranyl farnesyl diphosphate), TPS (terpene synthase)

1.1.3 Isoprene emission and terpenoid composition of *Populus × canescens* and *Picea abies*

After this short review about the function and biosynthesis of isoprenoids, the two plant species grey poplar (*P. canescens*) and Norway spruce (*P. abies*) will be characterized based on their terpenoid composition and isoprene emission.



Figure 3: *P. canescens* wildtype (3 months old) and *P. abies* wildtype (12 months old), grown at the MPI for Chemical Ecology, Jena (Pictures ©Toni Krause)

P. canescens, commonly known as grey poplar, is part of the Salicaceae family and occurs naturally in middle and Western Europe and Northern Africa. It is generally recognized as a hybrid from *Populus alba* and *Populus tremula* (Rajora and Dancik, 1992). The genome is not fully sequenced, but in many cases, as in this project, the genome from *Populus trichocarpa* can be used as a template for genetic analysis (see fully sequenced genome of *P. trichocarpa* (Tuskan et al., 2006)). The genus *Poplar* is used as a model organism for woody plants in the scientific community, as, amongst other characteristics, it is a fast-growing pioneer tree. Characterizing *P. canescens* by its isoprenoid production, it stands out that it emits high rates of isoprene. Isoprene is the quantitatively most emitted volatile organic compound from plants, which has an impact even on atmospheric chemistry due to its high concentrations (Guenther et al., 1995). Due to its overall high emission of isoprene, poplar species are intensively studied in terms of isoprene biosynthesis, regulation and function (Loivamaki et al., 2007; Wiberley et al., 2009; Schnitzler et al., 2010; Vickers et al., 2010). On the other hand, there is little constitutive synthesis and emission of terpenoids such as mono- or sesquiterpenes in poplar.

P. abies is commonly known as Norway spruce and is part of the Pinaceae family. In 2013 its whole genome has been sequenced (Nystedt et al., 2013). The species naturally occurs in Northern Europe, Siberia and at high altitudes in central Europe, being the dominant species in many forests (Caudullo et al., 2016). Its wood is economically important, as it grows relatively fast, is of good quality for construction and the manufacturing of furniture and instruments. A healthy spruce tree constitutively produces a mixture of terpenes as a defence mechanism against pathogens and herbivores. The mixture is composed by mono- or sesquiterpenes (some of them volatile) and non-volatile diterpenes. Linalool, camphor, farnesene, abietic acid and pimaric acid are only a few examples (Martin et al., 2003; Martin et al., 2004; Keeling and Bohlmann, 2006; Zulak and Bohlmann, 2010; Celedon and Bohlmann, 2019). Compared to the *Populus* species, *P. abies* is a weak emitter of isoprene (Bourtsoukidis et al., 2014).

This short characterization of grey poplar and Norway spruce should illustrate the differences of their isoprene emission and terpenoid production. Grey poplar emits high rates of isoprene and produces small amounts of longer-chain (C_{10} and higher) terpenoids whereas Norway spruce does the opposite. It emits low rates of isoprene and produces high amounts of mono-, sesqui- and diterpenes. Since isoprene is solely derived from DMADP and longer-chain terpenoids need only one molecule of DMADP, but many molecules of IDP for their synthesis (see Figure 2), different ratios of IDP and DMADP are assumed in the two species. So far this has not been published for *P. canescens* and *P. abies*. In the plant kingdom only IDP/DMADP ratios from *Ginkgo biloba* have been analysed *in vitro*. The hypothesis of different ratios existing throughout different plant species, leads to the following questions. At which point of the biosynthetic pathway is the ratio regulated? Is there any regulation at all? Does the HDR decide the ratio? To approach these questions investigation on different levels is needed such as the molecular, metabolomic and biochemical level.

This thesis focuses on the biochemical level, as little is known in literature about biochemical characteristics of the HDR from plants. The knowledge generated *in vitro* is, next to studies *in planta*, an important piece in understanding the regulation of isoprenoid biosynthesis.

Our hypothesis is that the HDR differs in its enzymatic activity and synthesis of product ratio in two plant species with different isoprenoid levels. We assume that a plant such as *P. canescens*, which emits high rates of isoprene, needs more DMADP and with that the HDR catalyses a relatively lower level of IDP/DMADP than plants such as *P. abies*, with a low emission of isoprene and a high production of longer-chain terpenoids. Furthermore, we

want to compare the enzyme activity of the HDR from those two species, which will be done by determining the Michaelis-Menten constant K_M and k_{cat} .

Before the results of this thesis will be presented and discussed, an introduction about the biosynthetic pathway of DMADP and IDP will be given and the current state of research of the HDR will be described.

1.2 The methylerythritol phosphate (MEP) pathway

The MEP pathway (see Figure 4) was discovered in 1993 independently by two research groups, one headed by Rohmer and the other by Arigoni (Lichtenthaler et al., 1997; Eisenreich et al., 1998; Rohmer, 1999). Even though almost 30 years have passed, there are still many open questions regarding the MEP pathway, especially in plants, as research has been conducted predominantly in microorganisms.

The first substrates of the pathway are pyruvate and glyceraldehyde-3-phosphate (GAP), which are converted to 1-deoxyxylulose 5-phosphate (DXP) by the enzyme named deoxyxylulose phosphate synthase (DXS). The DXS is often claimed to be a rate-limiting step for the MEP pathway and the following isoprenoid biosynthesis, as for example in *A. thaliana* (Estévez et al., 2001; Wright et al., 2014). It is also a regulatory point of the pathway as it can be feedback inhibited by DMADP (Ghirardo et al., 2014; Banerjee et al., 2016). The subsequent enzymes are listed in Figure 4 and fulfil chemical reactions such as a relocation of a methyl group, reduction of a ketone, addition of cytidine triphosphate (CTP) and a phosphate group (Rohmer, 1999; Rohdich et al., 2003). They transform DXP to the cyclic intermediate 2-C-methyl-D-erythritol-2,4-cyclodiphosphate (MEcDP). Some studies describe an accumulation of MEcDP in cells. Such was the case in spinach (Rivasseau et al., 2009) and *A. thaliana* (Wright et al., 2014). The reductive deoxygenation to 1-hydroxy-2-methyl-2-(*E*)-butenyl 4-diphosphate (HMBDP) by the 1-hydroxy-2-methyl-2-(*E*)-butenyl 4-diphosphate synthase (HDS) seems to be a critical step in the biosynthetic flux. Both the HDS and HDR have an $[4Fe-4S]^{2+}$ cluster (Wolff et al., 2003; Seemann et al., 2005). Rivasseau et al. suggested that damage of the cluster through molecular oxygen and reactive oxygen species, or more precisely the repairing mechanisms for such damaged clusters are the limiting factors for their activity (Rivasseau et al., 2009). Both enzymes are supposed to use the ferredoxin/ferredoxin reductase system as an electron source in plants (Frank and Groll, 2017; Johnson et al., 2017), and both catalyse a reductive dehydroxylation. How the

two last enzymes of the MEP pathway are regulated and whether they are regulated constitutively remains to be investigated by future research.

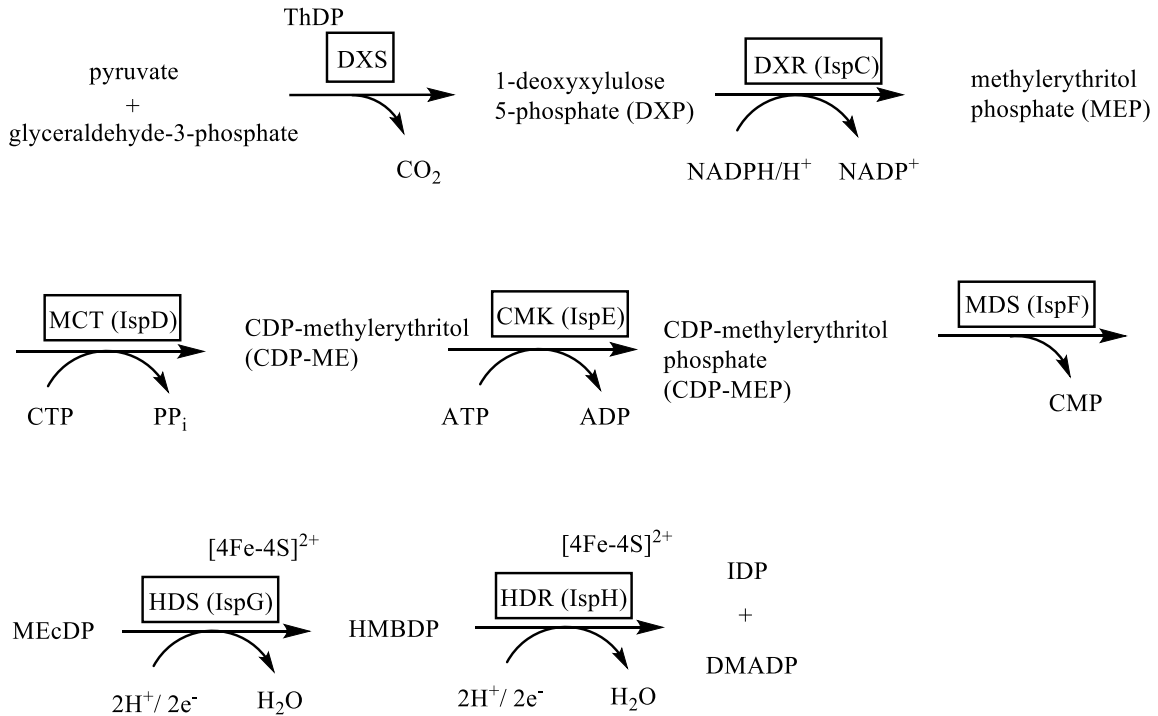


Figure 4: Scheme of the MEP pathway (adapted from (Frank and Groll, 2017) and (Lipko and Swiezewska, 2016)); enzymes have a frame, titles from *E. coli* are put in brackets: IspC-H; DXS (1-deoxy-D-xylulose-5-phosphate synthase), DXR (1-deoxy-D-xylulose-5-phosphate reductoisomerase), MCT (2C-methyl-D-erythritol 4-phosphate cytidyl transferase), CMK (4-(cytidine 5'-diphospho)-2-C-methyl-d-erythritol kinase), MDS (2-C-methyl-d-erythritol 2,4-cyclodiphosphate synthase), HDS (1-hydroxy-2-methyl-2-(*E*)-butenyl 4-diphosphate synthase), HDR (1-hydroxy-2-methyl-2-(*E*)-butenyl 4-diphosphate reductase); ThDP (thiamin diphosphate), NADPH (nicotinamide adenine dinucleotide phosphate (reduced)), NADP⁺ (nicotinamide adenine dinucleotide phosphate (oxidized)), CTP (cytidine triphosphate), PP (pyrophosphate), ATP (adenosine triphosphate), ADP (adenosine diphosphate), CMP (cytidine monophosphate), MEcDP (2-C-methyl-D-erythritol-2,4-cyclodiphosphate), HMBDP (1-hydroxy-2-methyl-2-(*E*)-butenyl 4-diphosphate), IDP (isopentenyl diphosphate), DMADP (dimethylallyl diphosphate)

1.3 The 1-hydroxy-2-methyl-2-(E)-butenyl 4-diphosphate reductase (HDR) in plants

A short overview of the current state of research of the HDR in plants will be given here, before passing on to explaining its reaction mechanism, which has been mainly described in microorganisms. This chapter will focus on the amino acid and enzyme level as this is also the main concern in the results chapter.

The first studies on plant HDR were published by Hsieh and Goodman in 2005. *A. thaliana* plants with a silenced *HDR* gene had an albino phenotype and the chloroplast stroma was identified as the enzyme's location in the cell. About ten years later Hsieh et al. (2014) assumed, based on amino acid sequence alignments and detection of conserved amino acids, that the HDR would incorporate an iron-sulfur cluster, as its homolog from *E. coli*, and have a similar reaction mechanism. *HDR* from *A. thaliana* could complement a lethal *E. coli ispH* (*E. coli* homolog for mutant (Hsieh and Goodman, 2005)). Such complementation assays were performed by several research groups. *HDR* genes from *Oncidium* orchid (Huang et al., 2009), *Stevia rebaudiana* (Kumar and Kumar, 2013), *Tripterygium wilfordii* (Cheng et al., 2017), *Ginkgo biloba* (Kim et al., 2008), *Pinus densiflora* (Kim et al., 2009), *Cucumis melo* L. (Saladié et al., 2014), from various angiosperms and the gymnosperm *Picea sitchensis* (Bongers et al., 2020) all showed successful complementation of an *E. coli ΔispH* mutant. However, such a complementation assay can only confirm the functionality of a putative gene, but cannot state anything about the activity, the reaction itself or the products. By fusion to a green fluorescent protein, the HDR from *Ginkgo biloba*, *Pinus taeda* and *Pinus densiflora* were confirmed to be located in the chloroplast (Kim et al., 2008; Kim et al., 2009). In 2014 Hsieh et al. published investigation on essential amino acids in the protein structure of *A. thaliana* by mutagenization and complementation assays. They also described an amino-terminal (N-terminal) domain after the transit peptide, which is highly conserved in photosynthetic organisms (Hsieh et al., 2014). Both topics will be discussed regarding spruce and poplar further on in the chapter where the results are presented. The first heterologous expression in *E. coli*, purification and *in vitro* analysis under anaerobic conditions of a plant HDR (from *Ginkgo biloba*) has been published in 2015 (Shin et al., 2015). As depicted here, research about the HDR in plants is rare and many questions remain to be answered. Most of the studies have been performed on the genetic level and only a few ones on the enzymatic level. This is probably also due to difficulties in handling the oxygen sensitive iron-sulfur cluster.

1.4 Reaction of the HDR

1.4.1 The iron-sulfur cluster

An overview will be given of the current state of research on the iron-sulfur cluster and the reaction mechanism. The project could not include any mechanistic or bio-organometallic studies. However, as it deals with the purified enzyme and to give a complete picture, it will be summarized here what is known from other organisms. So far, mechanistic studies have been conducted only on HDR enzymes from *E. coli*, *Aquifex aeolicus* and *Plasmodium falciparum*. The MEP pathway and the HDR enzyme of pathogens is proposed as a target for antibiotics (Seemann et al., 2009) and anti-malarial drugs (Gräwert et al., 2004). However, it is surprising that there have not been any mechanistic studies on plant HDR enzymes, as the MEP pathway is only present in bacteria, some fungi and photosynthetic organisms, but not in humans, animals or insects, and could be also a target for fungicides or herbicides.

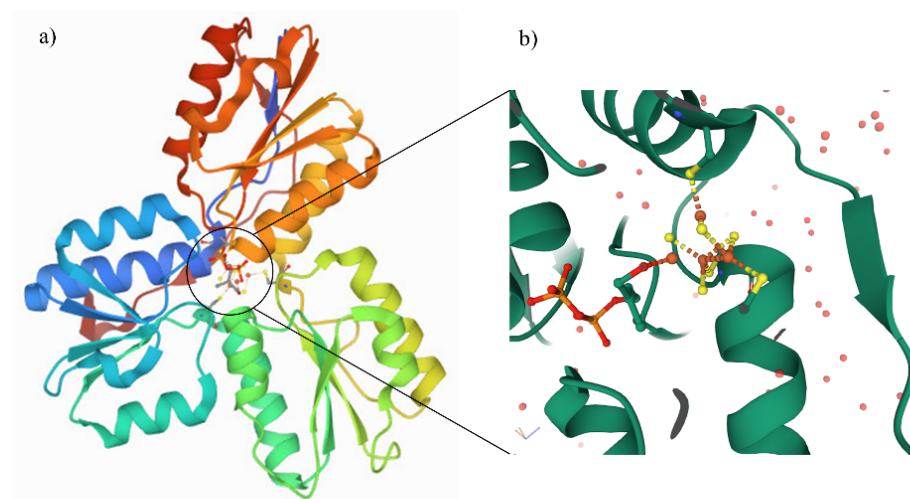


Figure 5: 3D-modell from *E. coli* HDR based on X-ray crystallographic data (PDB Database set: 3KE8), a) entire protein, b) zoomed in $[4\text{Fe-4S}]^{2+}$ cluster; one Fe-atom is interacting with the substrate HMBDP; orange dots: Fe, yellow dots: S (Gräwert et al., 2010)

The first to prove that the ispH protein from *E. coli* has a $[4\text{Fe-4S}]^{2+}$ cluster were Wolff et al. in 2003. They reconstituted the cluster under anaerobic conditions, analysed it with UV/VIS and electron paramagnetic resonance (EPR) spectroscopy and stated that the enzyme would only be active together with a reducing system (Wolff et al., 2003). These findings were confirmed one year later by Gräwert et al. (2004). Flavodoxin and flavodoxin reductase were used as a reducing system and three conserved cysteine residues were identified. Mutations of these conserved residues resulted in a strong loss of catalytic activity

of the HDR (Gräwert et al., 2004). In *Plasmodium falciparum* a ferredoxin/ferredoxin-NADP⁺ reductase redox system was found to be the reducing system (Röhrich et al., 2005). Today, the general consensus based on data from Mössbauer spectroscopy (Seemann et al., 2009) and protein crystallization (see Figure 5) (Gräwert et al., 2010) is that the ispH protein contains 4 iron and 4 sulfur atoms. Three of the iron atoms are coordinated to the three conserved cysteine residues (Gräwert et al., 2004), the fourth iron atom is directly involved in substrate binding and catalysis (Gräwert et al., 2010). When the first X-ray crystallographic structures from the HDR from *Aquifex aeolicus* (Rekittke et al., 2008) and *E. coli* (Gräwert et al., 2009) were introduced in 2008 and 2009, this represented considerable progress for the structure and reaction mechanism.

1.4.2 The reaction mechanism

Since the iron-sulfur cluster was first described, scientists explored how the hydroxyl group is reduced and how the apical iron coordinates the substrate over the time of the reaction. Two different models, a Birch reduction and a bio-organometallic reduction, have been discussed (Abdel-Azeim et al., 2015; Blachly et al., 2015). The common opinion now is that the HDR undergoes a bio-organometallic reaction mechanism. In 2012 Span et al. and Wang et al. and in 2020 Chaignon et al. showed evidence for this mechanism (see Figure 6) by mutation of relevant amino acids and by EPR, crystallographic and nuclear magnetic resonance (NMR) analysis (Span et al., 2012; Wang et al., 2012; Chaignon et al., 2020). Firstly, the hydroxy group of the substrate coordinates to the apical iron atom. The cluster is reduced by one electron. Relying on the HSAB (hard and soft (Lewis) acid and bases) concept, this leads to a softer iron atom, which can then better interact with the softer alkene (Chaignon et al., 2020). The hydroxy group can rotate and interact with the E126 (Rekittke et al., 2008; Span et al., 2012) and can be released as a water molecule (see Figure 6). The following $[4\text{Fe-4S}]^{3+}$ cluster interacts with the allylic anion and is reduced by a second electron (Chaignon et al., 2020). As a final step this anion is protonated either at the C4 or at the C2 carbon, which results in DMADP or IDP respectively.

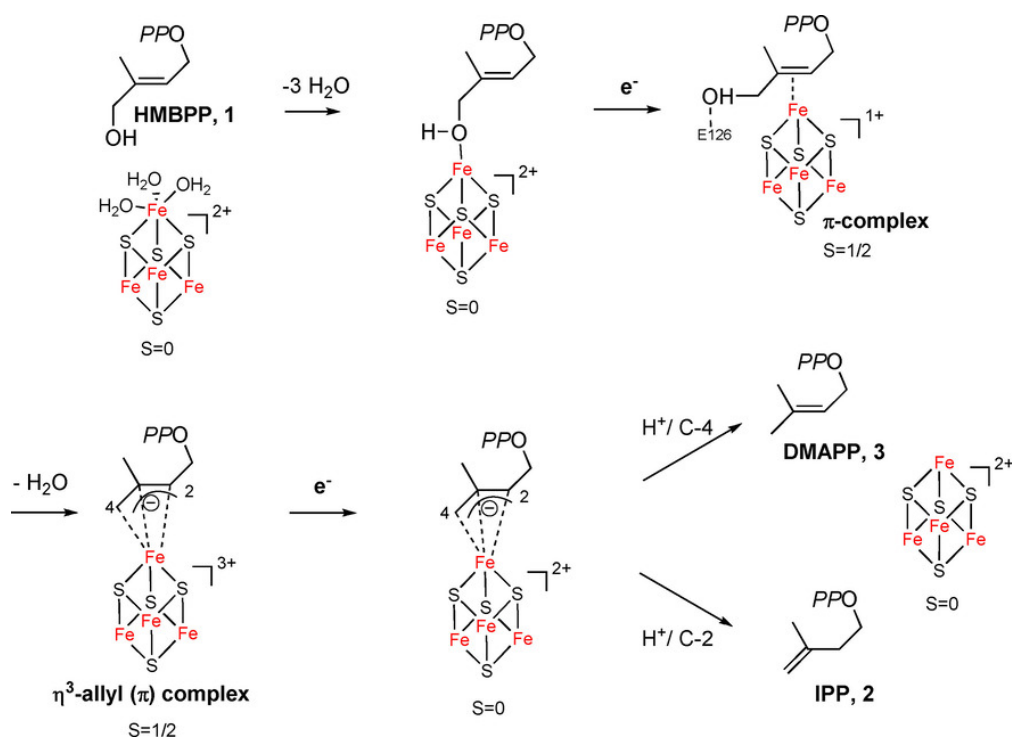


Figure 6: Scheme from Chaignon et al. (2020) of the mechanism proposed for the reaction catalyzed by the HDR from *E. coli*

1.4.3 The IDP/DMADP ratio

However, to this date no research has been conducted on whether the final protonation step is regulated and how the ratio of the two isomeric products is controlled. Is the regulation fulfilled by amino acid side chains of the enzyme, by the pH, depending on where the enzyme is localized in the cell, by other cofactors or simply by which chemical reaction is energetically preferred? This is a question which remains unanswered. The products were analysed separately only in a few studies, as their isomeric character displays an analytical challenge. This was done by analysing their alcohol derivatives through gas chromatography (GC) coupled to a flame ionization detector (FID) (Kwon et al., 2013) or MS (Shin et al., 2017) or analysis of the alcohol derivatives through radioactivity (Adam et al., 2002; Wolff et al., 2003), by NMR (Gräwert et al., 2004), by high performance liquid chromatography electrospray ionization mass spectrometry (HPLC-ESI-MS) using an anion exchange column (Altincicek et al., 2002; Röhrich et al., 2005) or by liquid chromatography mass spectrometry (LC-MS) using a chiral column (Köhling et al., 2014; Bongers et al., 2020). In Table 1 an overview is given on the HDRs from organisms where the IDP/DMADP ratio was determined *in vitro*.

Table 1: *In vitro* ratio of IDP/DMADP produced by the HDR from different organisms

Organism	IDP/DMADP ratio	Literature
<i>Burkholderia glumae</i>	2.2:1	(Kwon et al., 2013)
<i>Plasmodium falciparum</i>	4-5:1	(Röhrich et al., 2005)
<i>Aquifex aeolicus</i>	4-5:1	(Altincicek et al., 2002)
<i>Escherichia coli</i>	5-6:1	(Adam et al., 2002; Wolff et al., 2003; Gräwert et al., 2004)
<i>Ginkgo biloba</i>	16:1	(Shin et al., 2017)

To prevent confusion, it should be stated here that the ratios described in this thesis are always IDP/DMADP as the HDR produces more IDP than DMADP and the enzyme is characterized independently from other enzymes. The literature has to be read carefully as in some publications the ratio is the other way around (DMADP/IDP) (see for example (Bongers et al., 2020)). This is the case since there the ratio is measured *in vivo* from the plant and the isomerase IDI can change the ratio towards more DMADP.

In this work, the IDP/DMADP ratio of the HDR from *P. abies* and *P. canescens* shall be determined and added to this list. This is done with a Astec® Cyclobond® I 2000 column.

The method established by Krause et al. can separate the two isomers. By doing so it is possible to determine the components without chemical derivatisation (Krause et al., 2020).

1.5 Starting point of the project

The starting point of this project were genetic studies of the HDR from *P. abies* and *P. canescens*. Since the project was embedded in the research of the Conifer Defense group at the Biochemistry department of the Max-Planck-Institute for Chemical Ecology, antecedent studies on expression levels of putative *HDR* genes from grey poplar and Norway spruce had been performed. Two putative *HDR* genes from both species had been identified in the corresponding genome databases (<https://popgenie.org>, <https://phytozome.jgi.doe.gov> and <https://congenie.org>), they had been called PcHDR1 and PcHDR2 (*P. canescens*) and PaHDR1 and PaHDR2 (*P. abies*) (for titles in the databases see chapter 2.1.3.3). All four genes were tested on their expression pattern in the stem and leaves or needles by real-time quantitative polymerase chain reaction (RT-qPCR). The relative normalized expression data is shown in Figure 7.

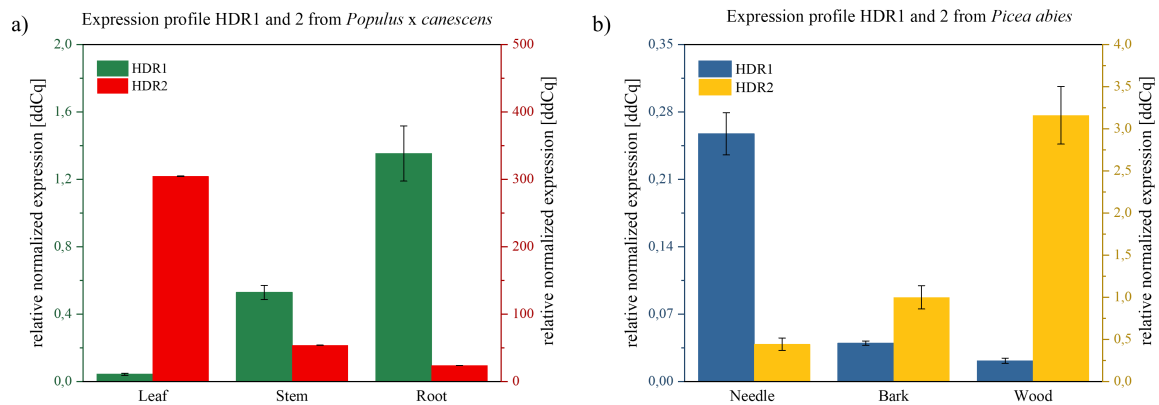


Figure 7: Relative normalized expression of the *HDR1* and *HDR2* from a) *P. canescens* and b) *P. abies* in different tissues, note the different units of the y-axis

To sum up, *HDR1* and *HDR2* from spruce showed similar expression levels, but slightly different expression patterns throughout the various organs. *HDR1* had a higher expression in needles than *HDR2*, and *HDR2* was higher expressed in the woody parts. Even though two putative *HDR* genes were also found in poplar, only *HDR2* from *P. canescens* is characterized in this work because *HDR2* from grey poplar showed 400 times higher expression than *HDR1* in leaves. Similar differences in expression levels are found in transcriptomic data (not published, information given in personal by Tobias Köllner, MPI

for Chemical Ecology, Jena). Due to these substantial differences, HDR1 was assumed to play a minor role, if a role at all, in poplar. Therefore, HDR2 of *P. canescens* will be named solely HDR in the entire thesis.

1.6 Aim of this work

Four observations were the basis of this project: first, the knowledge gained from the literature, that *P. abies* produces high amounts of mono-, sesqui- and diterpenes and *P. canescens* emits high amounts of isoprene; second, the observation that the HDR is an enzyme at the interface between the MEP pathway and the isoprenoid biosynthesis pathway and therefore it has to be a regulatory point; third, the assumption that the HDR from plants inherits an iron-sulfur cluster as catalytic centre such as the HDR from *E. coli* does and fourth, the information given about expression levels of putative HDRs from *P. canescens* and *P. abies*.

The driving questions of the project were: Do the HDRs from *P. canescens* and *P. abies* inherit conserved cysteine residues to bind an iron-sulfur cluster? If yes, how can we heterologously express and purify the HDRs to get an active enzyme? Does the procedure have to be carried out in an oxygen-free environment? Once the procedure is established, we can ask whether the HDRs from two different plant species differ in their enzyme activity. Furthermore, do these HDRs differ in the product ratios of IDP and DMADP they produce? To address these questions, a setup and a protocol to purify and test enzymes in a glove box have been established. Based on that, HDR1 and HDR2 from *P. abies* and HDR from *P. canescens* have been cloned. They were heterologously expressed in *E. coli* and purified and enzyme assays were performed and analysed via liquid-chromatography tandem mass spectrometry (LC-MS/MS). Kinetic studies were performed to address the enzyme activity of the three HDRs and the IDP/DMADP ratio has been determined.

2 Material and Methods

2.1 Materials

2.1.1 Chemicals, reagents, media and buffers

2.1.1.1 Chemicals

All chemicals, if not stated otherwise, were supplied by Carl Roth, Sigma-Aldrich Chemie GmbH, Merck KGaA or Honeywell Fluka (see <https://www.carlroth.com/de/de>, <https://www.sigmaaldrich.com/germany.html>, <https://www.merckmillipore.com/DE/de> and <https://lab.honeywell.com/en/fluka>).

2.1.1.2 Antibiotics

All antibiotic stocks were prepared with 50 mg/ml and later diluted 1:1000 in the corresponding application. The following antibiotics were used: Gentamicin (<https://www.duchefa-biochemie.com/>) and Carbenicillin (Carl Roth).

2.1.1.3 LB (lysogeny broth) medium

LB medium (Lennox `powder Gibco`) was composed by 10 g/l peptone, 5 g/l yeast extract and 10 g/l NaCl. LB agar (Lennox `powder Gibco`) was composed by 10 g/l peptone, 5 g/l yeast extract, 5 g/l NaCl and 35 g/l LB agar.

2.1.1.4 Buffers for protein purification and enzyme assays

All buffers were freed from O₂ prior to use by flushing them for 1 h with nitrogen gas.

MOPSO (3-(N-morpholino)-2-hydroxypropane sulphonic acid) Buffer

Table 2: MOPSO Buffer, pH 7.8

Component	Final concentration [mM]
MOPSO (β -Hydroxy-4-morpholine-propanesulfonic acid)	25
Magnesium chloride hexahydrate	25
Potassium chloride	50
Glycerine	10% (v/v)

MES/HEPES/CHES Buffer

2-(N-morpholino)ethanesulfonic acid / 4-(2-hydroxyethyl)-1-piperazineethanesulfonic acid / 2-(cyclohexylamino)ethanesulfonic acid buffer

Table 3: MES/HEPES/CHES Buffer, pH variable

Component	Final concentration [mM]
MES/HEPES/CHES	Each 100
Magnesium chloride hexahydrate	50
Sodium chloride	100
Glycerine	20% (v/v)

This buffer was used as a $2 \times$ buffer. Final concentrations in enzyme assays were hence half of the above mentioned. The three-buffer system was chosen according to Shin et al. (2015).

2.1.1.5 Reagents for sodium dodecyl sulfate polyacrylamide gel electrophoresis (SDS-PAGE)

10 \times SDS running buffer

0.25 M Tris Base, 1.9 M glycine and 0.03 M SDS were dissolved in double distilled water (ddH₂O). For application the solution was diluted 10 times.

Coomassie staining solution

50% (v/v) ethanol, 0.05% (w/v) Coomassie brilliant blue R250 and 10% (v/v) acetic acid were dissolved or diluted in ddH₂O.

Destaining solution

5% (v/v) acetic acid and 16.5% (v/v) ethanol were diluted in ddH₂O.

2.1.2 Bacterial strains

The following two *E. coli* strains were used for plasmid propagation or protein expression respectively. Both were delivered by Invitrogen life technologies (<https://www.thermofisher.com/de/de/home.html>).

Table 4: *E. coli* strains

Title	Genotype
One Shot® TOP10 <i>E. coli</i>	F- <i>mcrA</i> Δ (<i>mrr-hsdRMS-mcrBC</i>) Φ 80 <i>lacZ</i> Δ M15 <i>ΔlacX74 recA1 araD139 Δ(araleu)7697 galU galK</i> <i>rpsL (StrR) endA1 nupG</i>
One Shot® BL21-AI™ <i>E. coli</i>	F- <i>ompT hsdS_B (r_B⁻ m_B⁻) gal dcm araB::T7RNAP-tetA</i>

2.1.3 Primer, plasmids and constructs

2.1.3.1 Primer

All primer were supplied by Eurofins (<https://www.eurofins.de/>) and diluted to 10 μ M before further use.

Table 5: Primer for sequencing

Name	Sequence 5' → 3'
pDONR207_for_seq	GGCCTTCTGCTTAGTTTGATGC
pDONOR_rev_neu_seq	TAAATTCCGTCAGCCAGTTTAGTC
pDEST15_for_seq	CCTGAAATGCTGAAAATGTTCTGAAG
pDEST15_rev_seq	CTAGCGCTATATGCGTTGATGC
PcHDR_for_seq	GTTGGATCTTATGTTAGTTGTTGGC
PcHDR_rev_seq	CCATGTATACTCATAACCATTCTCC
PcHDR_for2_seq	GGAAATGTTACAGTCAAATTAGCC
PcHDR_rev2_seq	TATCCTCTGTTCACTGTCAATCC
PaHDR1_for_seq	TCTTATTCTTGTTGTAGGAGGATGG
PaHDR1_rev_seq	ATTGCTTCAAGAGTTTCTTCCTTGTC
PaHDR1_for2_seq	TGAAAGAGAACAACAATGAATACAC
PaHDR1_rev2_seq	TCCATCCTCCTACAACAAGAATAAG
PaHDR2_for_seq	GATGCAATGGATGATCTAGTAAAGG
PaHDR2_rev_seq	GTTAAGTTTTTCTGAAGGTCTTGGG
PaHDR2_for2_seq	GGACCAAGAGTACACGAGTGATC
PaHDR2_rev2_seq	CATCTTGTCTTTCCTGAGTGG

Table 6: Primer for Gateway cloning

Name	Sequence 5'→3'
<i>Pc</i> HDR-T_GW_pD15/17_for	GGGGACAAGTTTGTACAAAAAAGCAGGCTA CTGCGCTGGCGGTGATGACTCTAC
<i>Pc</i> HDR-T_GW_pD15/17_rev	GGGGACCACTTTGTACAAGAAAGCTGGGTC TTAAGCTACTTGTAAGCTTCGTC
<i>Pc</i> HDR+T GW pD15/17/24 for	GGGGACAAGTTTGTACAAAAAAGCAGGCTT CATGGCTATCTCTCTCCAACCTCTGCCGC
<i>Pc</i> DHR400-T_GW_pD15/17_for	GGGGACAAGTTTGTACAAAAAAGCAGGCTA CTGCGCCGGCGGTGATGGCTCTAC
<i>Pc</i> DHR400-T_GW_pD15/17_rev	GGGGACCACTTTGTACAAGAAAGCTGGGTC TCATGCTAGTTGCAAGCCTTCCTC
<i>Pa</i> HDR1-T_GW_pD15/17_for	GGGGACAAGTTTGTACAAAAAAGCAGGCTA CTGCGATGCTGCTCCCAGCGCTGTAG
<i>Pa</i> HDR1-T_GW_pD15/17_rev	GGGGACCACTTTGTACAAGAAAGCTGGGTC TTATACTGTCTGCAACGCCTCCTC
<i>Pa</i> HDR2-T_GW_pD15/17_for	GGGGACAAGTTTGTACAAAAAAGCAGGCTA CTGCGATGGAGGGGGAGCTGCTGCTG
<i>Pa</i> HDR2-T_GW_pD15/17_rev	GGGGACCACTTTGTACAAGAAAGCTGGGTC CTATGCTACTTGCAGAGCCTCTTC
<i>Pa</i> HDR2-T2_GW_pD15/17_for	GGGGACAAGTTTGTACAAAAAAGCAGGCTA CCATTCGGCTCTCGTGCATCATC

2.1.3.2 Plasmids

All plasmids were purchased by Invitrogen Life Technologies (<https://www.thermofisher.com/de/de/home/brands/invitrogen.html>). Plasmid maps are listed in the appendix in chapter 6.3.

Table 7: Plasmids for Gateway cloning

Name	Purpose
pDONR207	donor vector to form entry clone with putative HDR gene
pDEST15	destination vector with N-terminal GST-tag to form expression clone with putative HDR gene

2.1.3.3 Putative HDR constructs

For primer design and sequence analysis the following templates from the popgenie and congenie database (see 2.1.6) were used. Putative transit peptides, which were calculated and proposed by the online database ChloroP, are described here with T. Constructs designed with or without transit peptide are correspondingly entiteled with +/- T Sequences of the cloned putative HDR constructs are listed in the appendix in chapter 6.4. A detailed description and discussion of transit peptide length is given in chapter 3.1.4.

Table 8: Titles of putative HDR constructs and corresponding template genes

Putative HDR construct	Template gene
<i>Populus × canescens</i> HDR-T (<i>PcHDR-T</i>)	Potri.009G111600.1
<i>Populus × canescens</i> HDR+T (<i>PcHDR+T</i>)	Potri.009G111600.1
<i>Picea abies</i> HDR1-T (<i>PaHDR1-T</i>)	GQ03701_E06.1
<i>Picea abies</i> HDR2-T (<i>PaHDR2-T</i>)	MA_105092g0010
<i>Picea abies</i> HDR2-T2 (<i>PaHDR2-T2</i>)	MA_105092g0010

2.1.4 Plant material

Leaves were collected from a greenhouse grown *Populus × canescens* (clone INRA 717, WT) and phytochamber grown *Picea abies* (clone 3369-Schongau, WT; Samenklenge und Pflanzgarten, Laufen, Germany).

2.1.5 Equipment

2.1.5.1 General equipment

All work was performed in S1 laboratories, with its standard laboratory equipment and disposables.

2.1.5.2 Glove box

For anaerobic work in nitrogen atmosphere a glove box had to be set up and adapted for the work with oxygen-sensitive enzymes. The glove box P10 R0 T2 from GS GLOVEBOX Systemtechnik GmbH (<http://www.glovebox-systemtechnik.de/>) was used. A picture of the setup is listed in chapter 3.2.1.

The Oxygen level in the box was measured by a BW clip real time O₂ sensor from BW Technologies by Honeywell (<https://www.honeywellanalytics.com/de-de>). It can measure O₂ concentrations in % v/v. Before starting the work, the glove box was filled with N₂ to reach ~ 1% O₂ and was constantly flushed with 2 l/min of N₂ during work.

2.1.6 Software and databases

Table 9: Software and databases

Name / Website	Purpose
DNASTAR Lasergene 17: SeqBuilder Pro 17, SeqMan Pro 17 and MegAlign Pro 17	Primer design, sequence analysis, sequence alignments
Geneious Prime	Analysis of sequencing results
ChemDraw Professional 17.1	Drawing of chemical structures
Analyst Software (Version 1.6.3)	Analysis of LC-MS/MS data
SigmaPlot 14.0	Statistical analysis
Origin 2019	Creating of graphs, enzyme kinetic analysis
https://www.genome.jp/kegg/ (retrieved 03.03.21)	HDR enzyme number
Popgenie.org	sequences of poplar species
https://phytozome.jgi.doe.gov/pz/portal.html (retrieved 03.03.21)	sequences of various plant species for alignment
https://www.ncbi.nlm.nih.gov/gene/ (retrieved 03.03.21)	sequences of various plant species for alignment
Congenie.org	sequences of spruce species
ChloroP 1.1 Server http://www.cbs.dtu.dk/services/ChloroP/ (retrieved 03.03.21) (Emanuelsson et al., 1999)	For transit peptide analysis
https://web.expasy.org/compute_pi/ (retrieved 03.03.21)	Calculation of protein mass
https://swissmodel.expasy.org/ (retrieved 03.03.21)	3D-Modells of plant HDR

2.2 Methods

2.2.1 Ribonucleic acid (RNA) extraction

Plant material (see 0) was grinded under liquid N₂. For RNA extraction protocol 1 from the InviTrap® Spin Plant RNA Mini Kit 1017 (<https://www.invitex-molecular.com/home.html>) was used with the following amendments. For cell lysis ~100 mg of plant powder were added to 1100 µl of RT buffer and 12 µl 1 M DTT. This was incubated for 30 min at 22°C shaking for 14.000 rpm. Centrifugation was performed after adding 300 µl R1 buffer, then 70 µl RDD (<https://www.qiagen.com/us/>) mixed with 10 µl DNase were added and kept for 15 min at RT. After centrifugation, 300 µl R1 were added and centrifuged one last time before continuing with the second washing step. In the end RNA was eluted with 32 µl of fresh ddH₂O.

2.2.2 Reverse transcription to cDNA

For reverse transcription from RNA to cDNA the following components were used:

Table 10: Components for reverse transcription

Component	Volume / Concentration
Oligo(dT) ₂₀	1 µl (50 µM stock)
Total RNA	10 pg-5 µg
dNTP Mix	1 µl (10 mM each nucleotide at pH 7)
ddH ₂ O	fill up to 14 µl
5X First-Strand Buffer	4 µl
DTT	1 µl (0.1 M stock)
SuperScript™ III RT	1 µl (200 units/µl)

The oligonucleotides, total RNA, dNTPs and ddH₂O were mixed and heated to 65°C for 5 min and afterwards incubated on ice for 1 min. After a short centrifugation the buffer, DTT and SuperScript were added and gently mixed by pipetting: The incubation took place at 65°C for 5 min and at 55°C for 1h. The reaction was inactivated at 70°C for 15 min and stored at -20°C until further usage.

2.2.3 Gateway cloning

The gateway cloning system (Invitrogen Life Technologies) was used for the construction of plasmids for protein expression and purification. In this technology a PCR product of the gene of interest flanked by two attB sites recombines with the donor vector pDONR207 to form an entry clone. From this entry clone the gene of interest recombines with the destination vector pDEST15 to form an expression clone. For more detailed information see the Gateway cloning manual (<http://tools.thermofisher.com/content/sfs/manuals/gatewayman.pdf> retrieved 03.03.2021)

2.2.3.1 PCR with attB sites

For the attB-PCR suitable primer were designed and the following reaction was set up:

Table 11: Components for attB-PCR

Component	Volume / Concentration
5 × Q5 Reaction Buffer	5 µl
dNTPs	1 µl (10 mM each nucleotide stock)
Forward Primer	1.25 µl (10 µM stock)
Reverse Primer	1.25 µl (10 µM stock)
cDNA	1 µl
Q5 Polymerase	0.5 µl
ddH ₂ O	15 µl

The amplification of the fragment was done in a PCR cycler with the following program. 35 cycles were performed from step 2 to 4. If the amplification was not successful the primer annealing temperature was lowered to 55°C, the amplification raised to 70 sec and the cycle number increased to 50.

Table 12: Program for attB-PCR

Step	Temperature [°C]	Time
1.	98	30 sec
2.	98	10 sec
3.	58	30 sec
4.	72	1 min (40 sec/kb)
5.	72	2 min
6.	4	pause

The amplified fragments were extracted from an agarose gel with the Zymoclean Kit before performing the clonase reactions.

2.2.3.2 BP and LR reaction

The BP reaction took place ON at RT with 1 µl BP clonase, 150 ng attB-PCR product, 150 ng pDONR207 and TE-Buffer up to 10 µl. The LR reaction took place ON at RT with 1 µl LR clonase, 150 ng of entry clone, 150 ng of the destination vector and TE-Buffer up to 10 µl.

Both reactions were inactivated the next day by addition of 1 µl proteinase K and incubation for 10 min at 37°C. Until the transformation of the whole inactivated reaction, it was kept at 4°C.

2.2.4 Agarose gel electrophoresis

For DNA analysis 0.75% agarose gels were prepared with 0.5 × TBE (Tris Borate EDTA) buffer. For visualization 0.006% (v/v) Midori Green (<https://www.nippongenetics.eu/>) was used. Running conditions were usually 135 V for 20-40 min, depending on the fragment size. BlueJuice™ Gel Loading Buffer (10×) and Invitrogen 1 Kb Plus DNA Ladder were used (both ThermoFisher Scientific). Pictures were taken by Intas Gel Stick IMAGER (<https://www.intas.de/>).

2.2.5 Gel extraction with Zymoclean Gel DNA Recovery Kit

Gel extraction of PCR fragments was done with the Zymoclean Gel DNA Recovery Kit (<https://www.zymoresearch.de/>) and eluted with 8 µl ddH₂O.

2.2.6 Measuring RNA and DNA concentration

RNA and DNA concentrations were measured by a Nanodrop 2000c Spectrophotometer from ThermoScientific.

2.2.7 Sequencing

Sequencing was done in house by using the Sanger sequencing method.

The templates were prepared with fluorescent nucleotides by PCR using the following protocol:

Table 13: Components for PCR for sequencing

Component	Volume / final concentration
Big Dye TM Terminator (Applied Biosystems TM)	2 μ l
Plasmid DNA	150 ng
Primer (10 μ M; one way)	1 μ l / 1 μ M
ddH ₂ O	fill up to 10 μ l

The Big Dye (<https://www.fishersci.de/de/de/home.html>) had the following components: 2.5% MgCl₂, Polymerase-Buffer, AmpliTaq DNA Polymerase FS (fluorescence sequencing), desoxynucleoside triphosphates (dNTP), dye terminators (ddNTP) with the following dyes: G (dR110: blue colour), A (dR6G: green colour), T (dTamra: black colour) and C (dRox: red colour).

The following PCR program was generally used for all primers and templates, fulfilling a hot start at 96°C and using a ramp of 4°C/s and 35 cycles (turning from step 4 to step 2).

Table 14: Program for PCR for sequencing

Step	Temperature [°C]	Time
1.	96	5 min
2.	96	30 sec
3.	55	30 sec
4.	60	4 min
5.	4	pause

The PCR reaction was purified by sephadex G50 superfine (Sigma-Aldrich). For analysis ABI Prism® - Gen- Analysator 3130xl with 16 capillaries was used.

2.2.8 Culturing of bacteria

E. coli strains (see 2.1.2) were cultured in liquid LB medium with the corresponding antibiotic (1:1000) at 37°C shaking at 220 rpm ON or on LB-Agar plates with the corresponding antibiotic (1:1000) at 37°C ON.

2.2.9 Plasmid preparation

2 ml of an ON liquid culture from a single colony were used to prepare plasmids with the Invisorb Spin Plasmid Mini Two kit (<https://www.invitex-molecular.com/home.html>). The plasmid was eluted with 30 µl ddH₂O and stored at -20°C.

2.2.10 Transformation of *E. coli*

Transformation was performed the same way for every *E. coli* strain. Cells were thawed on ice, centrifuged down quickly and split up for different transformations. If all 50 µl of competent cells were used, 1-2 µl (10-20 ng) of plasmid were transformed. This cell-DNA solution was kept on ice for 30 min, then heat shocked in a water bath at 42°C for 30 sec and cooled on ice again for 2 min. Afterwards 150-250 µl pre-warmed (to 42°C) SOC medium (Invitrogen Life Technologies; Carlsbad, California, US) was added and incubated for 45 min at 37°C shaking horizontally at 220 rpm. Then the transformed cells could be plated on LB-Agar plates with the corresponding antibiotic and incubated ON at 37°C.

2.2.11 Heterologous Expression of HDR

2.2.11.1 Pre-culture

For expression of recombinant HDR a pre-culture of freshly transformed cells was grown in 12 ml LB with carbenicillin (1:1000) in a 150 ml Erlenmeyer flask for either 72 h, at 18°C or 48 h, at 25°C and shaking at 220 rpm.

2.2.11.2 Induction culture

For induction of protein expression 100 ml LB with carbenicillin (1:1000) were inoculated with 5 ml of the pre-culture. The medium was supplemented with 1 mM L-cysteine and ferric ammonium citrate (30 mg/l) to ensure the bacteria enough iron for uptake and formation of the iron-sulfur-cluster of the HDR according to Gräwert et al. (2009). The culture was grown in a 500 ml Erlenmeyer flask until OD₆₀₀ was 0.6. At this stage the culture was induced with 0.2% (w/v) L-arabinose and was grown ON, shaking at 18°C and 220 rpm.

2.2.12 Anaerobic extraction and purification of recombinant protein

2.2.12.1 *Harvesting and Sonication*

The induction culture was harvested by centrifugation in a 50 ml Falcon tube at $3000 \times g$, at 4°C for 10 min. Afterwards the cell pellet was covered with argon and transferred into the glove box. There it was resuspended in 3 ml MOPSO Buffer (see 2.1.1.4). The sonication took place on ice for 3 min, $2 \times 10\%$ cycle with 60% power. Then the disrupted cells were transferred to 2 ml tubes and centrifuged for 15 min, at RT and 14.500 rpm.

2.2.12.2 *Purification via GST-tag*

Purification via Thermo Scientific™ Pierce Glutathion-Agarose columns was performed according to the manufacturers protocol (Instructions Pierce®Glutathione Spin Columns; ThermoFisher Scientific) with the following adaptations due to handling in the glove box. All steps were carried out on ice and with gravity flow. To ensure that the column was oxygen-free, it was flushed with 1 ml 10 mM sodium dithionite between two equilibration steps of Wash Buffer. Binding of the enzyme to the column took place for 2 h on ice, while horizontally laying and being gently shaken every 30 min. For enzyme assays the elution fractions 1 – 2, 1 ml each, were united.

2.2.13 Sodium dodecyl sulfate polyacrylamide gel electrophoresis (SDS-PAGE)

3 μl of flow through and wash and 20 μl of the elution fractions were loaded on an SDS-PAGE (Mini-PROTEAN® TGX™ Precast Gels; <https://www.bio-rad.com/>). Before loading on the gel each fraction was denatured together with $4 \times$ Laemmli sample buffer (Bio-Rad Laboratories) for 2 min at 105°C . 3 μl of Page Ruler™ Plus Prestained Protein Ladder (ThermoFisher Scientific; Waltham, Massachusetts, USA) were used. The electrophoresis run at 150 V for about 1 h. SDS running buffer, coomassie staining and destaining solution are listed in 2.1.1.5. Pictures were taken by Intas Gel Stick IMAGER (Intas Science Imaging Instruments GmbH).

2.2.14 Determination of protein concentration

Protein concentrations were determined by Bradford Assay using the Quick Start™ Bradford Protein Assay kit (BioRad Laboratories GmbH). A calibration curve was prepared with Bovine Serum Albumin (BSA) standards.

2.2.15 Anaerobic enzyme assays

All enzyme assays were performed in the glove box in a total volume of 200 μ l. The components are listed in Table 15.

Table 15: Components of anaerobic enzyme assays

Component	Final concentration/amount
HMBDP	From 2.5 – 100 μ M
Methyl viologen	1 mM (2 μ l of 100 mM stock)
Sodium dithionite	3 mM (3 μ l of 200 mM stock)
Recombinant HDR	0.5 μ g
MES/HEPES/CHES buffer	100 μ l
ddH ₂ O	to 200 μ l

For temperature and pH-Optimization temperatures ranging from 8 - 50°C and pH ranging from 3.5 to 9.5 were chosen. The reaction took place at 30°C (for pH optimization), for 30 min with 50 μ M HMBDP. The setup for the enzyme assays was based on Gräwert et al (2009) and Shin et al (2015, 2017).

All reactions were stopped by adding 100 μ l chloroform and vortexing. The samples were centrifuged for 5 min, at 4°C and 20.000 rpm. Depending on the analytical method the upper aqueous phase was either directly transferred to a 1.5 ml LC-MS vial with a 200 μ l inlet (for 2.2.17.1) or diluted 1:1 with MeOH and after vortexing transferred to a LC-MS vial (for 2.2.17.2). Samples were stored at -20°C until analysis was performed. For long term storage a temperature of -80°C was used.

2.2.16 Calibration curve for DMADP, IDP and HMBDP quantification

For quantification of DMADP, IDP and HMBDP samples for a calibration curve were prepared as in Table 15 without enzyme. The amount of DMADP plus IDP was the same as the amount of HMBDP. Concentrations reached from 100 μ M to 1,5625 μ M.

2.2.17 Analytical methods

Two different analytical methods were used. The method described in 2.2.17.1 used a hydrophilic interaction liquid chromatography (HILIC) column and was applied for assay optimization and enzyme kinetics. The two isomers DMADP and IDP could not be separated by the column. The method described in 2.2.17.2 which utilizes a chiral cyclodextrin column can separate the two isomers and therefore was used for determination of the DMADP/IDP ratio.

An Agilent 1260 HPLC system coupled to an API 5000 triple quadrupole mass spectrometer (AB Sciex Instruments), with an electrospray ionization source in negative mode, was used for both methods. The ion spray voltage was at -4200 V (-4500 V for method 2.2.17.1) and ion source temperature at 700°C. Nebulizer, heating and curtain gas were set at 70, 60 (30) and 30 pounds per square inch (psi) respectively. All gases were nitrogen. Declustering potential (DP) was -45.0 V and collision energy (CE) -24.0 V. The detected ions had the m/z ratio 244.922 as precursor ion and 78.900 as product ion for DMADP and IDP and correspondingly 260.930 and 78.900 for HMBDP. 78.900 is the [phosphate-H]⁻ fragment (see chapter 4.2 in González-Cabanelas et al. (2016), Krause et al. (2020)).

2.2.17.1 Quantification of HMBDP and IDP+DMADP with XBridge BEH Amide column

Quantification of HMBDP and IDP+DMADP was performed according to the method described in González-Cabanelas et al. (2016) chapter 4.

The method was established to analyse all intermediates of the MEP-pathway. Those metabolites highly polar compounds due to their phosphate-groups. They interact with the polar aqueous layer which covers a polar stationary phase. In the hydrophilic interaction liquid chromatography (HILIC) the organic mobile phase increases in the amount of water over the run and with that the polar compounds elute. (González-Cabanelas et al., 2016)

XBridge BEH Amide XP Column (2.5 µm, 150×2.1 mm; Waters) was used together with a guard column and a precolumn filter. The injected volume was 5 µl, the flow rate was 0.5 ml/min, total runtime was 30 min and the separation took place at 25°C. The organic mobile phase contained two different solvents. Solvent A was 20 mM ammonium bicarbonate and solvent B 80% acetonitrile with 20 mM ammonium bicarbonate. Ammonium bicarbonate was adjusted to pH 10.5 with ammonium hydroxide before use. The solvent gradient profile is listed in Table 16.

Table 16: Solvent gradient profile for separation of MEP-pathway metabolites with XBridge BEH Amide XP Column

Time (min)	% Solvent A	% Solvent B
0	0	100
5	16	84
11	40	60
15.10	0	100

Elution occurred in the first ten minutes (retention time: DMADP and IDP ~ 7.5 min, HMBDP ~ 8.8 min), followed by washing for 5 minutes and column equilibration for 15 min. (see chapter 4.1 in González-Cabanelas et al. (2016))

2.2.17.2 Separation of DMADP and IDP with Astec® Cyclobond® I 2000 column

Analysis of DMADP and IDP was performed according to the method described in Krause et al. (2020) chapter 2.4.

A Astec® Cyclobond® I 2000 column (4.6 mm × 250 mm, 5 µm; Supelco) was used. The injected volume was 5 µl, the flow rate was 1 ml/min, total runtime was 47 min and the separation took place at 20°C. The mobile phase was constituted of solvent A with 50 mM ammonium acetate (pH 6.5) and solvent B with acetonitrile. The solvent gradient profile is listed in Table 17.

Table 17: Solvent gradient profile for separation of DMADP and IDP with Astec® Cyclobond® I 2000 column

Time (min)	% Solvent A	% Solvent B
0	20	80
15-30	Increase to 60	Decrease to 40
37	20	80

Elution of DMADP, IDP and HMBDP occurred in minute 30-37.

3 Results and Discussion

The molecular basis and sequence analysis of *HDR* genes will be described in this first chapter, before presenting the experimental setup (see chapter 3.2), the biochemical results (s. chapter 3.3) and the results on the IDP/DMADP ratio (s. chapter 3.4).

3.1 The genetic and molecular level of putative 1-hydroxy-2-methyl-2-(*E*)-butenyl 4-diphosphate reductases (HDRs)

3.1.1 Evolutionary aspects

Full genome sequences of *Populus trichocarpa* and *Picea abies* are available in the databases popgenie.org and congenie.org. The *P. trichocarpa* genome has been used as a template for *Populus × canescens*. Previous database searches have identified two putative *HDR* genes for both *P. abies* and *P. canescens*. Together with putative *HDR* sequences from *Ginkgo biloba* (Kang et al., 2013), *Picea sitchensis* (Bongers et al., 2020), *Pinus taeda* (Kim et al., 2008), *Pinus densiflora* (Kim et al., 2009) and *Arabidopsis thaliana* (Hsieh et al., 2014) a phylogenetic tree has been built with MegAlign Pro (see Figure 8).

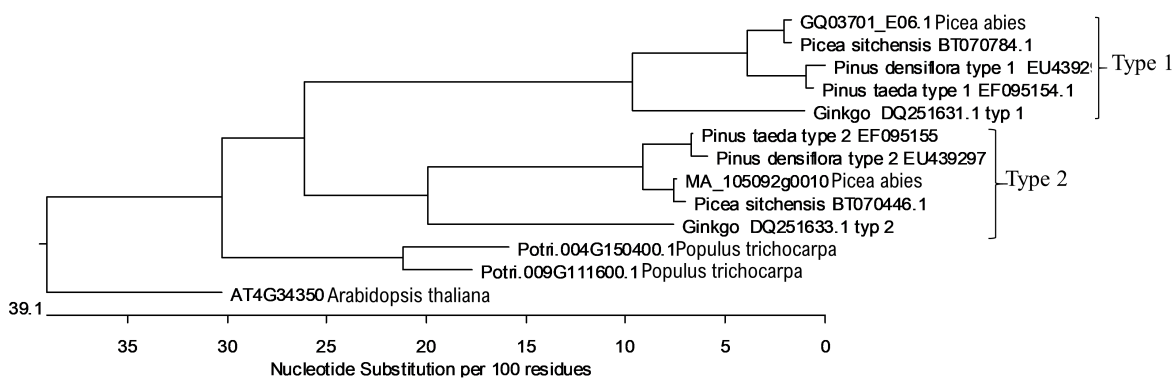


Figure 8: Phylogenetic tree of putative *HDR* genes from *Arabidopsis thaliana* (AT), *Populus trichocarpa* (Potri), *Ginkgo biloba* (Ginkgo), *Picea sitchensis*, *Picea abies* (MA and GQ), *Pinus taeda* and *Pinus densiflora*

The HDRs from gymnosperms divided into two clades, type 1 and type 2. Based on findings from *G. biloba* (Xiao et al.) (Kang et al., 2013) and their allocation in the phylogenetic tree, the putative *HDRs* from *P. abies* are named HDR1 and HDR2 respectively. Based on expression levels in various tissues, Kang et al. described that *GbHDR1* is related to housekeeping, whereas *GbHDR2* seems to be part of the secondary metabolism. Expression data from *P. abies HDR1* and *HDR2* have been presented in chapter 1 Figure 7. The data

shows that the two HDRs, *HDR1* and *HDR2*, are expressed at a similar level. Whether they are related to primary or secondary metabolism, has to be proven by more detailed expression analysis and investigation *in planta*. Therefore, the designations 1 and 2 are based solely on the phylogenetic analysis. *PaHDR1* and *PaHDR2* have an identity of 67% with the transit peptide. The truncated versions lacking the transit peptide have an identity of 75%. The putative transit peptide will be further explained in chapter 3.1.4.

The putative *HDRs* from the angiosperms *A. thaliana* and *P. trichocarpa* are not part of the two clades of gymnosperms in the phylogenetic tree. Transcriptome analysis had also revealed two putative *HDRs* for *P. trichocarpa*. As they are not assigned to the two clades, they are not named *HDR1* and *HDR2*, but Potri.004G150400.1 (Potri400) and Potri.009G111600.1 (Potri600) as they are named in the database. Furthermore, expression analysis (performed by Toni Krause and Marion Stäger at the MPI for Chemical Ecology, Jena) of the two *P. canescens* putative *HDR* genes via RT-qPCR showed about 300-fold higher expression of the corresponding Potri600 compared to Potri400 (see Figure 7). Comparable levels were obtained by transcriptomic data analysis (unpublished data, information given by Tobias Köllner, MPI CE Jena). The ortholog gene to Potri600 from *P. canescens* is named *PcHDR*. Potri600 and *PcHDR* have an 88% amino acid sequence identity and an 89% identity, if they lack the transit peptide. In this thesis only *PcHDR* (based on Potri600) is considered for genetic analysis and enzymatic characterization, as Potri400 (and so does the ortholog from *P. canescens*) is assumed to play a neglectable role in the plant's isoprenoid biosynthesis.

In their paper on *HDR* isoforms in melon (*Cucumis melo* L.), Saladié et al. compared about 30 different plant species in a phylogenetic tree. Based on this analysis, they formulated two hypotheses on gene duplication events. Firstly, they suggested that the *HDR* isoforms of *P. trichocarpa*, as well as from various other angiosperms, had evolved in a recent whole-genome duplication event (Saladié et al., 2014). In contrast to the angiosperms, similarity between the gymnosperm *HDRs* is higher within a clade than between paralogous pairs of one species (Saladié et al., 2014) (see Figure 8). Secondly, Saladié et al. assume that *HDR* isoforms in gymnosperms as well as cucurbits evolved in ancient individual gene duplication events, as the species lack polyploidy or partial genome duplications.

However, besides investigation on phylogeny, *in planta* studies could lead to a better understanding of the function of the two isoforms for plants.

3.1.2 Sequencing results

After categorizing *PcHDR*, *PaHDR1* and *PaHDR2* through phylogenetic analysis, the putative genes were cloned from fresh leaves and needles. The cloned sequences were checked by sequencing. The DNA as well as the amino acid sequences are listed in the appendix in the chapter 6.4.2. An alignment of these amino acid sequences and the corresponding orthologues from the databases is shown in Figure 9. Conserved regions are colored grey. Amino acids highlighted within the black frames are highly conserved and will be described in the following chapter 3.1.3. The putative transit peptides will be discussed in chapter 3.1.4. This section will focus on a short characterization and discussion of the sequences' general properties.

The cloned sequences from putative *P. abies* HDRs were identical to the Norway spruce sequences from the congenie database. Including the transit peptide, both putative *PaHDR1* and *PaHDR2* have a peptide sequence length of 486 amino acids and inherit the highly conserved amino acids.

Putative *PcHDR2* is 461 amino acids long and shares the highly conserved positions. Cloning of the putative HDR vof *P. canescens* from one cDNA template resulted in a few small mutations of the DNA sequence in multiple clones, which also led to changes in the amino acid sequence. The *HDR* from 18 different clones was sequenced and 10 variants were found. Throughout these variants six amino acids positions were mutated (positions 63, 223, 253, 360, 385 and 454, counted from +T without gap). None of these amino acids are placed in the transit peptide region and none of them were assumed to be essential for the enzyme activity according to Hsieh et al (2014). It requires further investigation to clarify how the variations of the gene could occur. As there were too many point mutations in the sequence to test all variants, one was expressed and its activity was tested. This variant was used for further optimization and for kinetics. We assume that there are no significant differences in activity among all other variants, as no highly conserved amino acids are affected. However, a second variant was tested as the sequence of the construct with the transit peptide (*PcHDR*+T) differed in four amino acids from the sequence of *PcHDR*-T. Both sequences are listed in the appendix in chapter 6.4.1. The -T version was used for the alignments shown in Figure 9 and Figure 25.

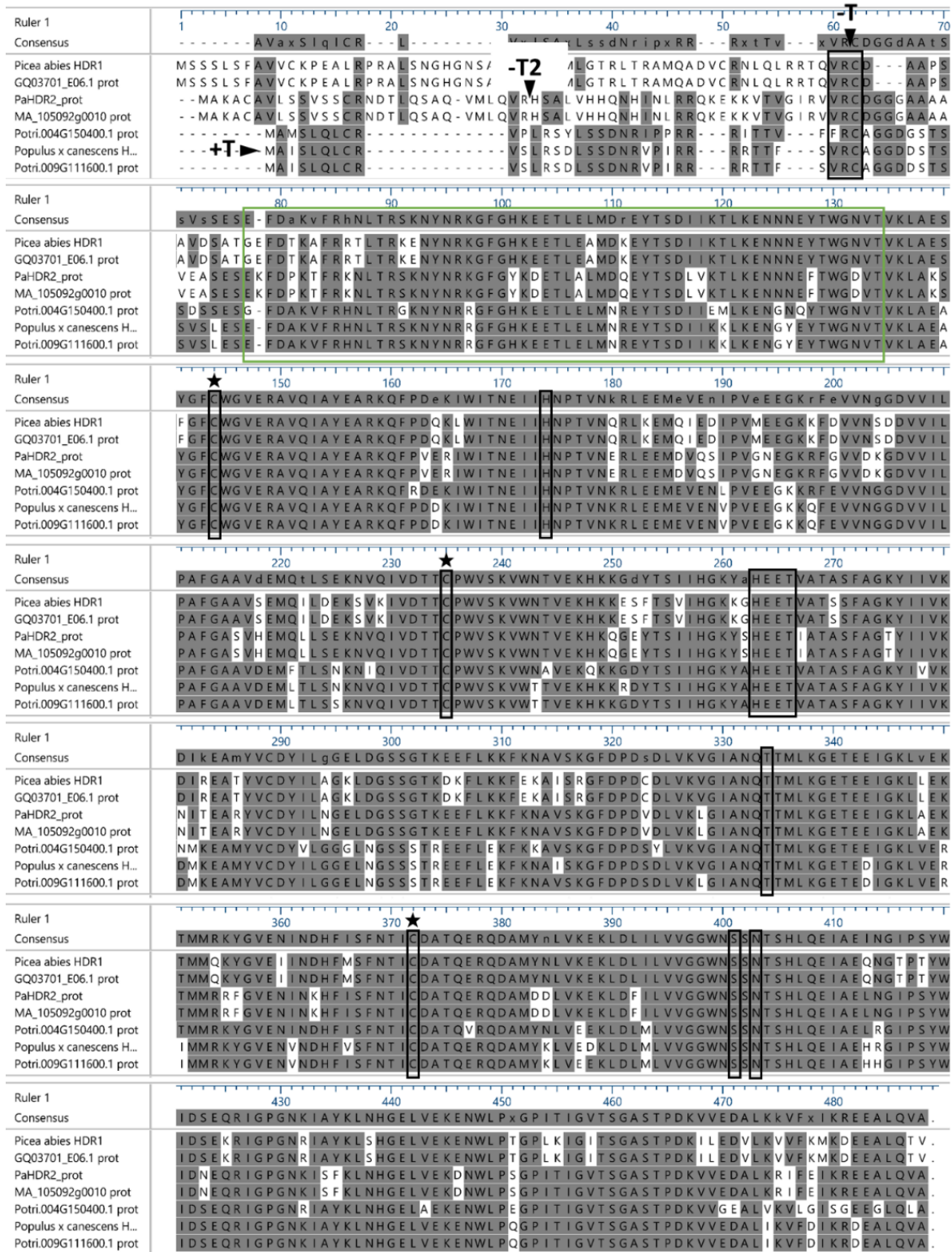


Figure 9: Alignment of HDR peptide sequences from *P. abies*, *P. canadensis* and *P. trichocarpa*; *P. abies* HDR1 (sequenced in this project), *P. abies* (GQ03701_E06.1 prot, identical to the previous sequence), *P. abies* (PaHDR2_prot, sequenced in this project), *P. abies* (MA_105092g0010 prot, identical to the previous sequence), *P. trichocarpa* Potri.004G150400.1 prot, *P. canadensis* HDR2 (sequenced in this project), *P. trichocarpa* Potri.009G111600.1 prot (identical to the previous sequence); aligned with MegAlign Pro ClustalW (GONNET); T: putative transit peptide, star: highly conserved cysteine residues, arrow: transit peptide end, black frames: other highly conserved amino acids relevant for substrate binding or reaction mechanism, green frame: N-terminal region conserved in photosynthetic organisms

3.1.3 Conserved amino acids and motifs – predictions on the iron-sulfur-cluster and binding pocket

In the following section, conserved motifs and amino acids, which could be critical for the enzymes' activity and are associated to the putative iron-sulfur cluster, will be discussed. Firstly, it has to be mentioned that all assumptions made in this chapter are based on bioinformatic analyses, namely alignments and 3D-structure predictions. To our best knowledge HDR1 from *G. biloba* is the only HDR from plants that has been characterized as recombinant enzyme *in vitro* in an oxygen-free environment (Shin et al., 2015). Other putative HDRs, to be found in the alignment Figure 25, were tested for their activity by complementation assays in the literature.

The amino acid sequence alignments in Figure 9 are supported by a larger alignment in the appendix (see Figure 25). The alignments show that the three cystein residues, which coordinate three of the four irons in the cluster (Gräwert et al., 2004), are conserved also in *PcHDR*, *PaHDR1* and *PaHDR2*. Apart from these three cystein residues, Hsieh et al. (2014) revealed further conserved amino acids that are supposed to play a role in substrate binding and catalysis in the HDR from *A. thaliana*. As illustrated in the alignments, they are conserved in *P. canescens*, *P. abies* and *E. coli* HDRs as well. Regarding the catalytic mechanism, E126 (from *E. coli*) is predicted to be the first proton donor to release water with the hydroxyl group (scheme see Figure 6). This glutamate is highly conserved (see HEET motive). This provides further evidence for the hypothesis, that the mechanism could be the same, or similar, in plants.

To support this theory a 3D-protein model prediction was made by the bioinformatic database SWISS-MODEL-Expasy. This database predicts 3D-structures of proteins based on the given amino acid sequence and on available X-ray crystallographic data. *PcHDR-T*, *PaHDR1-T* and *PaHDR2-T* were predicted with this tool and are presented in Figure 10, while the characteristic values for the homology modelling are listed in the appendix in Table 21 and Table 22. Although the expected accuracy (GMQE value) and quality of the model (QMEAN value) are rather low and the sequence identity lies between 26 and 29%, all three target sequences were predicted to have similar tertiary structures to the HDR of *E. coli*. These similarities are visualized in Figure 10. A magnification of the catalytic centre is shown there, too. The three conserved cysteine residues are coloured yellow. They are in spatial proximity to each other and could coordinate an $[4\text{Fe-4S}]^{2+}$ cluster (Span et al., 2012), such as in Figure 10 a).

However, this visual evaluation is only a first step. In order to be able to make more precise predictions, *in silico* analysis has to be performed in the future. To prove whether the same amino acids, as proposed by Hsieh et al. (2014), are part of the active site and essential for enzyme activity, site directed mutagenesis and activity tests could be carried out in future experiments. Other tests, that should be carried out, concern the iron-sulfur cluster, as the assumption is only based on sequence alignments. Various approaches are possible to determine, whether the HDR from *P. canescens* and *P. abies* also inherits a $[4\text{Fe-4S}]^{2+}$ cluster. One test would be to determine the absorption of a Fe^{2+} -ferene complex at 532 nm (Shin et al., 2015). UV/VIS spectra of the purified enzyme incorporating iron show a characteristic shoulder at 410 nm (Wolff et al., 2003). Other analytical methods would be elemental analysis (Brumby and Massey, 1967), EPR spectroscopy (Wolff et al., 2003) or even *in vivo* Mössbauer-Spectroscopy (Seemann et al., 2009).

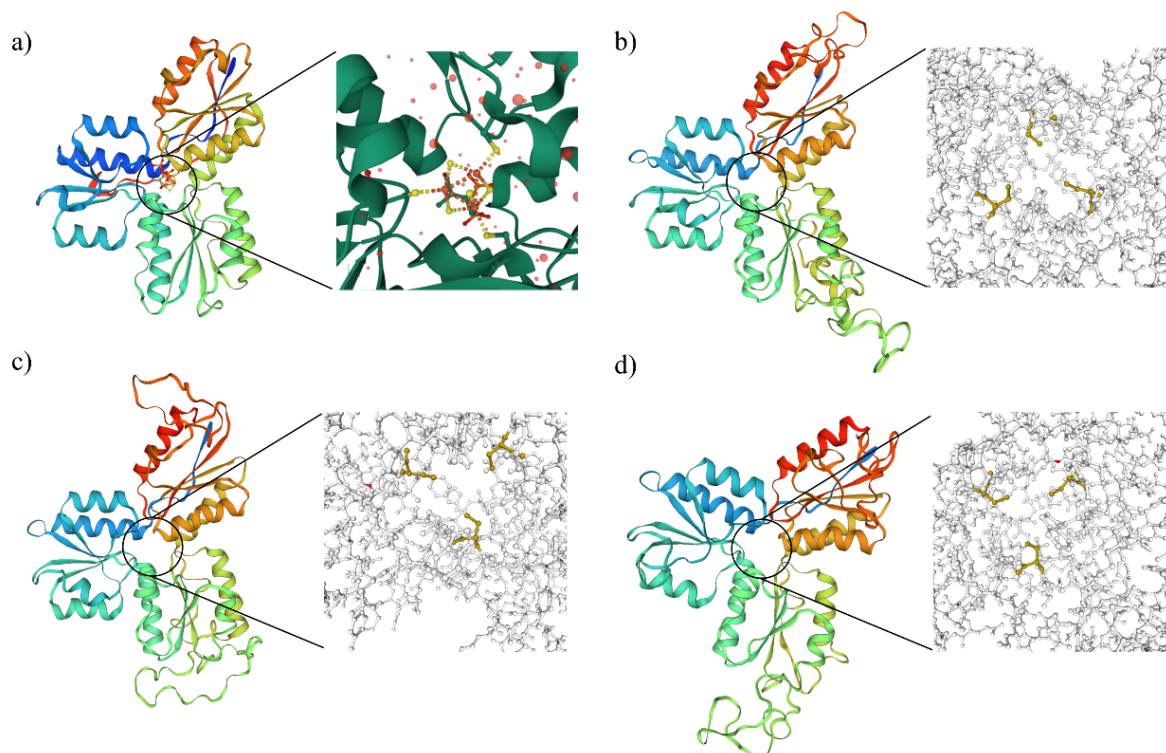


Figure 10: 3D models of the HDRs from *E. coli*, *Populus × canescens* and *Picea abies* (models made by SWISS-MODEL Expasy); a) *E. coli* HDR based on X-ray crystallographic data from the PDB database (PDB code: 3SZU) (Span et al., 2012), zoom-in shows $[4\text{Fe-4S}]^{2+}$ cluster coordinated by 3 cystein residues; b) *P. canescens* HDR-T based on homology modelling, c) *P. abies* HDR1-T based on homology modelling, d) *P. abies* HDR2-T based on homology modelling; zoom-ins show 3 yellow cystein residues which could coordinate an $[4\text{Fe-4S}]^{2+}$ cluster

We assume that a reaction mechanism in the catalytic centre is similar to the mechanism in *E. coli* (Chaignon et al., 2020). Based on this assumption, we can start thinking about the source of the electrons for the reaction. This question has been addressed for plants only by *in silico* docking models. Such a docking model was published by Johnson et al. in 2017. They performed docking analysis with a ferredoxin (Fd) and ferredoxin-NADP⁺ reductase (FNR) and concluded that the HDR from *Mentha × piperita* could be reduced by this pair (Johnson et al., 2017). The model is depicted in Figure 11. By *in silico* docking analysis or *in vitro* assays it could be proven whether the redox system Fd-FNR could be the electron donor for *PcHDR*, *PaHDR1* and *PaHDR2*, too.

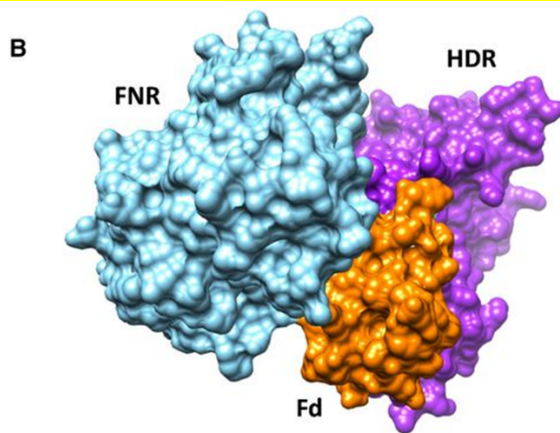


Figure 11: *In silico* docking model of ferredoxin (Fd) and ferredoxin-NADP⁺ reductase (FNR) with HDR from *Mentha × piperita* (adapted figure from Johnson et al., 2017)

Hsieh et al. (2014) suggested that – besides the highly conserved cysteines, which could bind an iron-sulfur cluster in plant HDRs – all HDRs from oxygen-evolving photosynthetic organisms have a conserved N-terminal domain located following the transit peptide. This domain seems to be essential for their functioning and is also present in *P. canescens* and *P. abies* HDRs (highlighted with a green frame in the alignment Figure 9 and Figure 25).

3.1.4 The transit peptide

When the cloning and heterologous expression was planned, the question arose whether the expression host *E. coli* could deal with the transit peptide or would on the contrary hinder the bacterium to express a functional enzyme. To solve this problem, we designed one construct of the *P. canescens* HDR with the transit peptide (for sequence of +T see appendix chapter 6.4.1.2). Expression and enzyme assay results of *PcHDR*+T are illustrated in chapter 3.3.1 and 3.3.3.

However, the aim was to characterize the enzyme's activity in its natural conformation in the chloroplast. Usually transit peptides, which transport the protein to the chloroplast, are truncated (Richter and Lamppa, 2002). We assume this applies to the HDR, too. Therefore, we had to decide where the putative transit peptide ends and had to design constructs without it. Predictions were performed by the ChloroP database (data see appendix Table 20) (Emanuelsson et al., 1999). The predictions for the putative *PcHDR* and *PaHDR1* gene were unequivocal and are shown in Figure 9 (see -T). The cleavage site was determined to be at the motif "VRC" between the arginine and the cysteine. The alignment shown in Figure 9 as well as the alignment with putative HDRs of other gymnosperms confirmed this conserved motif (see appendix Figure 25) and so do two publications (Huang et al., 2009; Hsieh et al., 2014). Even though the putative *PaHDR2* gene also contains this motif the prediction was equivocal. ChloroP predicted that it would not have any transit peptide or if any then at a "VRH" motive between arginine and histidine (see Figure 9 "-T2"). Due to this ambiguous prediction, two different constructs with transit peptide cleavage at both options (-T and -T2), were designed. Expression and enzyme assay results of *PaHDR-T2* are shown in chapter 3.3.1 and 3.3.3. However, only the construct *PaHDR2-T* was chosen for kinetic analysis, to be comparable with *PcHDR-T* and *PaHDR1-T*. Sequences of the constructs are listed in the appendix in 6.4.

As the "VRC" motif is conserved in all the putative HDRs (*P. canescens* and *P. abies*) analysed here, we assume that the transit peptide cleavage site is the same for all three. Optimization and kinetic analyses were performed only with the constructs containing the transit peptide cleaved at this conserved site (-T).

3.2 Establishing the experimental setup

To our best knowledge the only HDR from plants characterized *in vitro* as recombinant enzyme is from *G. biloba* (Shin et al., 2015; Shin et al., 2017). Indications from their experimental procedure together with literature from *E. coli* HDR (Gräwert et al., 2009) and the evidence gained from pre-tests led to the final experimental setup. The procedure which led to the final protocol is described here.

3.2.1 Setup of the glove box

Before setting up the glove box a pre-test had been performed. The test included the heterologous expression of all three putative HDR constructs in *E. coli* BL21AI and enzyme purification in standard laboratory air conditions. The enzyme could be visualized on an SDS-PAGE (corresponding to what is depicted in Figure 14, Figure 15 and Figure 16), but no enzyme activity could be detected. When enzyme purification and assays were conducted under anaerobic conditions in the glove box, an oxygen-sensitivity control (see Figure 13) was performed. After taking the enzyme out of the glove box, it was exposed to the environmental oxygen and only at that point in time the substrate was added. No products (IDP and DMADP) could be detected in this enzyme assay. The lacking activity when the HDR comes into contact with oxygen and the previously depicted highly conserved cysteine residues, lead us to the conclusion, that the three HDRs we analysed are oxygen-sensitive such as the HDR from *E. coli* (Gräwert et al., 2004).

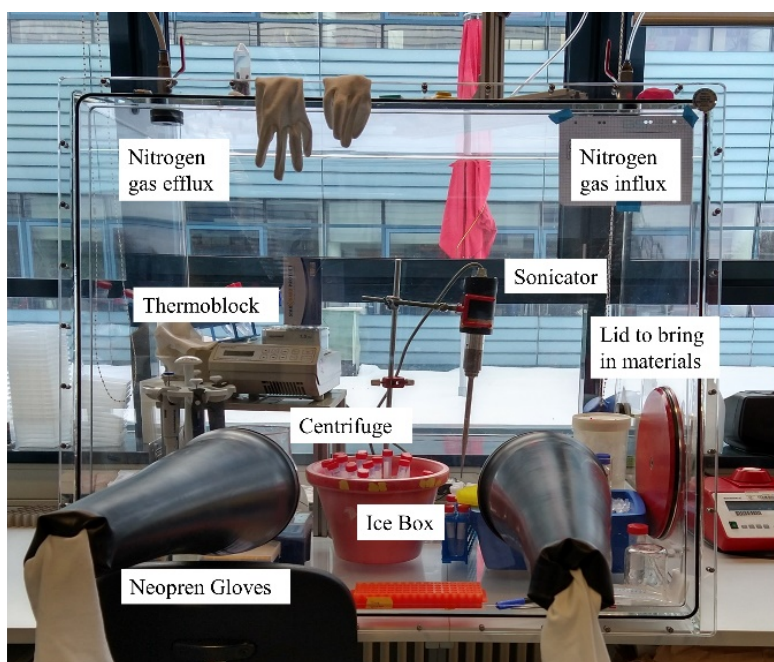


Figure 12: Experimental setup in the glove box

As mentioned previously, purification and enzyme assays carried out at standard laboratory conditions did not lead to any activity. Therefore, an oxygen-free environment had to be provided. A P10 R0 T2 glove box from GS GLOVEBOX Systemtechnik GmbH was kindly supplied by the MPI for Biogeochemistry (Jena). The experimental procedure was then established in the glove box, where experiments were carried out at ~1% O₂. The setup is illustrated in Figure 12.

When working in an oxygen-free environment it is critical to degas all buffers and free the purification column from oxygen. Furthermore, all consumable materials, such as pipet tips and tubes should either be filled with argon to oust oxygen, or must stay in the glove box in nitrogen atmosphere for at least one day.

However, it has to be mentioned here that it usually is other types of glove boxes that are used for enzymatic experiments, such as the so called Coy glove boxes. In the Coy glove box the atmosphere there is controlled N₂/H₂ (95%/5%) and residual oxygen is removed, for example, with a palladium catalyst (Rekittke et al., 2008; Gräwert et al., 2009). They also incorporate a floodgate. The glove box P10 R0 T2 was designed for person's protection, whereas Coy boxes are for product protection. Working conditions are more difficult and less controllable without a floodgate as oxygen flows in when opening the gate. Therefore, a constant nitrogen flow has to be guaranteed, to oust the remaining oxygen. However, this unusual setup leads to some interesting new questions: First, is there any remaining oxygen (in the ppm range) in the glove box and in the buffers? If there is, how can the plant's enzymes cope with it and at which oxygen limit is the activity completely lost? Hsieh et al. suggested that the N-terminal domain (NCD), which is conserved throughout oxygen-evolving photosynthetic organisms, could protect the HDR from high oxygen concentrations (Hsieh and Hsieh, 2015). To address these questions, experimental setups could be designed with controlled varying oxygen concentrations in the buffers and in the glove box. Furthermore, a construct without NCD could be prepared and tested in parallel to a full construct at those different oxygen levels.

3.2.2 Establishing the protocol

According to Gräwert et al. (2004) ferric ammonium citrate and L-cysteine were added to the expression culture to ensure that *E. coli* would have enough raw material to correctly synthesize the enzyme and inorganic cluster. Other research groups (Rekittke et al., 2008; Shin et al., 2015) regenerated the cluster after the purification. As the enzymes showed activity, a re-assembly seemed not to be necessary. However, we could not prove, if all enzymes had a fully assembled functional iron-sulfur cluster, or if *E. coli* could not guarantee this status.

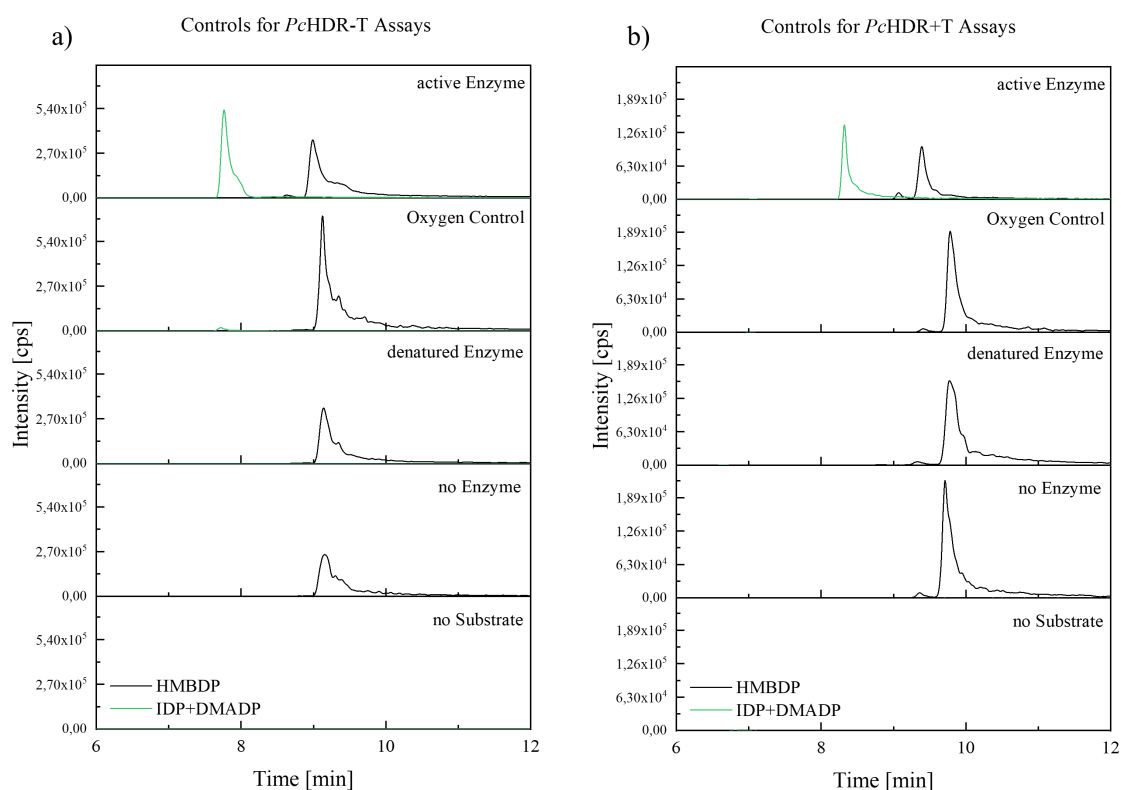
Various test runs were performed to establish a working protocol. Time and temperature of culturing conditions were tested. Yields of ~50 µg/ml purified protein, which were needed to perform kinetic assays, were achieved either by growing precultures for two nights at 25°C or by growing them for three nights at 18°C. To achieve such yields, two flasks each with 100 ml of induction culture had to be set on. They were kept at 18°C for one night. Induction of the T7 promotor by 2% L-arabinose led to the highest protein yields compared to induction with the Novagen® Overnight Express™ autoinduction medium or isopropyl β-d-1-thiogalactopyranoside (IPTG). Buffers were degassed from O₂ by flushing them for 1 h with nitrogen gas.

Initially a MOPSO buffer (pH 7.8) was used, but in order to be able to test a wide range of pH values the three-component buffer MES/HEPES/CHES was established according to Shin et al. (2015). Magnesium chloride was added to the buffer. We assumed that the HDR is in need of Mg²⁺ for its activity, as this divalent cation is an essential cofactor for other enzymes of isoprenoid biosynthesis, for instance the isopentenyl diphosphate isomerase (IDI) (Agranoff et al., 1960) and the isoprenyl diphosphate synthase (Nystedt et al.) (Chen et al., 2011). Magnesium is involved in binding the diphosphate groups to the IDS during catalysis (Tarshis et al., 1996).

Fd-FNR was previously mentioned to be assumed to be the *in planta* redox system donating electrons for the reaction catalysed by the HDR. However, for *in vitro* studies in this thesis, the redox system constituted from methyl viologen and sodium dithionite was used. This redox system was predominantly found in the literature.

Before performing pH and temperature optimization as well as kinetic studies on PcHDR-T, PaHDR1-T and PaHDR2-T, all constructs, including PcHDR+T and PaHDR2-T2, were tested for their activity. Enzyme and substrate concentrations and the reaction time were varied to determine conditions that yield the proper amounts of products which can be

analysed via LC-MS/MS. The development process is not described here in detail, but controls for each construct are shown in Figure 13. As can be seen there, no IDP+DMADP was produced in the negative controls and only the substrate HMBDP was detected. It was also tested for which period the enzyme could be stored without losing its entire catalytic power. The storage conditions were the elution buffer (see 2.2.12.2), 4°C and a cautiously sealed tube to prevent oxygen to flow into the tube. After one day the enzyme suffered a major activity loss (see appendix Figure 28 a)). It is not known if residual oxygen in the buffer oxidized the [4Fe-4S]²⁺ cluster, or the protein denatured.



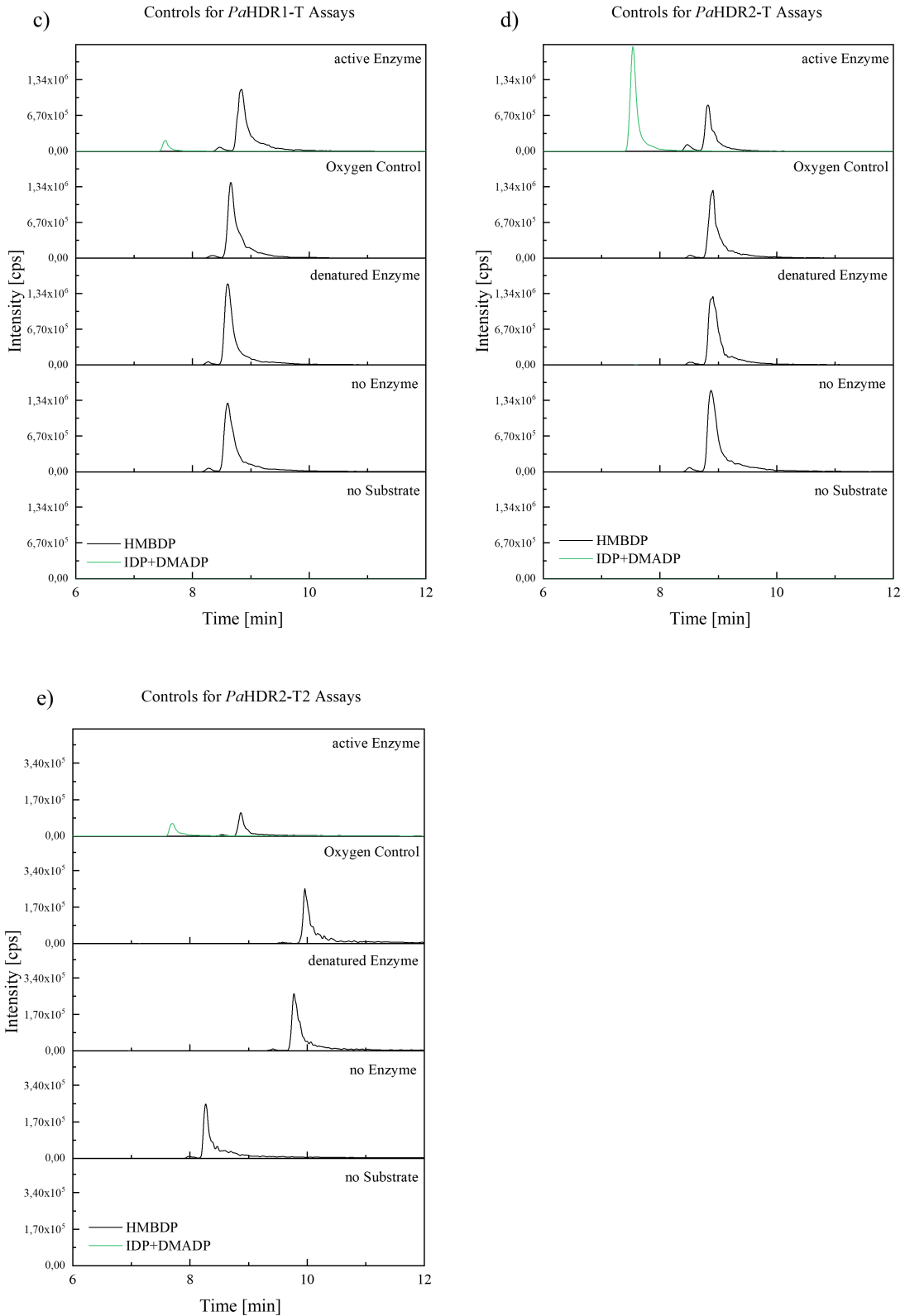


Figure 13: Chromatograms of controls for a) *PcHDR-T*, b) *PcHDR+T*, c) *PaHDR1-T*, d) *PaHDR2-T* and e) *PaHD2-T2*, assays measured with XBridge BEH Amide column; section of 6-12 min retention time; controls top down: active enzyme (positive control), oxygen control (negative control: enzyme was exposed to oxygen before adding HMBDP), denatured enzyme (negative control, enzyme was denatured at 95°C for 10 min), no enzyme (negative control), no substrate (negative control); retention time shifts are due to change of running buffers

3.3 Enzymatic characterization

3.3.1 Purification of HDR constructs

After expression of the glutathione S-transferase tagged (GST-tag) putative HDR genes in BL21AI *E. coli* cells, the proteins were purified via a glutathione column. The following fractions were collected: flow through (FT), three wash steps (W1-3) and three elution steps (E1-3) each 1 ml. All fractions were loaded on an SDS-PAGE to check for the right protein size and for purity of the fractions. Pictures of the SDS-PAGES are shown in Figure 14 to Figure 16.

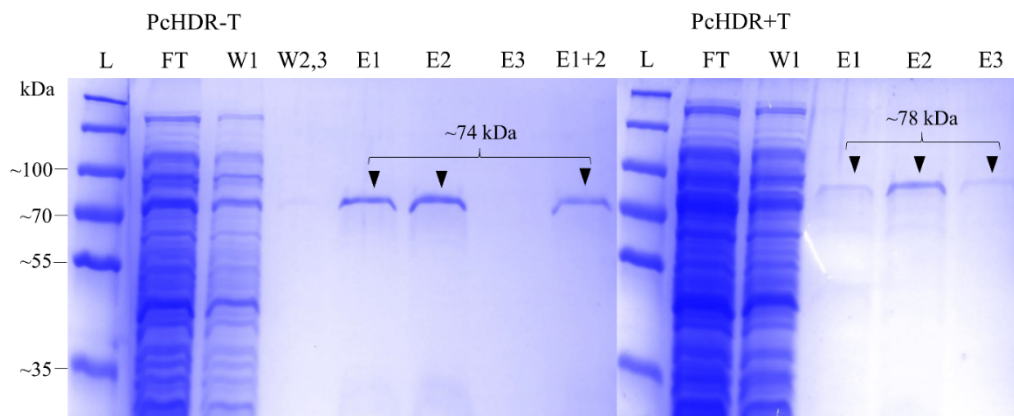


Figure 14: SDS-PAGE of *PcHDR-T*+GST-tag (~74 kDa) and *PcHDR+T*+GST-tag (~78 kDa), GST-tag ~26 kDa; kDa: Kilodalton, L: Page Ruler™ Plus Prestained Protein Ladder, FT: Flow through, W1-3: Wash fraction 1 to 3, E1-3: Elution fraction 1 to 3

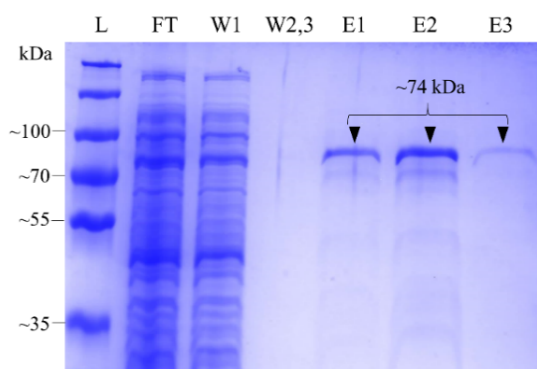


Figure 15: SDS-PAGE of *PaHDR1-T*+GST-tag (~74 kDa), GST-tag ~26 kDa; kDa: Kilodalton, L: Page Ruler™ Plus Prestained Protein Ladder, FT: Flow through, W1-3: Wash fraction 1 to 3, E1-3: Elution fraction 1 to 3

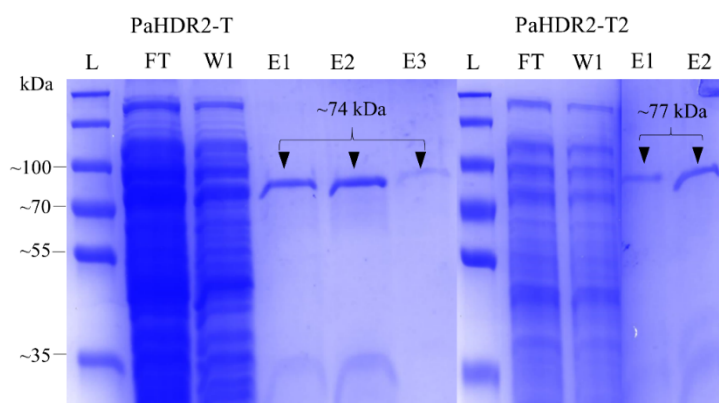


Figure 16: SDS-PAGE of *PaHDR2-T*+GST-tag (~74 kDa) and *PaHDR2-T2*+GST-tag (~77 kDa), GST-tag ~26 kDa; kDa: Kilodalton, L: Page Ruler™ Plus Prestained Protein Ladder, FT: Flow through, W1-3: Wash fraction 1 to 3, E1-3: Elution fraction 1 to 3

The molecular weight (MW) of all constructs was calculated with the ExPASy compute pI/Mw tool (https://web.expasy.org/compute_pi/) and the MWs are listed in the appendix in chapter 6.4. According to instructions from ThermoFisher Scientific (see 2.2.12.2) the purification of proteins via a GST-tag (~26 kDa) usually leads to a purity of more than 90%. In the elution fractions only one band is clearly visible, and it appears at the expected molecular weight. However, in the FT and W1 fraction a band of the same MW as the putative HDR appears. It suggests that some of the protein of interest did not fully bind to the column and was eluted already in those two fractions. The assumption is proved by enzyme assays performed with these two fractions which produce IDP and DMADP (see *PaHDR1-T* exemplary for all constructs in appendix Figure 28 b)). To improve binding of the GST-tag to the glutathione on the column, conditions such as the used buffer, the duration of the binding process and the rotation of the column during the process, should be optimized. The elution fractions 1 and 2 were combined for enzyme assays, as they showed the highest yield on the SDS-PAGE and in the Bradford Assay used for protein quantification. Although the GST-tag is rather large it did not hinder the HDRs in their activity. However, we do not know if the catalytic activity is somehow altered by the tag. To check this, the tag could be cleaved off by a protease.

3.3.2 Calibration curve

To determine the amount of the products, DMADP and IDP, a calibration curves was made (see Figure 17). The samples were measured with the XBridge BEH Amide column. With this curve, the concentrations of the products (DMADP+IDP) in the enzyme assays, were calculated.

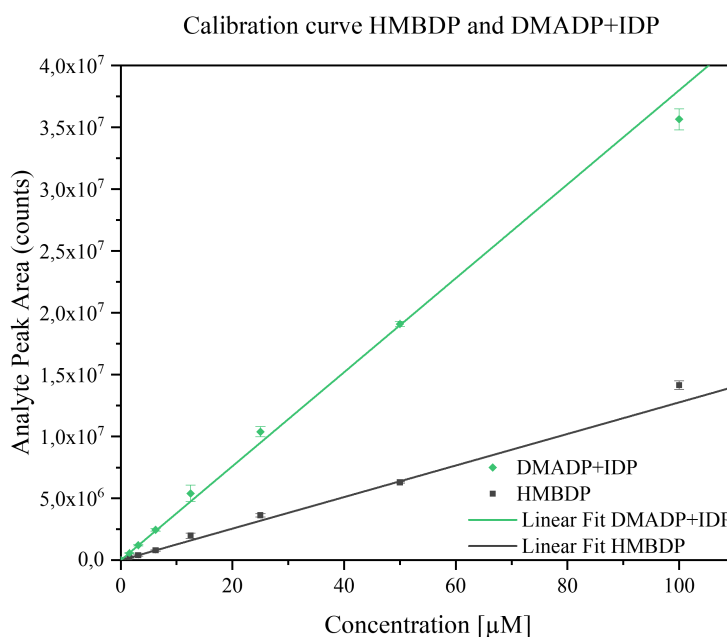


Figure 17: Calibration curve for HMBDP and IDP+DMADP (measured in triplicates); formula for the linear fit of IDP+DMADP: $y = (970.65 \pm 685.39) + (379955.29 \pm 5226.54) * x$, Pearson's r: 0.99; For HMBDP: $y = (1112.86 \pm 483.58) + (127606.70 \pm 2421.81) * x$, Pearson's r: 0.99

3.3.3 Activity profile of *Pc*HDR+T and *Pa*HDR2-T2

To address whether the putative transit peptide (explanation see chapter 3.1.4) influences *E. coli* BL21AI to express the putative HDR and whether this peptide hinders the enzyme in its activity, the two constructs *Pc*HDR+T and *Pa*HDR2-T2 were tested. Figure 14 and Figure 16 prove the correct expression of both. Based on this result the activity was tested.

Enzyme assays with 2.96 μg of *Pc*HDR+T and 10 μM HMBDP were performed at 30°C in MOPSO buffer (pH 7.8). At these conditions the product formation reaches saturation after about 20 min (see Figure 18 a)). For testing *Pa*HDR2-T2, assays with 2.41 μg enzyme and 10 μM HMBDP were performed at 30°C in MOPSO buffer (pH 7.8). Product saturation is achieved at about 25 min (see Figure 18 b)).

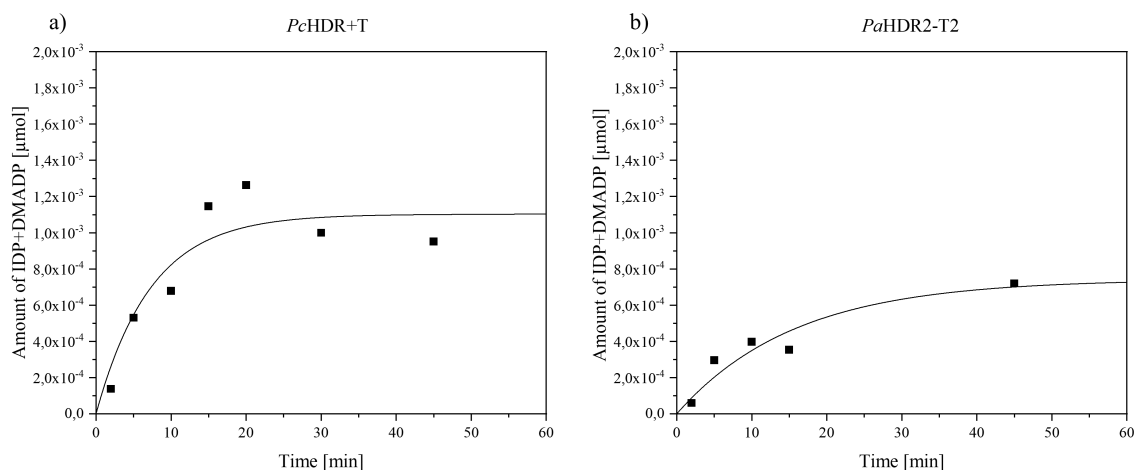


Figure 18: Assay to proof activity of *PcHDR+T* and *PaHDR2-T2*; amount of IDP+DMADP was measured, curve fitting was performed with OriginPro 2019, Model: BoxLucas1, Equation: $y = a * (1 - \exp(-b * x))$, product saturation was achieved; a) *PcHDR+T*: assay conditions: 2.96 µg enzyme, 10 µM HMBDP, MOPSO buffer pH 7.8, 30°C, b) *PaHDR2-T2*: assay conditions: 2.41 µg enzyme, 10 µM HMBDP, MOPSO buffer pH 7.8, 30°C

It has to be mentioned here, that the results only show that the constructs are active and that product saturation is achieved. The data sets cannot be compared with each other or with data sets from the other constructs, as the enzyme concentrations differ and the substrate concentration is not in the saturation range. To address whether the transit peptides alter the enzymes affinity to the substrate or catalytic activity, kinetic studies have to be performed. However, due to time constraints, this was not done in this thesis, and the characterization of the enzymes was only performed on truncated constructs lacking the transit peptide, as this is how it is usually present in the chloroplast (Richter and Lamppa, 2002). In conclusion, it can be said that HDR constructs including the transit peptide, or a variant of it, are expressed by *E. coli*. These constructs show activity and product saturation.

3.3.4 Optimization of reaction conditions for *PaHDRs* and *PcHDR*

The optimal reaction conditions for the enzyme had to be established, before performing kinetic studies, to determine the Michaelis-Menten constant K_M and the catalytic constant k_{cat} . Enzyme assays were performed at different pH and temperatures. Some enzymes also need cofactors, such as metal ions, for their activity. In the MEP pathway this is for instance the case for all enzymes beside HDS and HDR, which both have an iron-sulfur cluster (Frank and Groll, 2017). Apart from this bioorganometallic cluster, some cofactors were referred about in literature (Gräwert et al., 2004; Xiao et al., 2008) yet they had no positive effect on

the catalytic activity of the HDR. Therefore, apart from the previously mentioned Mg^{2+} , no additional metal ions were considered here.

3.3.4.1 pH optimization

The activity of *PcHDR-T*, *PaHDR1-T* and *PaHDR2-T* was tested at nine different pH levels ranging from pH 3.5 to pH 9.5 (see Figure 19). The buffer was a three-buffer system constituted from the sulfonic-acid derivatives MES, HEPES and CHES. All tests were performed for 30 min at 30°C with 0.5 μ g enzyme and 50 μ M HMBDP, which means at saturated conditions. Good activity was achieved in the range from pH 5.5 to 7.5 and optimum activity at pH 6-6.5. The highest amount of product was determined at pH 6.5 for all three HDRs. The pH dependent activity profiles are shown in Figure 19.

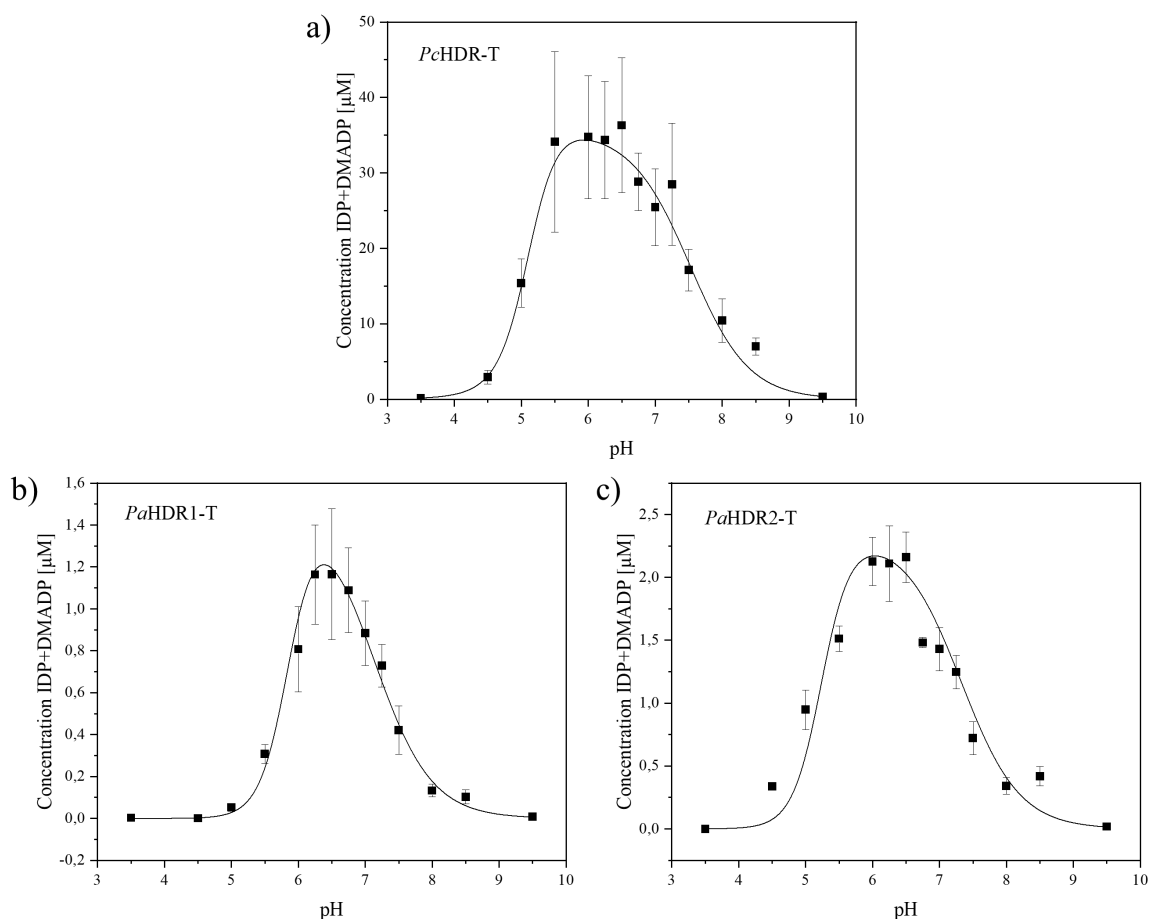


Figure 19: Activity profile of a) *PcHDR-T*, b) *PaHDR1-T* and c) *PaHDR2-T* at different pH values (MES/HEPES/CHES buffer), pH 3.5, 4.5, 5, 5.5, 6, 6.25, 6.5, 6.75, 7, 7.25, 7.5, 8, 8.5, 9.5; concentration of IPD+DMADP is measured; assay conditions: 0.5 μ g enzyme, 50 μ M HMBDP, 30 min, 30°C; highest activity at pH 6-6.5; curve fitting was performed with OriginPro 2019, Model: Bell_Shaped_With_Plateau, Equation: $V_{maxlim} * (\alpha + 10^{(pKb - x)}) / (1 + 10^{(pKa + pKb - 2 * x + 10^{(pKb - x + 10^{(x - pKc)})})})$

Shin et al. (2015) tested a pH range from 5 to 10 using the above mentioned three-buffer system, when characterizing HDR1 from *G. biloba*. The optimum enzyme activity was at pH 8. The pH at which the enzyme has its best activity usually reflects the localisation in the cell. In this work no experiments have been performed regarding the localisation of the HDR from *P. canescens* and *P. abies*. However, Hsieh et al. (2015) showed that the HDR from *A. thaliana* is located in the stroma of the chloroplast. Due to the reactions of the photosynthetic apparatus and the proton-gradient needed for adenosine triphosphate (ATP) synthesis, the ΔpH is about 2.5 higher in the stroma (pH ~7.5-8) than in the thylakoid inner space (pH ~5.5) (Heldt et al., 1973). Relying on the pH values in the compartments of the chloroplast, we would locate *PcHDR-T*, *PaHDR1-T* and *PaHDR2-T* in the thylakoid inner space. However, the data is in contrast to the pH optimum from the *G. biloba* HDR and localisation of *A. thaliana* HDR. To address this contradiction, further investigation have to be done. One approach to determine the localisation of the HDR would be to fuse a green-fluorescent protein to the HDR and localize it through microscopy (Hsieh and Goodman, 2005).

3.3.4.2 Temperature optimization

As for the pH, the enzyme activity at different temperatures was also tested to determine optimum conditions for enzyme kinetic studies. Six different temperatures, ranging from 25 to 45°C (5°C interval) were chosen. Assays were performed for 30 min at pH 6.5 with 0.5 μg enzyme and 50 μM HMBDP. The results are shown in Figure 20. Since the assays were performed first and served for the development of the conditions, the temperatures for the HDR from *P. canescens* differ from the ones chosen for the two HDRs from *P. abies*. However, we assume that the optimum temperature is still at about 35°C for all three HDRs. The overall activity was reduced in these experiments, as they were performed with enzymes which had been purified the previous day.

Shin et al. (2015) had also performed temperature-dependent activity assays with HDR from *G. biloba*. They measured activity between 0 and 50°C and the highest activity was detected at 50°C. No temperature optimum was described. Therefore, no direct comparison can be carried out with the data obtained here.

Kinetic studies for *PcHDR-T*, *PaHDR1-T* and *PaHDR2-T* were performed at 35°C.

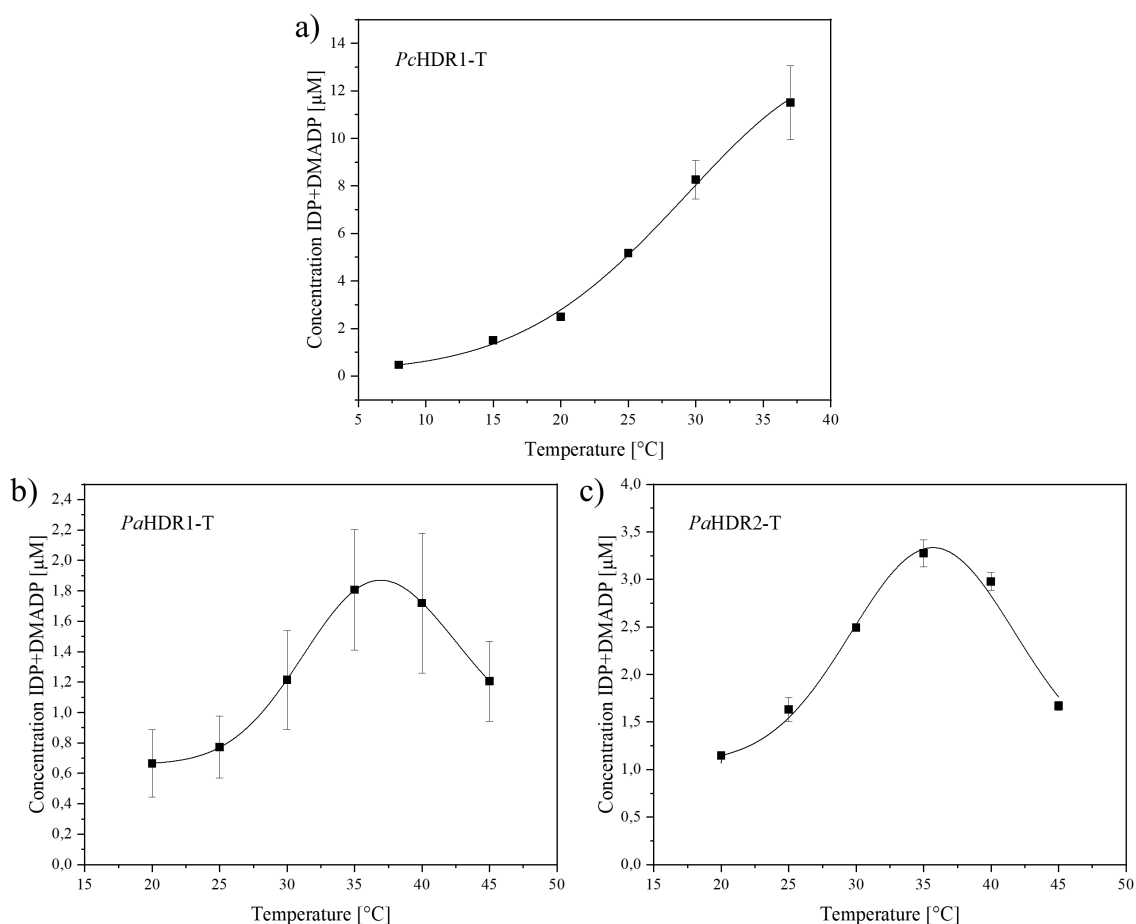


Figure 20: Activity profile of a) *PcHDR-T*, b) *PaHDR1-T* and c) *PaHDR2-T* at different temperatures; concentration of IPD+DMADP is measured, assay conditions: 0.5 μg enzyme, 50 μM HMBDP, 30 min, pH 6.5; highest activity at 35°C; curve fitting was performed with OriginPro 2019, Model: GaussMod, Equation: $double\ z = (x - xc)/w - w/t0$

3.3.5 Kinetic studies on the HDR – determination of K_M and k_{cat}

The Michaelis-Menten constant (K_M) and catalytic constant (k_{cat}) were determined; both characterize an enzyme in its affinity to a substrate and catalytic activity respectively. By definition the K_M is the concentration of substrate where the reaction speed is at half maximum ($v_{max}/2$). Therefore, the K_M is an index for the affinity of the enzyme to the substrate. If the K_M is low, the affinity to the substrate is high. The catalytic constant describes the amount of substrate which is converted to product in one minute by one enzyme. The catalytic efficiency is defined as k_{cat}/K_M .

To determine those two constants, the initial catalytic velocity of the enzyme had to be determined with different substrate concentrations. Therefore, the assay were stopped at five different points in time (at minute 5, 10, 15, 30 and 60). This was done for *PcHDR-T*, *PaHDR1-T* and *PaHDR2-T*. Substrate concentrations for *PcHDR-T* were 10, 25, 50, 75 and

100 μM and for *PaHDR1-T* and *PaHDR2-T* 2.5, 5, 10, 25 and 50 μM . The graphs were plotted with OriginPro 2019 and are shown in Figure 21. The initial velocities of the catalysed reaction at the different substrate concentrations were determined by fitting the BoxLucas1 model to the data sets (see subtitles for equation).

PcHDR-T was the first to be tested and too many high HMBDP concentrations were applied. Due to time constraints of the thesis, the experiment could not be repeated. The plot is not accurate and error bars are high. Nonetheless, a Lineweaver-Burk and Michaelis-Menten plot were performed. This is acceptable in order to understand in which range the constants are located. Yet, in order to achieve more accurate data, the experiments should be repeated with lower substrate concentrations. Assays with *PaHDR1-T* and *PaHDR2-T* were performed with adjusted HMBDP concentrations and show smaller errors.

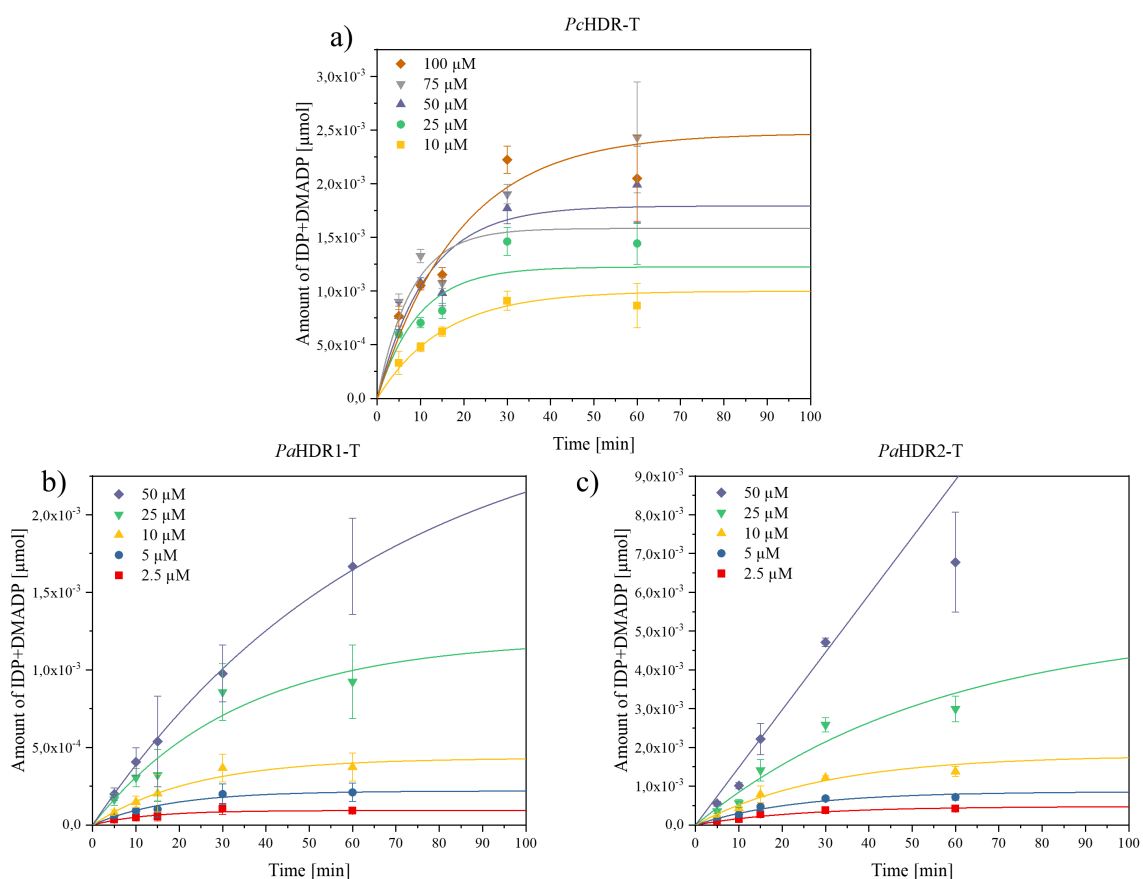


Figure 21: Measurements for the determination of the initial velocities of product formation by a) *PcHDR-T*, b) *PaHDR1-T* and c) *PaHDR2-T* at different substrate concentrations; amount of IDP+DMADP was measured at five different points in time (5, 10, 15, 30 and 60 min), assay conditions: 0.5 μg enzyme, pH 6.5, 35°C; curve fitting was performed with OriginPro 2019, Model: BoxLucas1, Equation: $y = a * (1 - \exp(-b * x))$, initial velocities were determined by $y(0,0) = a * b$

The determined values of initial velocities were then plotted in a Lineweaver-Burk and Michaelis-Menten plot to determine the K_M and k_{cat} . The Lineweaver-Burk plot is the

reciprocal representation of the Michaelis-Menten plot. The first is presented in Figure 22, as it is commonly accepted to be more accurate, and it has the advantage of having the K_M at the intercept with the x-axis ($-1/K_M$) and v_{max} at the intercept with the y-axis ($1/v_{max}$). The slope is K_M/v_{max} . The Michaelis-Menten plot is listed in the appendix in chapter 6.6. The Lineweaver-Burk plot is based on a linear fit (for equations see subtitles of the figures).

The Lineweaver-Burk plot for *PcHDR-T* is shown in Figure 22 a). As mentioned before, the data is not accurate and error margins are high. However, K_M was determined to be $21.4 \mu M$, v_{max} $2.1 \cdot 10^{-4} \mu mol/min$ and k_{cat} $31.6 min^{-1}$.

The data of *PaHDR1-T* and *PaHDR2-T* gives accurate plots, which are shown in Figure 22 b) and c). K_M , v_{max} and k_{cat} were determined to be $15.9 \mu M$, $5.2 \cdot 10^{-5} \mu mol/min$ and $7.8 min^{-1}$ respectively for *PaHDR1-T* and $21.2 \mu M$, $1.9 \cdot 10^{-4} \mu mol/min$ and $28 min^{-1}$ for *PaHDR2-T*.

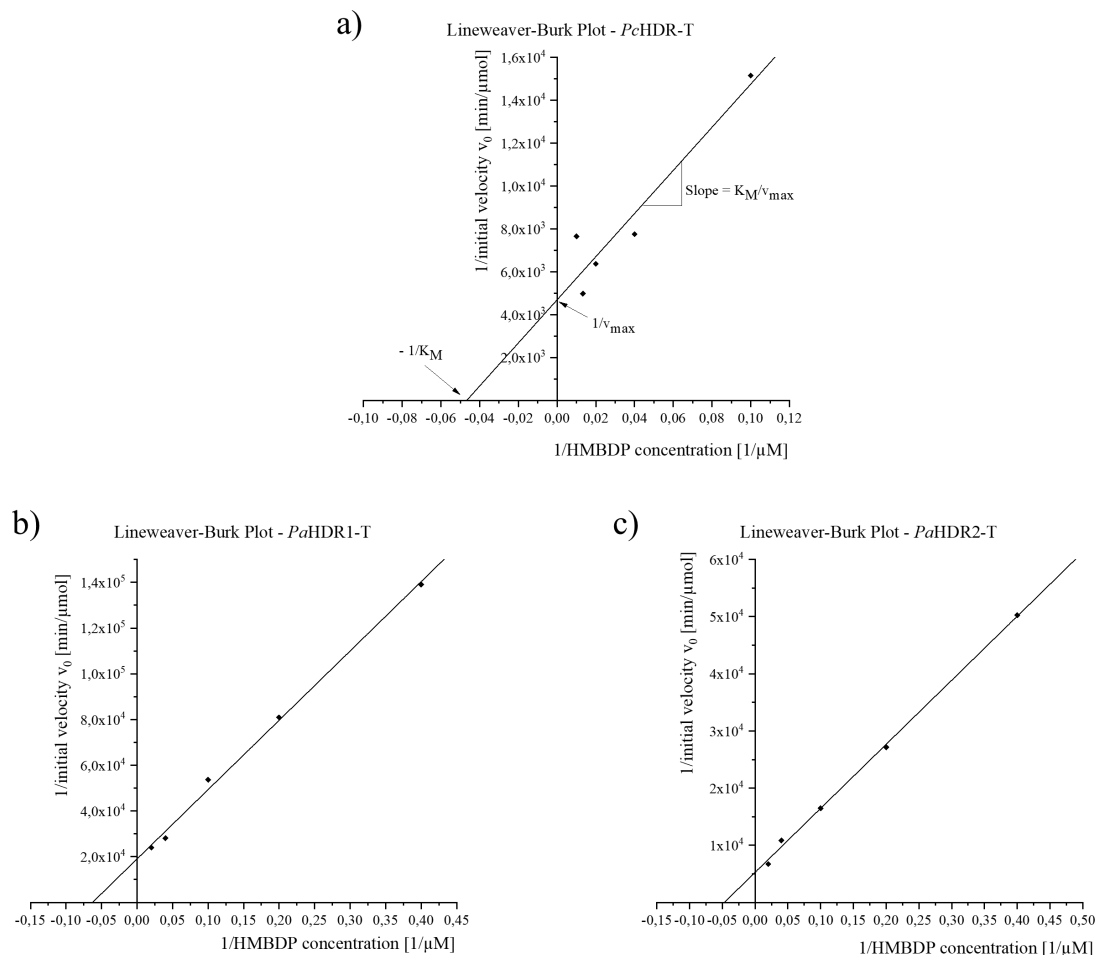


Figure 22: Lineweaver-Burk plots to determine K_M , v_{max} and k_{cat} of a) *PcHDR-T*, b) *PaHDR1-T* and c) *PaHDR2-T*; reciprocal initial velocities determined from Figure 21 and reciprocal substrate concentrations were plotted; fitting was performed with OriginPro 2019, Lineweaver-Burk: $k_{cat} = v_{max}[\mu mol/min]/E[\mu mol]$, intercept with y-axis is $1/v_{max}$, intercept with x-axis is $-1/K_M$, slope is K_M/v_{max} ; a) $v_{max} = 2.1 \cdot 10^{-4} \mu mol/min$, $K_M = 21.4 \mu M$, b) $v_{max} = 5.2 \cdot 10^{-5} \mu mol/min$, $K_M = 15.9 \mu M$, c) $v_{max} = 1.9 \cdot 10^{-4} \mu mol/min$, $K_M = 21.2 \mu M$

Plotting all three HDR candidates in one Lineweaver-Burk plot (Figure 23), the differences and similarities become visible. *PcHDR-T* and *PaHDR2-T* have a similar catalytic efficiency (k_{cat}/K_M) and a similar K_M value, whereas the catalytic efficiency of *PaHDR1-T* makes up for only about a third of the other two HDRs. In addition, the K_M and therefore the substrate affinity are lower.

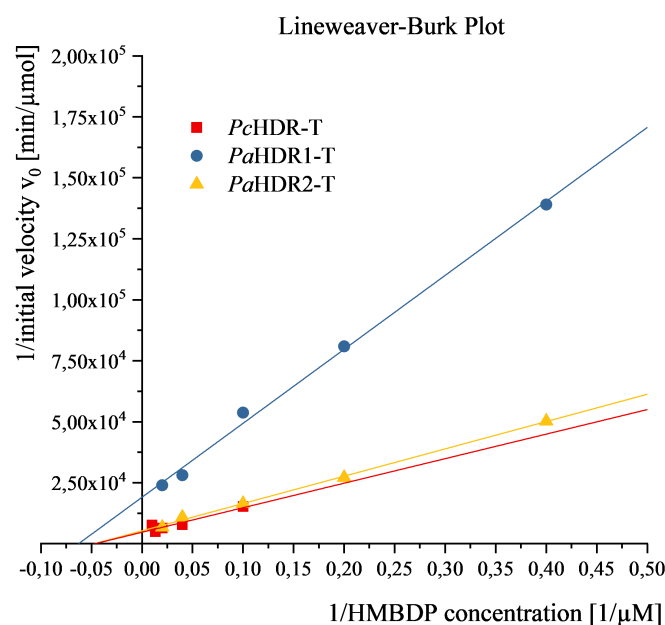


Figure 23: Lineweaver-Burk plot to compare K_M and v_{max} of *PcHDR-T*, *PaHDR1-T* and *PaHDR2-T*; for data see Figure 21 and Figure 22

As far as we know this is the first time that two HDRs from one organism have been biochemically characterized *in vitro* so far. As discussed previously in the context of the phylogenetic tree, further investigation need to be carried out to be able to tell whether the HDRs have different functions. One approach, which is currently pursued in the research group, are transgenic poplar and spruce trees, where the HDR had been downregulated by an RNAi-approach. Expression of different genes involved in the pathway and metabolites are measured to gain understanding of the function of the HDR and the regulation of terpene biosynthesis at this regulatory point.

To give an overview about the current state of research, the biochemical values from other organisms are listed in Table 18. The K_M values are mostly in a similar range between 6 and 40 μM , but the catalytic efficiency from HDRs characterized in this work is rather low compared to other organisms. However, comparisons should be carried out carefully, as all listed k_{cat} and K_M values were determined in different experimental conditions. One factor are the used redox systems, which are assumed to have an impact on the enzymes activity

(Xiao et al., 2009). In addition, apart from different optimization approaches, the analytical method can also have an influence, depending on its accuracy.

Table 18: Characteristic biochemical values of HDRs from different organisms

Organism	k_{cat} [min^{-1}]	K_M [μM]	k_{cat}/K_M [$\mu\text{M}^{-1} \text{min}^{-1}$]	Reference
<i>Populus × canescens</i> (HDR-T)	31.6	21.4	1.5	This work
<i>Picea abies</i> (HDR1-T)	7.8	15.9	0.5	This work
<i>Picea abies</i> (HDR2-T)	28.0	21.2	1.3	This work
<i>Burkholderia glumae</i> (BgHDR1)	187.0	6.0	31.17	(Kwon et al., 2013)
<i>Burkholderia glumae</i> (BgHDR2)	66.6	21.2	3.14	(Kwon et al., 2013)
<i>Ginkgo biloba</i> (Type 1)	347 ± 12	14.9 ± 2.3	23.3 ± 3.7	(Shin et al., 2017)
<i>E. coli</i>	11.6	<15 30	-	(Xiao et al., 2008) (Gräwert et al., 2004)
<i>Aquifex aeolicus</i>	$3.7 \pm 0.2 \text{ s}^{-1}$	590 ± 60	-	(Altincicek et al., 2002)
<i>Plasmodium falciparum</i>	$\sim 1.3 \text{ s}^{-1}$	39	-	(Röhrich et al., 2005)

3.4 Determination of IDP/DMADP ratio

After the characterization of *PcHDR-T*, *PaHDR1-T* and *PaHDR2-T* by their biochemical values the second driving question will be addressed in this chapter: do they catalyze different product ratios? Selected samples with different pH values (pH 5, 6.5 and 8), different temperatures (25, 35 and 45°C) and at five different points in time (kinetic assays with 50 μ M HMBDP) were chosen and measured with the Astec® Cyclobond® I 2000 column. By using this method, it is possible to separate the two isomers DMADP and IDP and to determine the ratio. The results can be seen in Figure 24.

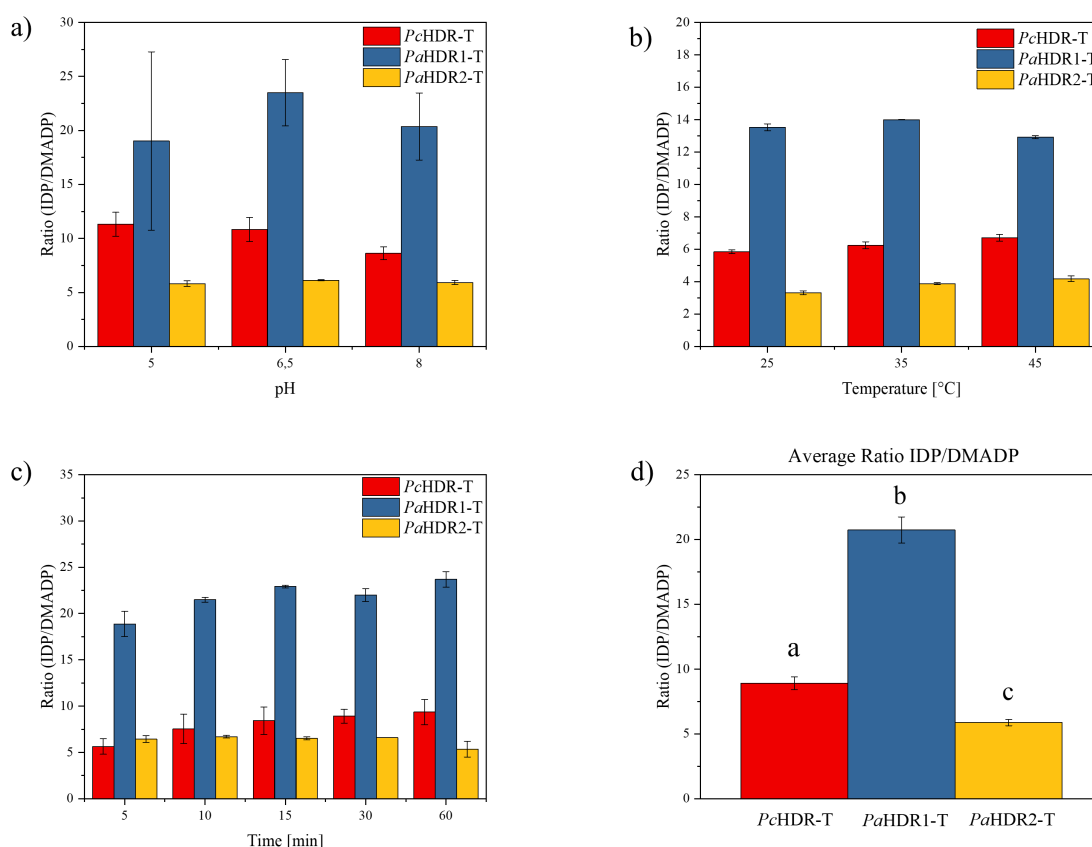


Figure 24: IDP/DMADP ratios synthesized by *PcHDR-T*, *PaHDR1-T* and *PaHDR2-T* at a) pH 5, 6.5 and 8, b) 25, 35 and 45°C, c) after 5, 10, 15, 30 and 60 minutes reaction time: no significant difference between samples of one construct; d) pooled data from a) and c); statistical analysis was performed with SigmaPlot, ANOVA oneway test was performed, significant difference of the IDP/DMADP ratios exists between the three constructs (pooled data; see letters a, b, c)

No significantly different ratios were detected between samples of different pH or temperature and neither between samples stopped at different points in time of one construct. Ratios from pH and time assays were then pooled. *PcHDR-T* produced a ratio of about 9:1, *PaHDR1-T* of 21:1 and *PaHDR2-T* of about 5:1. The differences of the ratios between the constructs are statistically significant (see Figure 24 d)). The high IDP/DMADP ratio of *PaHDR1-T* is exceptional. The table with IDP/DMADP ratios presented in the introduction is listed here again (Table 19) and data from this work is added.

Table 19: *In vitro* ratio of IDP/DMADP produced by the HDR from various organisms

Organism	IDP/DMADP ratio	Literature
<i>Burkholderia glumae</i>	2.2:1	(Kwon et al., 2013)
<i>Plasmodium falciparum</i>	4-5:1	(Röhrich et al., 2005)
<i>Aquifex aeolicus</i>	4-5:1	(Altincicek et al., 2002)
<i>Escherichia coli</i>	5-6:1	(Adam et al., 2002; Wolff et al., 2003; Gräwert et al., 2004)
<i>Ginkgo biloba</i>	16:1	(Shin et al., 2017)
<i>Populus</i> × <i>canescens</i> (HDR)	~9:1	This work
<i>Picea abies</i> (HDR1)	~21:1	This work
<i>Picea abies</i> (HDR2)	~6:1	This work

Gräwert et al. (2004) claimed that the product ratio would be controlled kinetically. However, Shin et al. (2017) claimed that the relatively high ratio of 16:1 in *G. biloba* is controlled by a phenylalanine residue in the protein sequence. The phenylalanine at position 217 in our alignment (Figure 25) is conserved in all listed plant species. Therefore, either all plant HDR should produce similarly high amounts of IDP as *G. biloba*, which is not the case for *PcHDR-T* and *PaHDR2-T*, or the assumption made by Shin et al. is questionable.

The initial hypothesis was, that the HDR of *P. canescens*, which emits high rates of isoprene, would have a lower IDP/DMADP ratio than *P. abies* which produces high levels of mono-, sesqui- and diterpenes. This hypothesis could not be confirmed. Interestingly there is a big difference of the ratios between the two HDRs from *P. abies* (21:1 and 6:1). The ratio catalyzed by *PcHDR* (9:1), though, resembles the ratio catalyzed by *PaHDR2-T* (6:1).

Further research has to be done to address how and if the ratio is controlled, whether there is an application of the different ratios and how the regulation is done *in vivo*. However, we have to take into account that the isomerase (IDI) is present *in vivo*. The IDI catalyzes the isomerization from IDP to DMADP and vice versa, but the equilibrium is towards the formation of DMADP (Ramos-Valdivia et al., 1997). When the ratio of the two isomers is measured *in planta*, DMADP is usually higher (see (Bongers et al., 2020)). It remains to be explained in the future, at which step of the isoprenoid biosynthesis the ratio of the two isomers is regulated. Heterologous expression of *PcHDR-T*, *PaHDR1-T* and *PaHDR2-T* and *in vitro* enzyme assays to determine the product ratio are one contribution to understand this regulation.

4 Conclusion and Outlook

In this thesis, an experimental setup and protocol for working with an oxygen-sensitive enzyme in a glove box have been established. This is a prerequisite to be able to perform assays with enzymes which inherit an iron-sulfur cluster, such as the HDR. The setup can now be used for further investigation on the HDR or on the HDS which is another oxygen-sensitive enzyme of the MEP pathway.

Besides the method development, one putative HDR from *P. canescens* and two from *P. abies* have been successfully heterologously expressed in *E. coli* and have been purified as well as characterized biochemically in a nitrogen atmosphere in the glove box. By performing enzyme kinetics of the recombinant proteins, we could tell that *PcHDR* and *PaHDR2-T* have similar enzymatic characteristics. Additionally, the IDP/DMADP ratio which they catalyse is in a similar range. In comparison to *PcHDR* and *PaHDR2-T*, *PaHDR1-T* has a lower substrate affinity and a lower catalytic efficiency but produces a two-to-three-fold higher IDP/DMADP ratio.

These findings are a contribution to a better understanding of the isoprenoid biosynthesis in plants. However, further investigation is needed to classify the role of *PcHDR*, *PaHDR1-T* and *PaHDR2-T* *in planta* and to get a full picture of the pathway and its regulation. As previously mentioned, HDR RNAi transgenic plants are available. A next experimental step would be to establish a protocol for the isolation of the HDR from *planta*. Freshly isolated enzymes from HDR RNAi transgenic plants, as well as from wildtype, vector control and HDR overexpression plants could be analyzed in a nitrogen atmosphere for their activity. Additionally, data from the expression of the *HDR* genes and the expression of other relevant enzymes of the pathway and data from the metabolic content of the plants, is currently collected in the research group. This data, together with future findings from extracted HDRs and together with the characteristics of recombinant *PcHDR*, *PaHDR1-T* and *PaHDR2-T* determined in this thesis, will help to gain a better understanding of the biosynthesis of isoprenoids.

5 Literature

- Abdel-Azeim S, Jedidi A, Eppinger J, Cavallo L** (2015) Mechanistic insights into the reductive dehydroxylation pathway for the biosynthesis of isoprenoids promoted by the IspH enzyme. *Chemical Science* **6**: 5643-5651
- Adam P, Hecht S, Eisenreich W, Kaiser J, Gräwert T, Arigoni D, Bacher A, Rohdich F** (2002) Biosynthesis of terpenes: studies on 1-hydroxy-2-methyl-2-(E)-butenyl 4-diphosphate reductase. *Proceedings of the National Academy of Sciences* **99**: 12108-12113
- Agranoff BW, Eggerer H, Henning U, Lynen F** (1960) Biosynthesis of Terpenes: VII. ISOPENTENYL PYROPHOSPHATE ISOMERASE. *Journal of Biological Chemistry* **235**: 326-332
- Altincicek B, Duin EC, Reichenberg A, Hedderich R, Kollas A-K, Hintz M, Wagner S, Wiesner J, Beck E, Jomaa H** (2002) LytB protein catalyzes the terminal step of the 2-C-methyl-D-erythritol-4-phosphate pathway of isoprenoid biosynthesis. *Febs Letters* **532**: 437-440
- Banerjee A, Preiser AL, Sharkey TD** (2016) Engineering of Recombinant Poplar Deoxy-D-Xylulose-5-Phosphate Synthase (Pt DXS) by Site-Directed Mutagenesis Improves Its Activity. *PloS one* **11**: e0161534
- Blachly PG, Sandala GM, Giammona DA, Bashford D, McCammon JA, Noodleman L** (2015) Broken-Symmetry DFT Computations for the Reaction Pathway of IspH, an Iron-Sulfur Enzyme in Pathogenic Bacteria. *Inorganic Chemistry* **54**: 6439-6461
- Boncan DAT, Tsang SS, Li C, Lee IH, Lam H-M, Chan T-F, Hui JH** (2020) Terpenes and Terpenoids in Plants: Interactions with Environment and Insects. *International Journal of Molecular Sciences* **21**: 7382
- Bongers M, Perez-Gil J, Hodson MP, Schrübbers L, Wulff T, Sommer MOA, Nielsen LK, Vickers CE** (2020) Adaptation of hydroxymethylbutenyl diphosphate reductase enables volatile isoprenoid production. *eLife* **9**: e48685
- Bourtsoukidis E, Williams J, Kesselmeier J, Jacobi S, Bonn B** (2014) From emissions to ambient mixing ratios: online seasonal field measurements of volatile organic compounds over a Norway spruce-dominated forest in central Germany. *Atmospheric Chemistry and Physics* **14**: 6495-6510
- Brumby PE, Massey V** (1967) [73] Determination of nonheme iron, total iron, and copper. *In Methods in enzymology*, Vol 10. Elsevier, pp 463-474
- Caudullo G, Tinner W, de Rigo D** (2016) *Picea abies* in Europe: distribution, habitat, usage and threats. In: San-Miguel-Ayanz, J.; de Rigo, D.; Caudullo, G.; Houston Durrant, T.; Mauri, A. (ed.) *European Atlas of Forest Tree Species*. Luxembourg: Publication Office of the European Union: pp 114-116
- Celedon JM, Bohlmann J** (2019) Oleoresin defenses in conifers: chemical diversity, terpene synthases and limitations of oleoresin defense under climate change. *New Phytologist* **224**: 1444-1463
- Chaignon P, Petit BE, Vincent B, Allouche L, Seemann M** (2020) Methylerythritol Phosphate Pathway: Enzymatic Evidence for a Rotation in the LytB/IspH-Catalyzed Reaction. *Chemistry – A European Journal* **26**: 1032-1036

- Chen F, Tholl D, Bohlmann J, Pichersky E** (2011) The family of terpene synthases in plants: a mid-size family of genes for specialized metabolism that is highly diversified throughout the kingdom. *The Plant Journal* **66**: 212-229
- Cheng QQ, Tong YR, Wang ZH, Su P, Gao W, Huang LQ** (2017) Molecular cloning and functional identification of a cDNA encoding 4-hydroxy-3-methylbut-2-enyl diphosphate reductase from *Tripterygium wilfordii*. *Acta Pharmaceutica Sinica B* **7**: 208-214
- Christianson DW** (2017) Structural and chemical biology of terpenoid cyclases. *Chemical reviews* **117**: 11570-11648
- Eisenreich W, Schwarz M, Cartayrade A, Arigoni D, Zenk MH, Bacher A** (1998) The deoxyxylulose phosphate pathway of terpenoid biosynthesis in plants and microorganisms. *Chemistry & biology* **5**: R221-R233
- Emanuelsson O, Nielsen H, Heijne GV** (1999) ChloroP, a neural network-based method for predicting chloroplast transit peptides and their cleavage sites. *Protein Science* **8**: 978-984
- Estévez JM, Cantero A, Reindl A, Reichler S, León P** (2001) 1-Deoxy-D-xylulose-5-phosphate synthase, a limiting enzyme for plastidic isoprenoid biosynthesis in plants. *Journal of Biological Chemistry* **276**: 22901-22909
- Frank A, Groll M** (2017) The Methylerythritol Phosphate Pathway to Isoprenoids. *Chemical Reviews* **117**: 5675-5703
- Gershenson J, Dudareva N** (2007) The function of terpene natural products in the natural world. *Nature Chemical Biology* **3**: 408-414
- Ghirardo A, Wright LP, Bi Z, Rosenkranz M, Pulido P, Rodríguez-Concepción M, Niinemets Ü, Brüggemann N, Gershenson J, Schnitzler J-P** (2014) Metabolic Flux Analysis of Plastidic Isoprenoid Biosynthesis in Poplar Leaves Emitting and Nonemitting Isoprene. *Plant Physiology* **165**: 37-51
- González-Cabanelas D, Hammerbacher A, Raguschke B, Gershenson J, Wright LP** (2016) Chapter Ten - Quantifying the Metabolites of the Methylerythritol 4-Phosphate (MEP) Pathway in Plants and Bacteria by Liquid Chromatography–Triple Quadrupole Mass Spectrometry. *In* SE O'Connor, ed, *Methods in Enzymology*, Vol 576. Academic Press, pp 225-249
- Gräwert T, Kaiser J, Zepeck F, Laupitz R, Hecht S, Amslinger S, Schramek N, Schleicher E, Weber S, Haslbeck M, Buchner J, Rieder C, Arigoni D, Bacher A, Eisenreich W, Rohdich F** (2004) IspH Protein of *Escherichia coli*: Studies on Iron–Sulfur Cluster Implementation and Catalysis. *Journal of the American Chemical Society* **126**: 12847-12855
- Gräwert T, Rohdich F, Span I, Bacher A, Eisenreich W, Eppinger J, Groll M** (2009) Structure of active IspH enzyme from *Escherichia coli* provides mechanistic insights into substrate reduction. *Angewandte Chemie International Edition* **48**: 5756-5759
- Gräwert T, Span I, Eisenreich W, Rohdich F, Eppinger J, Bacher A, Groll M** (2010) Probing the reaction mechanism of IspH protein by x-ray structure analysis. *Proceedings of the National Academy of Sciences of the United States of America* **107**: 1077-1081

- Guenther A, Hewitt CN, Erickson D, Fall R, Geron C, Graedel T, Harley P, Klinger L, Lerdau M, McKay W** (1995) A global model of natural volatile organic compound emissions. *Journal of Geophysical Research: Atmospheres* **100**: 8873-8892
- Heldt HW, Werdan K, Milovancev M, Geller G** (1973) Alkalization of the chloroplast stroma caused by light-dependent proton flux into the thylakoid space. *Biochimica et Biophysica Acta (BBA)-Bioenergetics* **314**: 224-241
- Hsieh MH, Goodman HM** (2005) The arabidopsis IspH homolog is involved in the plastid nonmevalonate pathway of isoprenoid biosynthesis. *Plant Physiology* **138**: 641-653
- Hsieh WY, Hsieh MH** (2015) The amino-terminal conserved domain of 4-hydroxy-3-methylbut-2-enyl diphosphate reductase is critical for its function in oxygen-evolving photosynthetic organisms. *Plant Signaling & Behavior* **10**: e988072
- Hsieh WY, Sung TY, Wang HT, Hsieh MH** (2014) Functional Evidence for the Critical Amino-Terminal Conserved Domain and Key Amino Acids of Arabidopsis 4-HYDROXY-3-METHYLBUT-2-ENYL DIPHOSPHATE REDUCTASE. *Plant Physiology* **166**: 57-69
- Huang JZ, Cheng TC, Wen PJ, Hsieh MH, Chen FC** (2009) Molecular characterization of the *Oncidium* orchid HDR gene encoding 1-hydroxy-2-methyl-2-(E)-butenyl 4-diphosphate reductase, the last step of the methylerythritol phosphate pathway. *Plant Cell Reports* **28**: 1475-1486
- Jalil SU, Ansari MI** (2020) Isoprenoids in Plant Protection Against Abiotic Stress. *In: Roychoudhury A, Tripathi DK (ed.) Protective Chemical Agents in the Amelioration of Plant Abiotic Stress*, pp 424-436
- Johnson SR, Lange I, Srividya N, Lange BM** (2017) Bioenergetics of monoterpenoid essential oil biosynthesis in nonphotosynthetic glandular trichomes. *Plant Physiology* **175**: 681-695
- Kang MK, Nargis S, Kim SM, Kim SU** (2013) Distinct expression patterns of two *Ginkgo biloba* 1-hydroxy-2-methyl-2-(E)-butenyl-4-diphosphate reductase/isopentenyl diphosphate synthase (HDR/IDS) promoters in Arabidopsis model. *Plant Physiology and Biochemistry* **62**: 47-53
- Keeling CI, Bohlmann J** (2006) Diterpene resin acids in conifers. *Phytochemistry* **67**: 2415-2423
- Kim S-M, Kuzuyama T, Kobayashi A, Sando T, Chang Y-J, Kim S-U** (2008) 1-Hydroxy-2-methyl-2-(E)-butenyl 4-diphosphate reductase (IDS) is encoded by multicopy genes in gymnosperms *Ginkgo biloba* and *Pinus taeda*. *Planta* **227**: 287-298
- Kim Y-B, Kim S-M, Kang M-K, Kuzuyama T, Lee JK, Park S-C, Shin S-c, Kim S-U** (2009) Regulation of resin acid synthesis in *Pinus densiflora* by differential transcription of genes encoding multiple 1-deoxy-d-xylulose 5-phosphate synthase and 1-hydroxy-2-methyl-2-(E)-butenyl 4-diphosphate reductase genes. *Tree Physiology* **29**: 737-749
- Köhling R, Meier R, Boertz J, Schönenberger B, Wohlgemuth R** (2014) Analysis of Isoprenoid Pathway Metabolites by LC-MS. Buchs, Switzerland: Biofiles, Sigma-Aldrich

- Krause T, Reichelt M, Gershenzon J, Schmidt A** (2020) Analysis of the isoprenoid pathway intermediates, dimethylallyl diphosphate and isopentenyl diphosphate, from crude plant extracts by liquid chromatography tandem mass spectrometry. *Phytochemical Analysis* **31**: 770-777
- Kumar H, Kumar S** (2013) A functional (E)-4-hydroxy-3-methylbut-2-enyl diphosphate reductase exhibits diurnal regulation of expression in *Stevia rebaudiana* (Bertoni). *Gene* **527**: 332-338
- Kwon M, Shin BK, Lee J, Han J, Kim SU** (2013) Characterization of *Burkholderia glumae* BGR1 4-hydroxy-3-methylbut-2-enyl diphosphate reductase (HDR), the terminal enzyme in 2-C-methyl-d-erythritol 4-phosphate (MEP) pathway. *Journal of the Korean Society for Applied Biological Chemistry* **56**: 35-40
- Lichtenthaler HK, Schwender J, Disch A, Rohmer M** (1997) Biosynthesis of isoprenoids in higher plant chloroplasts proceeds via a mevalonate-independent pathway. *FEBS letters* **400**: 271-274
- Lipko A, Swiezewska E** (2016) Isoprenoid generating systems in plants—A handy toolbox how to assess contribution of the mevalonate and methylerythritol phosphate pathways to the biosynthetic process. *Progress in lipid research* **63**: 70-92
- Loivamaki M, Louis S, Cinege G, Zimmer I, Fischbach RJ, Schnitzler JP** (2007) Circadian rhythms of isoprene biosynthesis in Grey poplar leaves. *Plant Physiology* **143**: 540-551
- Martin DM, Fäldt J, Bohlmann J** (2004) Functional characterization of nine Norway spruce TPS genes and evolution of gymnosperm terpene synthases of the TPS-d subfamily. *Plant physiology* **135**: 1908-1927
- Martin DM, Gershenzon J, Bohlmann J** (2003) Induction of volatile terpene biosynthesis and diurnal emission by methyl jasmonate in foliage of Norway spruce. *Plant physiology* **132**: 1586-1599
- Nystedt B, Street NR, Wetterbom A, Zuccolo A, Lin Y-C, Scofield DG, Vezzi F, Delhomme N, Giacomello S, Alexeyenko A, Vicedomini R, Sahlin K, Sherwood E, Elfstrand M, Gramzow L, Holmberg K, Hällman J, Keech O, Klasson L, Koriabine M, Kucukoglu M, Käller M, Luthman J, Lysholm F, Niittylä T, Olson Å, Rilakovic N, Ritland C, Rosselló JA, Sena J, Svensson T, Talavera-López C, Theißen G, Tuominen H, Vanneste K, Wu Z-Q, Zhang B, Zerbe P, Arvestad L, Bhalerao R, Bohlmann J, Bousquet J, Garcia Gil R, Hvidsten TR, de Jong P, MacKay J, Morgante M, Ritland K, Sundberg B, Lee Thompson S, Van de Peer Y, Andersson B, Nilsson O, Ingvarsson PK, Lundeberg J, Jansson S** (2013) The Norway spruce genome sequence and conifer genome evolution. *Nature* **497**: 579-584
- Opitz S, Nes WD, Gershenzon J** (2014) Both methylerythritol phosphate and mevalonate pathways contribute to biosynthesis of each of the major isoprenoid classes in young cotton seedlings. *Phytochemistry* **98**: 110-119
- Phillips MA, D'Auria JC, Gershenzon J, Pichersky E** (2008) The *Arabidopsis thaliana* type I isopentenyl diphosphate isomerases are targeted to multiple subcellular compartments and have overlapping functions in isoprenoid biosynthesis. *The Plant Cell* **20**: 677-696

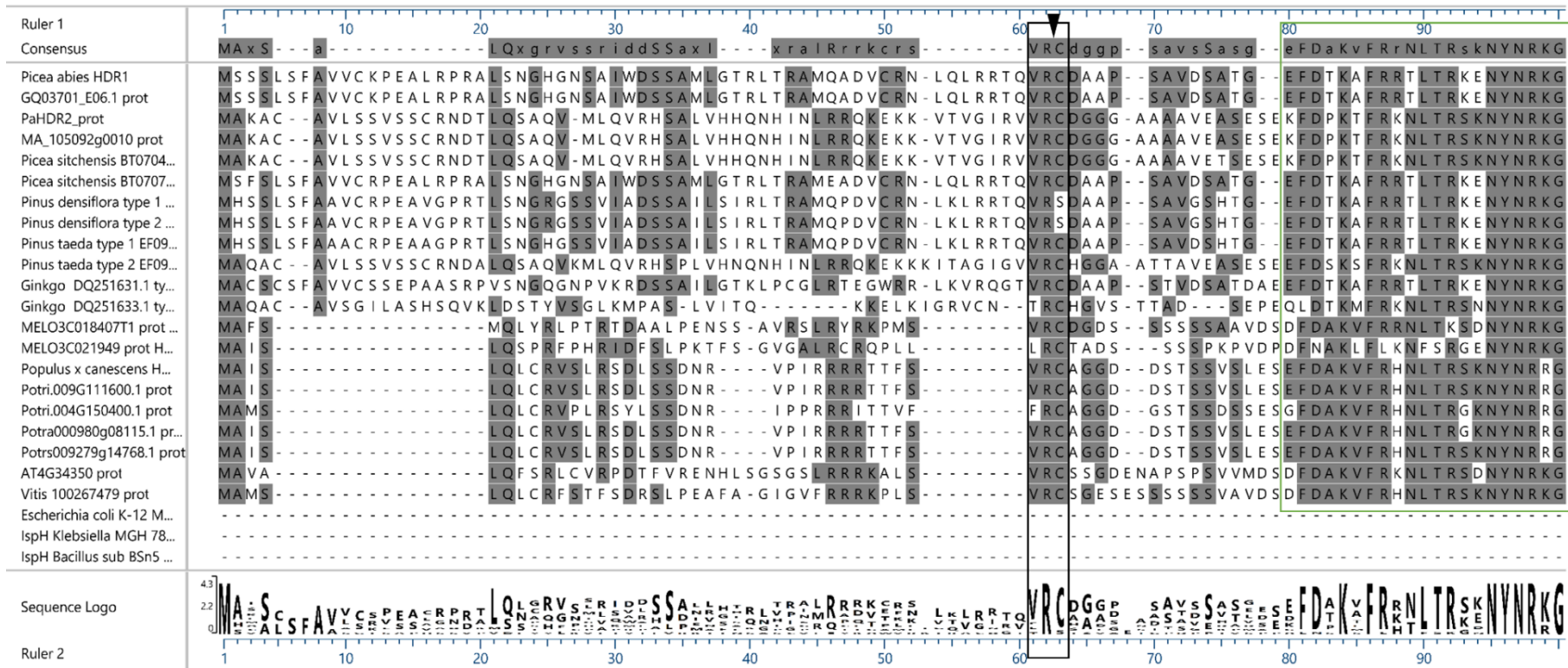
- Pichersky E, Gershenzon J** (2002) The formation and function of plant volatiles: perfumes for pollinator attraction and defense. *Current opinion in plant biology* **5**: 237-243
- Rajora O, Dancik B** (1992) Genetic characterization and relationships of *Populus alba*, *P. tremula*, and *P. x canescens*, and their clones. *Theoretical and Applied Genetics* **84**: 291-298
- Ramos-Valdivia AC, van der Heijden R, Verpoorte R** (1997) Isopentenyl diphosphate isomerase: a core enzyme in isoprenoid biosynthesis. A review of its biochemistry and function. *Natural product reports* **14**: 591-603
- Rekittke I, Wiesner J, Röhrich R, Demmer U, Warkentin E, Xu W, Troschke K, Hintz M, No JH, Duin EC** (2008) Structure of (E)-4-hydroxy-3-methyl-but-2-enyl diphosphate reductase, the terminal enzyme of the non-mevalonate pathway. *Journal of the American Chemical Society* **130**: 17206-17207
- Richter S, Lamppa GK** (2002) Determinants for Removal and Degradation of Transit Peptides of Chloroplast Precursor Proteins*. *Journal of Biological Chemistry* **277**: 43888-43894
- Rivasseau C, Seemann M, Boisson AM, Streb P, Gout E, Douce R, Rohmer M, Bligny R** (2009) Accumulation of 2-C-methyl-d-erythritol 2,4-cyclodiphosphate in illuminated plant leaves at supraoptimal temperatures reveals a bottleneck of the prokaryotic methylerythritol 4-phosphate pathway of isoprenoid biosynthesis. *Plant Cell and Environment* **32**: 82-92
- Rohdich F, Hecht S, Bacher A, Eisenreich W** (2003) Deoxyxylulose phosphate pathway of isoprenoid biosynthesis. Discovery and function of ispDEFGH genes and their cognate enzymes. *Pure and Applied Chemistry* **75**: 393-405
- Rohmer M** (1999) The discovery of a mevalonate-independent pathway for isoprenoid biosynthesis in bacteria, algae and higher plants. *Natural product reports* **16**: 565-574
- Röhrich RC, Englert N, Troschke K, Reichenberg A, Hintz M, Seeber F, Balconi E, Aliverti A, Zanetti G, Köhler U** (2005) Reconstitution of an apicoplast-localised electron transfer pathway involved in the isoprenoid biosynthesis of *Plasmodium falciparum*. *FEBS letters* **579**: 6433-6438
- Ruzicka L** (1953) The isoprene rule and the biogenesis of terpenic compounds. *Experientia* **9**: 357-367
- Saladié M, Wright LP, Garcia-Mas J, Rodriguez-Concepcion M, Phillips MA** (2014) The 2-C-methylerythritol 4-phosphate pathway in melon is regulated by specialized isoforms for the first and last steps. *Journal of Experimental Botany* **65**: 5077-5092
- Schmidt A, Gershenzon J** (2007) Cloning and characterization of isoprenyl diphosphate synthases with farnesyl diphosphate and geranylgeranyl diphosphate synthase activity from Norway spruce (*Picea abies*) and their relation to induced oleoresin formation. *Phytochemistry* **68**: 2649-2659
- Schnitzler JP, Louis S, Behnke K, Loivamaki M** (2010) Poplar volatiles - biosynthesis, regulation and (eco)physiology of isoprene and stress-induced isoprenoids. *Plant Biology* **12**: 302-316
- Schrader J, Bohlmann J** (2015) Biotechnology of isoprenoids. *Advances in Biochemical Engineering/Biotechnology*, Vol 148. Springer

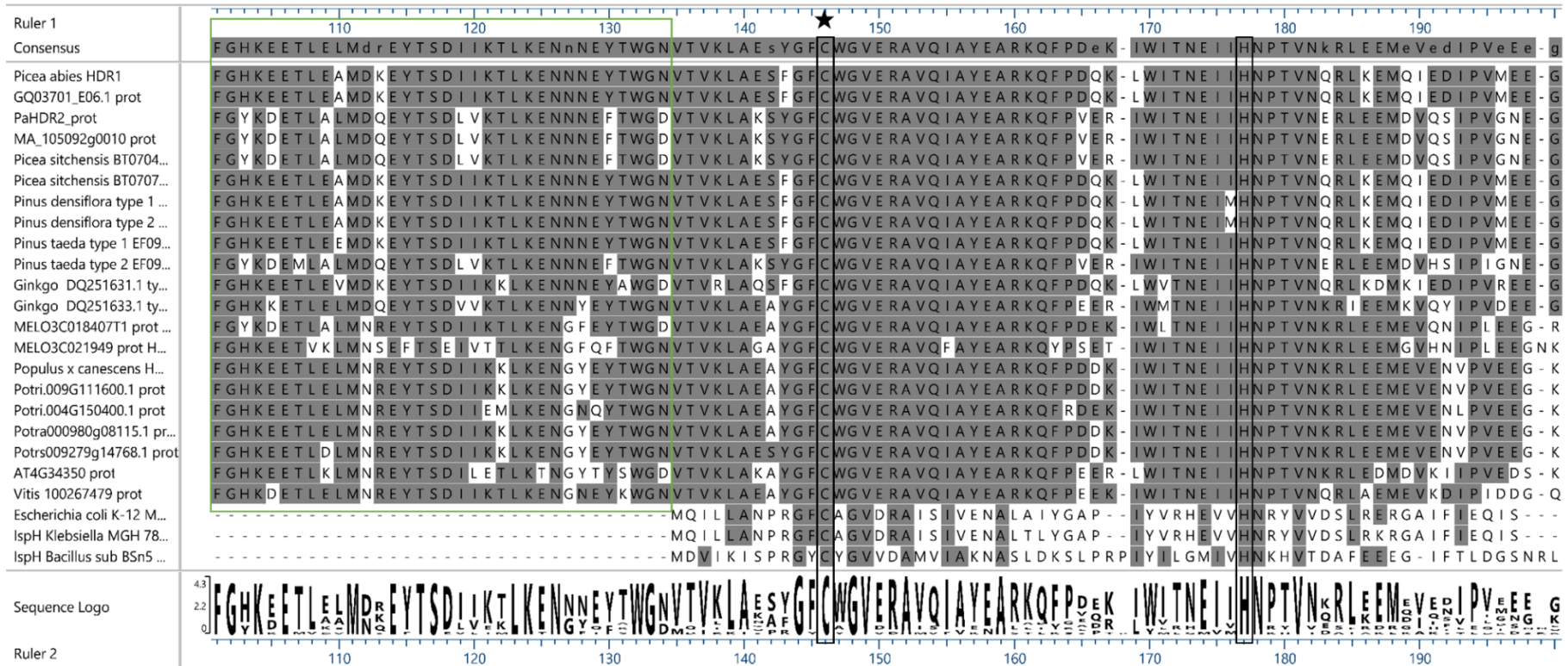
- Seemann M, Janthawornpong K, Schweizer J, Böttger LH, Janoschka A, Ahrens-Botzong A, Tambou EN, Rotthaus O, Trautwein AX, Rohmer M, Schünemann V** (2009) Isoprenoid Biosynthesis via the MEP Pathway: In Vivo Mössbauer Spectroscopy Identifies a [4Fe-4S]₂⁺ Center with Unusual Coordination Sphere in the LytB Protein. *Journal of the American Chemical Society* **131**: 13184-13185
- Seemann M, Wegner P, Schünemann V, Bui BTS, Wolff M, Marquet A, Trautwein AX, Rohmer M** (2005) Isoprenoid biosynthesis in chloroplasts via the methylerythritol phosphate pathway: the (E)-4-hydroxy-3-methylbut-2-enyl diphosphate synthase (GcpE) from *Arabidopsis thaliana* is a 4Fe-4S protein. *Journal of Biological Inorganic Chemistry* **10**: 131-137
- Shin BK, Ahn JH, Han J** (2015) N-terminal region of GbIspH1, *Ginkgo biloba* IspH type 1, may be involved in the pH-dependent regulation of enzyme activity. *Bioinorganic chemistry and applications* **2015**: 1-8
- Shin BK, Kim M, Han J** (2017) Exceptionally high percentage of IPP synthesis by *Ginkgo biloba* IspH is mainly due to Phe residue in the active site. *Phytochemistry* **136**: 9-14
- Span I, Gräwert T, Bacher A, Eisenreich W, Groll M** (2012) Crystal Structures of Mutant IspH Proteins Reveal a Rotation of the Substrate's Hydroxymethyl Group during Catalysis. *Journal of Molecular Biology* **416**: 1-9
- Tarshis L, Proteau PJ, Kellogg BA, Sacchettini JC, Poulter CD** (1996) Regulation of product chain length by isoprenyl diphosphate synthases. *Proceedings of the National Academy of Sciences* **93**: 15018-15023
- Tuskan GA, Difazio S, Jansson S, Bohlmann J, Grigoriev I, Hellsten U, Putnam N, Ralph S, Rombauts S, Salamov A** (2006) The genome of black cottonwood, *Populus trichocarpa* (Torr. & Gray). *science* **313**: 1596-1604
- Vickers CE, Gershenzon J, Lerdau MT, Loreto F** (2009) A unified mechanism of action for volatile isoprenoids in plant abiotic stress. *Nature Chemical Biology* **5**: 283-291
- Vickers CE, Possell M, Hewitt CN, Mullineaux PM** (2010) Genetic structure and regulation of isoprene synthase in Poplar (*Populus* spp.). *Plant Molecular Biology* **73**: 547-558
- Wang WX, Wang K, Span I, Jauch J, Bacher A, Groll M, Oldfield E** (2012) Are Free Radicals Involved in IspH Catalysis? An EPR and Crystallographic Investigation. *Journal of the American Chemical Society* **134**: 11225-11234
- Wiberley AE, Donohue AR, Westphal MM, Sharkey TD** (2009) Regulation of isoprene emission from poplar leaves throughout a day. *Plant, Cell & Environment* **32**: 939-947
- Wolff M, Seemann M, Tse Sum Bui B, Frapart Y, Tritsch D, Estrabot AG, Rodríguez-Concepción M, Boronat A, Marquet A, Rohmer M** (2003) Isoprenoid biosynthesis via the methylerythritol phosphate pathway: the (E)-4-hydroxy-3-methylbut-2-enyl diphosphate reductase (LytB/IspH) from *Escherichia coli* is a [4Fe-4S] protein. *FEBS Letters* **541**: 115-120
- Wright LP, Rohwer JM, Ghirardo A, Hammerbacher A, Ortiz-Alcaide M, Raguschke B, Schnitzler JP, Gershenzon J, Phillips MA** (2014) Deoxyxylulose 5-Phosphate Synthase Controls Flux through the Methylerythritol 4-Phosphate Pathway in *Arabidopsis*. *Plant Physiology* **165**: 1488-1504

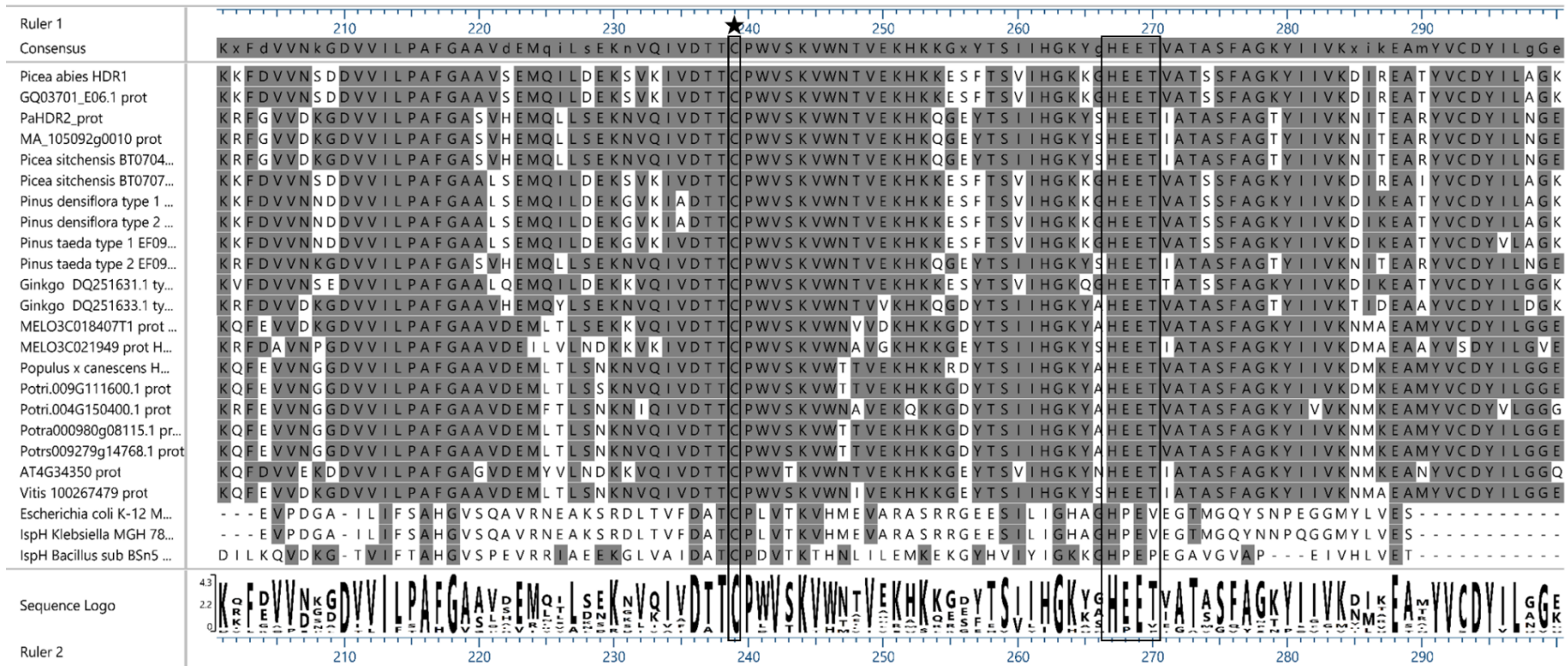
- Xiao Y, Chu L, Sanakis Y, Liu P** (2009) Revisiting the IspH Catalytic System in the Deoxyxylulose Phosphate Pathway: Achieving High Activity. *Journal of the American Chemical Society* **131**: 9931-9933
- Xiao Y, Zhao ZK, Liu P** (2008) Mechanistic Studies of IspH in the Deoxyxylulose Phosphate Pathway: Heterolytic C–O Bond Cleavage at C4 Position. *Journal of the American Chemical Society* **130**: 2164-2165
- Zulak KG, Bohlmann J** (2010) Terpenoid Biosynthesis and Specialized Vascular Cells of Conifer Defense. *Journal of Integrative Plant Biology* **52**: 86-97

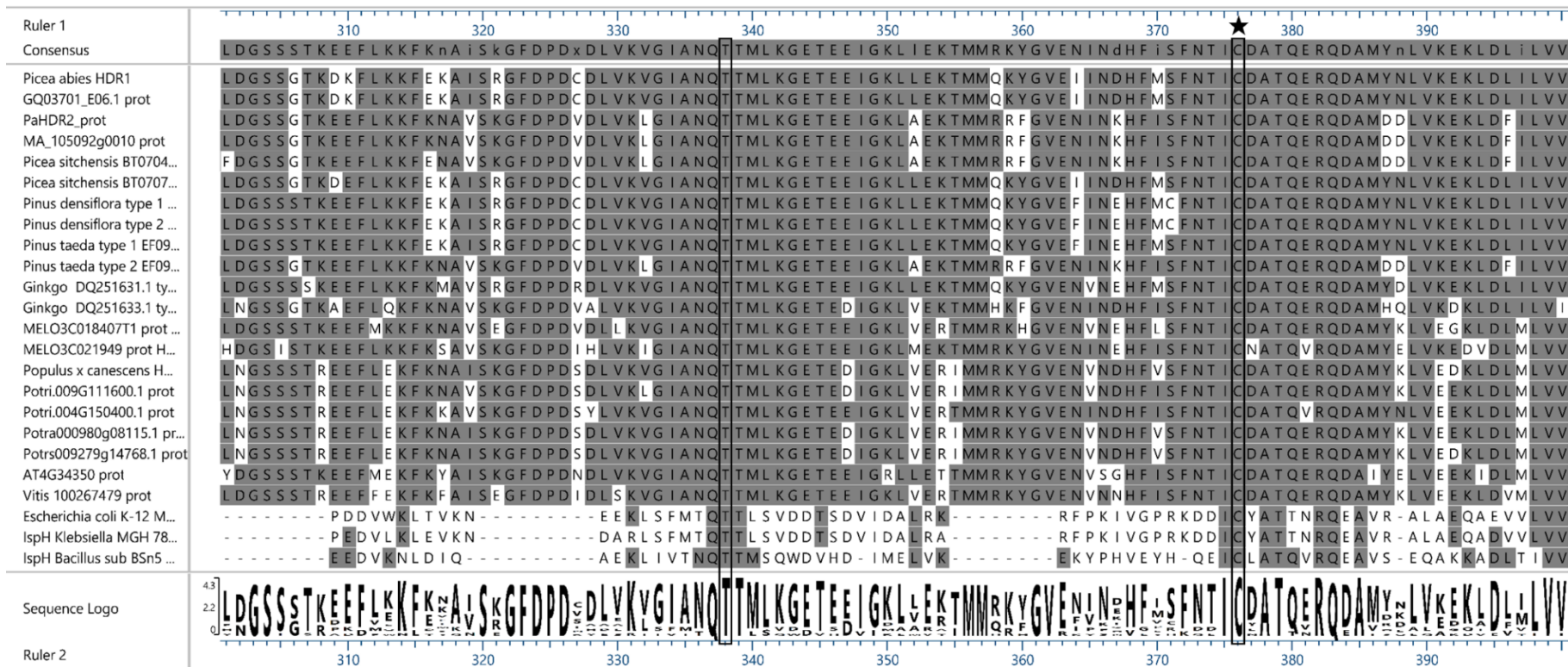
6 Appendix

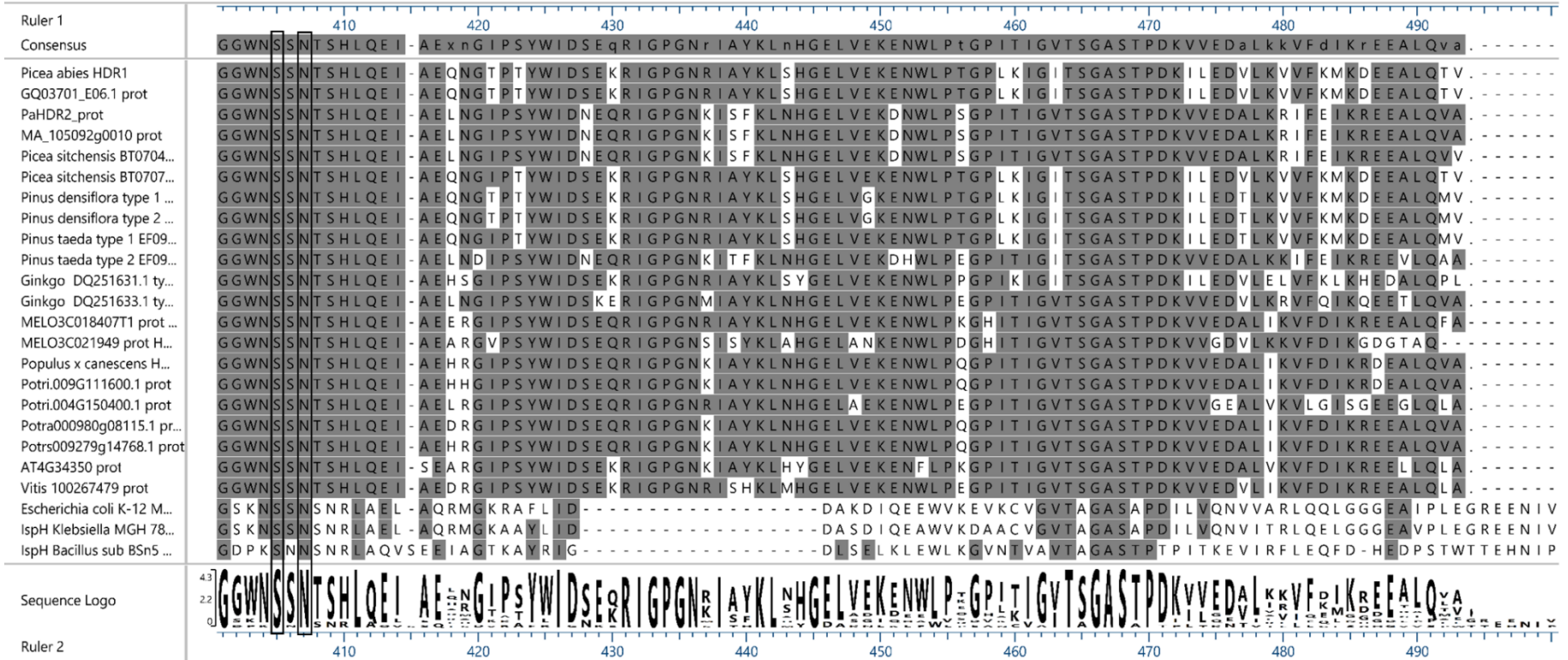
6.1 Alignments











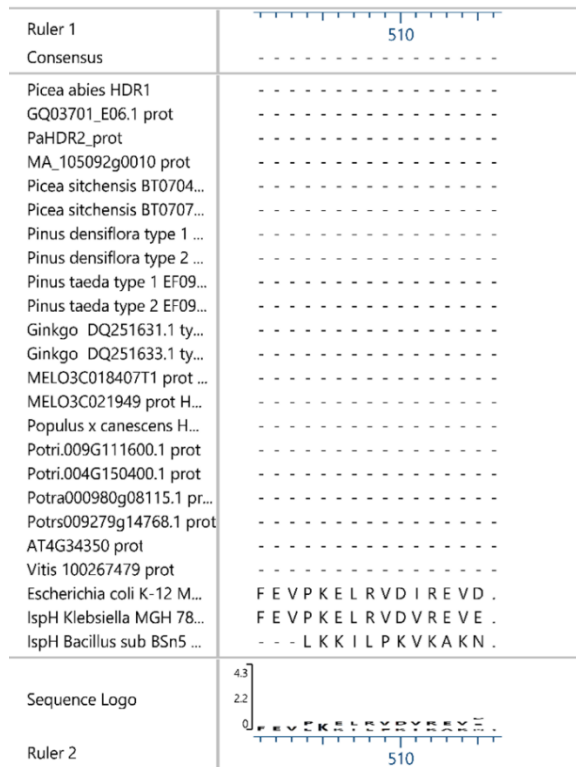


Figure 25: Alignment of peptide sequences from different organisms with MegAlign Pro ClustalW algorithm (GONNET); star: highly conserved cysteine residues, arrow: transit peptide end, black boxes: other highly conserved aminoacids relevant for substrate binding or reaction mechanism, green box: N-terminal region in photosynthetic organisms; Top down: *Picea abies* HDR1 (sequenced in this work), *Picea abies* (GQ03701_E06.1 prot.), *Picea abies* (PaHDR2_prot.), *Picea abies* (MA_105092g0010 prot.), *Picea sitchensis* (BT070446.1 prot), *Picea sitchensis* (BT070784.1 prot), *Pinus densiflora* type 1 (EU439296.1 prot), *Pinus densiflora* type 2 (EU439297 prot), *Pinus taeda* type 1 (EF095154.1 prot), *Pinus taeda* type 2 (EF095155 prot), *Ginkgo biloba* (DQ251631.1 typ 1 prot), *Ginkgo biloba* (DQ251631.1 typ 1 prot), *Cucumis melo* L. (MELO3C018407T1 prot HDR1), *Cucumis melo* L. (MELO3C021949 prot HDR2), *Populus × canescens* HDR2 (sequenced in this work), *Populus trichocarpa* (Potri.009G111600.1 prot), *Populus trichocarpa* (Potri.009G111600.4 prot), *Populus tremula* (Potra000980g08115.1 prot), *Populus tremuloides* (Potrs009279g14768.1 prot), *Arabidopsis thaliana* (AT4G34350 prot), *Vitis vinifera* (100267479 prot), *Escherichia coli* K-12 (MG1655 prot), IspH *Klebsiella* MGH 78578 prot, IspH *Bacillus subtilis* BSn5 prot; sequences from <https://phytozome.jgi.doe.gov/pz/portal.html>, <https://www.ncbi.nlm.nih.gov/gene/>, <https://popgenie.org> or <https://congenie.org>

6.2 Transit peptides

Table 20: Predictions about the transit peptide of *PcHDR*, *PaHDR1* and *PaHDR2* from ChloroP, *PcHDR* template sequence Potri.009G111600.1, *PaHDR1* template sequence GQ03701_E06.1, *PaHDR2* template sequence MA_105092g0010

Name	Length	Score	cTP	CS-score	cTP-length
Potri.009G111600.1	460	0.531	Y	7.817	34
GQ03701_E06.1	485	0.503	Y	10.613	61
MA_105092g0010	485	0.487	-	3.805	29

6.3 Plasmid maps

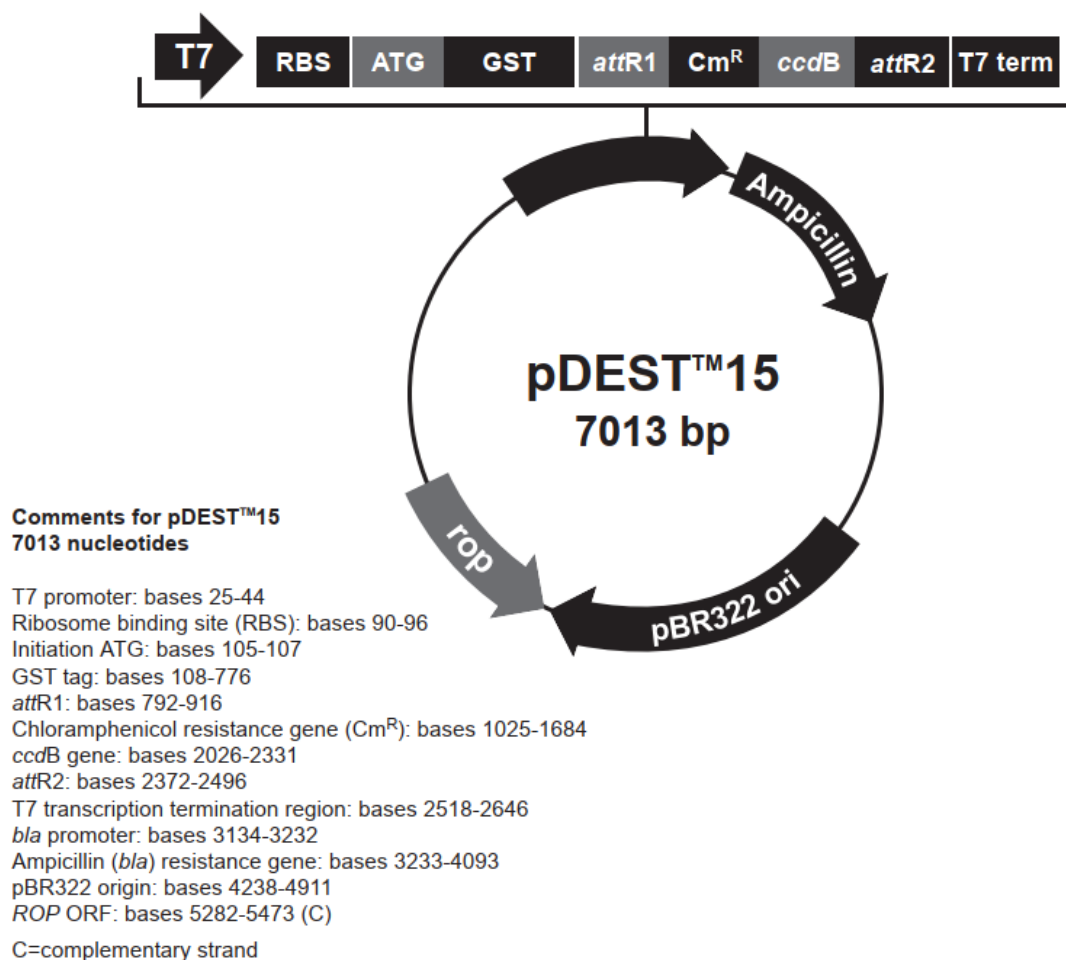
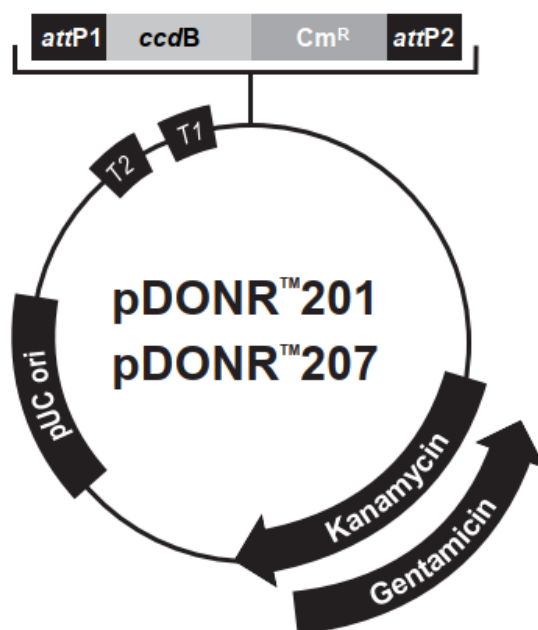


Figure 26: pDEST™15 plasmid map
 (https://www.embl.de/pepcore/pepcore_services/strains_vectors/vectors/pdf/pdest15_map.pdf retrieved 21.03.21)



Comments for:

	pDONR™201 4470 nucleotides	pDONR™207 5585 nucleotides
<i>rrnB</i> T2 transcription termination sequence (c):	73-100	73-100
<i>rrnB</i> T1 transcription termination sequence (c):	232-275	232-275
Recommended forward priming site:	300-324	300-324
<i>attP1</i> :	332-563	332-563
<i>ccdB</i> gene (c):	959-1264	959-1264
Chloramphenicol resistance gene (c):	1606-2265	1606-2265
<i>attP2</i> (c):	2513-2744	2513-2744
Recommended reverse priming site:	2769-2792	2769-2792
Kanamycin resistance gene:	2868-3677	---
Gentamicin resistance gene (c):	---	3528-4061
pUC origin:	3794-4467	4909-5582

(c) = complementary strand

Figure 27: pDONR™201 and pDONR™207 plasmid map
 (<https://content.fccc.edu/yen/docs/pDONR201+207%20info..pdf> retrieved 21.03.21)

6.4 Sequences

Transit peptides are underlined.

6.4.1 *Populus × canescens* HDR DNA and amino acid sequences

6.4.1.1 *PcHDR-T*

DNA sequence *PcHDR-T*

TGCGCTGGCGGTGATGACTCTACTTCTTCAGTCTCTTTGGAATCGGAATTTGAC
GCTAAAGTCTTCAGACATAACCTGACAAGAAGCAAGAATTATAATCGTAGAGG
TTTTGGTCACAAAGAAGAGACACTTGAGCTCATGAATCGCGAGTACACCAGTG
ATATAATAAAGAAATTGAAGGAGAATGGTTATGAGTATACATGGGGAAATGTT
ACAGTCAAATTAGCCGAAGCTTATGGATTTTGCTGGGGAGTAGAGCGAGCTGT
TCAGATTGCTTACGAAGCCAGAAAACAGTTTCCAGATGACAAGATTTGGATTA
CTAACGAGATTATCCACAATCCGACTGTTAATAAGAGGTTAGAGGAGATGGAA
GTTGAAAACGTTCTGTTGAGGAAGGGAAGAAACAGTTTGAAGTTGTAAATGG
TGGTGATGTTGTGATTTTGCCTGCATTTGGAGCGGCAGTGGATGAGATGTTGAC
TTTGAGTAACAAAAATGTACAAATTGTTGATACAACTTGCCCTTGGGTATCCAA
GGTTTGGACTACTGTTGAGAAGCACAGAAGAGAGATTATACCTCAATTATTC
ATGGAAAATATGCTCACGAGGAACTGTAGCAACCGCTTCTTTTGCAGGAAAG
TACATTATTGTGAAGGATATGAAAGAGGCAATGTATGTGTGTGATTACATTCTT
GGGGgTGA ACTTAATGGATCTAGCTCAACCAGAGAGGAGTTTCTAGAGAAATT
TAAAAATGCAATTTCTAAGGGGTTTGATCCTGATAGTGACCTGGTGAAAGTTG
GTATTGCAAATCAA ACTACAATGCTCAAGGGAGAAACAGAAGACATTGGAAA
ATTGGTGGAGAGGATCATGATGCGCAAGTATGGAGTGGAAAATGTAAATGATC
ACTTCGTAAGCTTCAACACCATTTGTGATGCTACTCAGGAGAGACAAGATGCA
ATGTATAAACTGGTGGAGGACAAGTTGGATCTTATGTTAGTTGTTGGCGGGTG
GAACTCAAGTAACACCTCCCACCTCCAAGAAATTGCTGAGCACCGTGGAATTC
CTTCATACTGGATTGACAGTGAACAGAGGATCGGCCCCAGGAAACAAAATAGCT
TATAAGTTGAATCATGGGGAGTTGGTTGAGAAAGAGAACTGGCTTCCACAAGG
CCCCATTACAATTGGTGTGACATCAGGCGCCTCTACACCAGACAAGTTGTGCG
AAGATGCCCTTATCAAGGTGTTTCGACATCAAACGTGACGAAGCTTTACAAGTA
GCTTAA

Amino acid sequence *PcHDR-T* (48101.33 Da)

CAGGDDSTSSVSLESEFDAKVFRHNLTRSKNYNRRGFGHKEETLELMNREYTS
KCLKENGYEYTWGNVTVKLAEAYGFCWGVERAVQIAYEARQKFPDDKIWITNEI
HNPTVNRLEEMEVENVPVEEGKKQFEVVNGGDVVILPAFGAAVDEMLTSLNKN
VQIVDTPWVSKVWTTVEKHKKRDYTSIIHGKYAHEETVATASFAGKYIIVKDM
KEAMYVCDYILGGELNGSSSTREEFLEKFKNAISKGFDPSDLVKVGIANQTTMLK
GETEDIGKLVERIMMRKYGVENVNDHFVSFNTICDATQERQDAMYKLVEDKLDL
MLVVGWNSNTSHLQEIAEHRGIPSYWIDSEQRIGPGNKIAYKLNHGELVEKEN
WLPQGPITIGVTSGASTPDKVVEDALIKVFDIKRDEALQVA.

6.4.1.2 *Pc*HDR+T

DNA sequence *Pc*HDR+T

ATGGCTATCTCTCTCCAACTCTGCCGCGTATCACTCCGCTCCGACCTCTCCTCC
GACAATCGCGTACCTATCCGCGCCCGTAGAACCACTTTCTCCGCTCCGCTGCGCT
GGCGGTGATGACTCTACTTCTTCAGTCTCTTTGGAATCGGAATTTGACGCTAAA
GTCTTCAGACATAACCTGACAAGAAGCAAGAATTATAATCGTAGAGGTTTTGG
TCACAAAGAAGAGACACTTGAGCTCATGAATCGCGAGTACACCAGTGATATAA
TAAAGAAATTGAAGGAGAATGGTTATGAGTATACATGGGGAAATGTTACTGTC
AAATTAGCCGAAGCTTATGGTTTTTCTGCTGGGGAGTAGAGCGAGCTGTTTCAGAT
TGCTTACGAAGCCAGAAAACAGTTTCCAGATGACAAGATTTGGATTACTAACG
AGATTATCCACAATCCGACTGTTAATAAGAGGTTAGAGGAGATGGAAGTTGAA
AACGTTCTGTTGAGGAAGGGAAGAAACAGTTTGAAGTTGTAAATGGTGGTGA
TGTTGTGATTTTGCCTGCATTTGGAGCGGCAGTGGATGAGATGTTGACTTTGAG
TAACAAAAATGTACAAATTGTTGATACAACCTTGCCCTTGGGTATCCAAGGTTTG
GACTACTGTTGAGAAGCACAAGAAGGGAGATTATACCTCAATTATTCATGGAA
AATATGCTCACGAGGAAACTGTAGCAACCGCTTCTTTTGCAGGAAAGTACATT
ATTGTGAAGAATATGAAAGAGGCAATGTATGTGTGTGATTACATTCTTGGGGG
TGAACCTAATGGATCTAGCTCAACCAGAGAGGAGTTTCTAGAGAAATTTAAA
ATGCAATTTCTAAGGGGTTTGATCCTGATAGTGACCTGGTGAAAGTTGGTATTG
CAAATCAAACCTACAATGCTCAAGGGAGAAACAGAAGACATTGGAAAATTGGT
GGAGAGGATCATGATGCGCAAGTATGGAGTGGAAAATGTAAATGATCACTTCG
TAAGCTTTAACACCATTGTTGATGCTACTCAGGAGCGACAAGATGCAATGTAT
AACTGGTGGAGGAAAAGTTGGATCTTATGTTAGTTGTTGGCGGGTGGAACTC
AAGTAACACCTCCCACCTCCAAGAAATTGCTGAGGACCGTGGAATTCCTTCAT
ACTGGATTGACAGTGAACAGAGGATAGGCCCAGGAAACAAAATAGCTTATAA
GTTGAACCATGGGGAGTTGGTTGAGAAAGAGAAGTGGCTTCCACAAGGCCCA
TTACAATTGGTGTGACATCAGGCGCCTCTACACCAGACAAGGTTGTGGAAGAT
GCCCTTATCAAGGTGTTTCGACATCAAACGTGACGAAGCTTTACAAGTAGCTTA
A

Amino acid sequence *Pc*HDR+T (51965.84 Da)

MAISLQLCRVSLRSDLSSDNRVPIRRRRRTTFSVRCAGGDDSTSSVSLESEFDAKVFR
HNLTRSKNYNRRGFGHKEETLELMNREYTSDIKKLKENGYEYTWGNVTVKLAE
AYGFCWGVERAVQIAYEARQFPDDKIWITNEIIHNPTVVKRLEEMEVENVPVEE
GKKQFEVVNGGDVVILPAFGAAVDEMLTSLNKNVQIVDTTCPWVSKVWTTVEKH
KKGDYTSIIHGKYAHEETVATASFAGKYIIVKNMKEAMYVCDYILGGELNGSSSTR
EEFLEKFKNAISKGFDPDSL VKVGIANQTTMLKGETEDIGKLVERIMMRKYGVE
NVNDHFVSNFNTICDATQERQDAMYKLVEEKLDLMLVVGWNSNTSHLQEI AED
RGIPSYWIDSEQRIGPGNKIAYKLNHGELVEKENWLPQGPITIGVTSGASTPDKVVE
DALIKVFDIKRDEALQVA.

6.4.2 *Picea abies* HDR DNA and amino acid sequences

6.4.2.1 *Pa*HDR1

DNA sequence *Pa*HDR1

ATGTCTTCCAGCCTCAGCTTTGCTGTAGTTTGCAAACCCGAAGCTCTACGACCA
AGAGCTTTAAGCAATGGACATGGGAATTCAGCGATTTGGGATTCATCGGCCAT
GTTGGGCACAAGATTGACTCGTGCAATGCAAGCAGATGTTTGCAGAACTTGC
AGCTGAGGCGGACACAAGTTAGGTGCGATGCTGCTCCCAGCGCTGTAGATTCA
GCTACAGGGGAATTTGATACCAAAGCCTTCAGGAGGACTTTGACTAGAAAAGA
GAATTATAACAGAAAGGGATTTGGTCACAAGGAAGAACTCTTGAAGCAATG
GACAAAGAGTATACCAGTGATATCATTAAAACATTGAAAGAGAACAACAATG
AATACACTTGGGGTAATGTAAGCTGTTAAGCTTGTGAATCATTGGATTCTGTT
GGGGTGTGGAACGAGCTGTTCAAATTGCATATGAAGCAAGAAAGCAATTTCCA
GATCAGAAGCTATGGATTACCAATGAAATCATAACAATCCAAGTGTGAATCA
GAGATTGAAGGAGATGCAGATTGAAGACATTCCTGTAATGGAAGAAGGGAAA
AAATTTGATGTTGTAAACAGTGATGATGTGGTTATTCTTCCAGCTTTTGGAGCA
GCAGTAAGTGAAATGCAGATTCTTGATGAAAAAAGTGTGAAGATTGTGGACAC
TACATGTCCATGGGTTTCCAAGGTTTGGAACTGTGGAGAAGCATAAGAAGG
AAAGCTTTACTTCTGTAATCCATGGAAAGAAAGGGCATGAAGAACTGTTGCC
ACTTCATCATTGTCAGGGAAATATATAATTGTAAAGGACATCAGGGAGGCAAC
ATATGTGTGTGACTACATTCTGGCTGGCAAGCTTGATGGTTCTAGTGGTACTAA
AGACAAATTTCTTAAAAAATTTGAAAAGGCTATTTCAAGAGGATTTGATCCTG
ATTGCGACTTGGTCAAAGTGGGAATTGCTAACCAGACAACAATGTTGAAAGGA
GAAACCGAAGAGATAGGAAAATTTCTCGAGAAAACAATGATGCAAAAATATG
GGGTGGAAATTATCAATGACCATTTTATGAGTTTCAACACTATATGTGATGCAA
CACAGGAAAGGCAAGATGCCATGTATAACTTGGTGAAGGAGAAGCTTGATCTT
ATTCTTGTGTAGGAGGATGGAATTCTAGCAATACATCCCATTTACAAGAAATC
GCAGAGCAGAATGGAAGTCCAAGTATTGGATTGATTCCGAGAAGCGCATAGG
ACCTGGTAACCGCATTGCATACAAGCTTAGTCACGGTGAGCTGGTGGAGAAGG
AAAATTGGCTTCCAAGTGGTCCACTCAAATTTGGAATCACTTCAGGTGCATCA
ACTCCTGATAAGATATTGGAGGATGTGTTGAAAGTCGTTTTCAAGATGAAGGA
TGAGGAGGCGTTGCAGACAGTATAA

Amino acid sequence *Pa*HDR1 (+T: 54518.13 Da; -T: 47819.38 Da)

MSSSLSFVAVVCKPEALRPRALSNGHGNSAIWDSSAMLGTRLTRAMQADVCRNLQ
LRRTQVRCDAAPSAVDSATGEFDTKAFRRTLTRKENYNRKGFGHKEETLEAMDK
EYTSDIKTLKENNEYTWGNVTVKLAESFGFCWGVERAVQIAYEARQFPDQKL
WITNEIIHNPTVNQRLKEMQIEDIPVMEEGKKFDVVNSDDVVILPAFGAAVSEMQL
LDEKSVKIVDTPWVSKVWNTVEKHKKESFTSVIHGKKGHEETVATSSFAGKYII
VKDIREATYVCDYILAGKLDGSSGTDKFLKFKFEKAISRGFDPDCDLVKVGIANQT
TMLKGETEEIGKLLKTMQKYGVEIINDHFMSFNTICDATQERQDAMYNLVKEK
LDLILVGGWNSNTSHLQEIAEQNGTPTYWIDSEKRIGPGNRIAYKLSHGELVEK
ENWLPTGPLKIGITSGASTPKILEDVLKVVFKMKDEEALQTV.

6.4.2.2 *Pa*HDR2

DNA sequence *Pa*HDR2

ATGGCTAAAGCGTGCGCAGTGTTGAGCTCTGTCTCCTCGTGCAGAAATGACAC
GTTGCAGAGTGCCCAAGTGATGTTGCAGGTGAGGCATTCGGCTCTCGTGCATC
ATCAAATCATATAAATCTCAGGAGGCAGAAGGAGAAGAAGGTTACAGTTGG
AATTCGTGTTGTTTCGATGCGATGGAGGGGGAGCTGCTGCTGCTGTGGAGGCCT
CCGAGTCAGAGAAATTCGACCCCAAGACCTTCAGAAAAAACTTAACCAGAAG
CAAGAATTATAACAGAAAAGGATTTGGGTACAAGGATGAGACGCTGGCCTTG
ATGGACCAAGAGTACACGAGTGATCTGGTGAAGACTCTAAAAGAAAATAACA
ATGAGTTTACTTGGGGGGATGTGACGGTCAAATTGGCCAAGTCCTATGGTTTCT
GCTGGGGCGTAGAACGTGCAGTGCAAATTGCATATGAAGCCAGGAAGCAATTC
CCTGTTGAAAGGATCTGGATCACTAATGAAATTATACACAATCCCACCGTGAA
TGAGAGATTGGAGGAAATGGATGTCCAATCTATTCCTGTAGGAAATGAAGGAA
AACGATTTGGTGTGTTGACAAGGGAGACGTGGTGATTTTGCCTGCATTTGGA
GCATCTGTACATGAAATGCAGTTGTTAAGTGAGAAAAATGTACAGATTGTGGA
CACAACCTGTCCATGGGTGTCTAAGGTTTGGAACTGTTGAGAAGCACAAAC
AAGGAGAGTACACCTCCATCATTGAAATATTCTCATGAAGAAACCATT
GCAACTGCTTCTTTGCAGGAAGTTATATTATTGTAAGAACATTACCGAGGCA
AGATATGTTTGCGATTACATCCTCAATGGTGAGCTTGATGGATCTAGTGGAAC
AAAAGAGGAATTCCTTAAGAAATTTAAGAATGCAGTTTCCAAGGGTTTCGACC
CAGATGTTGACTTGGTCAAGTTGGGCATTGCAAACCAACAACAATGCTGAAA
GGGGAAACAGAGGAGATAGGAAAAGACTAGCGGAAAAGACAATGATGCGTAGAT
TTGGTGTGAAAACATAAACAAGCATTTCATAAGCTTCAACACTATTTGTGATG
CCACTCAGGAAAGACAAGATGCAATGGATGATCTAGTAAAGGAGAAGCTTGA
TTTCATATTGGTAGTTGGTGGATGGAATTCCAGCAATACTTCACACCTTCAAGA
AATAGCTGAGTTGAATGGCATACTTCATACTGGATTGACAATGAGCAGCGTA
TTGGTCCTGAAAATAAAAATTCCTTTAAATTGAATCATGGGGAGTTGGTGGAG
AAAGATAACTGGCTGCCATCAGGCCCCATTACAATTGGGGTCACATCGGGTGC
TTCAACACCAGACAAGGTTGTTGAAGATGCCCTGAAAAGGATATTTGAGATCA
AACGAGAAGAGGCTCTGCAAGTAGCATAG

Amino acid sequence *Pa*HDR2 (+T: 54409.75 Da; -T: 47894.10 Da; -T2: 51330.13Da)

Double line is -T2

MAKACAVLSSVSSCRNDTLQSAQVMLQVRHSALVHHQNHINLRRQKEKKVTVGI
RVVRCDGGGAAAAVEASESEKFDPKTFRKNLTRSKNYNRKGFYKDETLALMDQ
EYTSDLVKTLKENNNEFTWGDVTVKLAQSYGFCWGVERAVQIAYEARQFPVER
IWITNEIIHNPTVNERLEEMDVQSIPVGNKRFVVDKGDVVILPAFGASVHEMQ
LLSEKNVQIVDTPWVSKVWNTVEKHKQGEYTSIIHGKYSHEETIATASFAGTYII
VKNITEARYVCDYILNGELDGSSGTKEEFLKKFKNAVSKGFDPDVLDVVLGIANQ
TTMLKGETEEIGKLAEKTMRRFGVENINKHFISFNTICDATQERQDAMDDLVEK
KLDLILVVGWNSNTSHLQEI AELNGIPSYWIDNEQRIGPGNKISFKLNHGELVEK
DNWLPSGPITIGVTSASTPKVVEDALKRIFEIKREALQVA.

6.5 3D-Models Infos

Table 21: Data about accuracy and quality of 3D-model predictions of *PcHDR*, *PaHDR1* and *PaHDR2* by SWISS-MODEL Expasy

Target Sequence	File	Built with	Oligo-State	Ligands	GMQE	QMEAN
<i>PcHDR</i> -T	PDB	ProMod3 3.2.0	monomer	None	0.44	-5.08
<i>PaHDR1</i> -T	PDB	ProMod3 3.2.0	monomer	None	0.44	-4.48
<i>PaHDR2</i> -T	PDB	ProMod3 3.2.0	monomer	None	0.45	-5.39

Table 22: Comparison of 3D-model predictions of *PcHDR*, *PaHDR1* and *PaHDR2* to template 3szu (PDB title) by SWISS-MODEL Expasy

Target Sequence	Template	Seq Identity	Oligo-state	QSQE	Found by	Method	Resolution	Seq Similarity	Range	Coverage	Description
<i>PcHDR</i> -T	3szu.1.A	27.82	monomer	0.00	HHblits	X-ray	1.40Å	0.34	71 - 420	0.67	
<i>PaHDR1</i> -T	3szu.1.A	26.76	monomer	0.00	HHblits	X-ray	1.40Å	0.34	69 - 418	0.67	4-hydroxy-3-methylbut-2-enyl diphosphate reductase
<i>PaHDR2</i> -T	3szu.1.A	28.52	monomer	0.00	HHblits	X-ray	1.40Å	0.34	72 - 421	0.67	

6.6 Loss of enzyme activity and activity in FT and W1 fractions

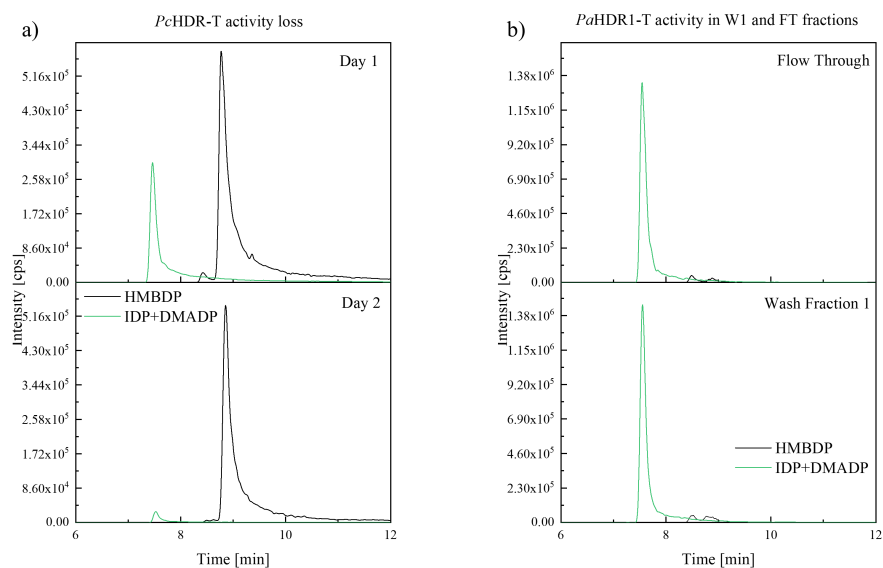


Figure 28: Loss of enzyme activity after one day of storage and present activity in Flow through and Wash 1 fraction; a) Loss of activity of *PcHDR* from day1 to day 2, amount of IDP+DMADP (green line) has decreased by about 30 times, assay conditions on both days: 0.5 μg enzyme, 50 μM HMBDP, 30 min, pH 6.5, 35°C; b) Enzyme activity is detected in Flow through and Wash 1 fractions of *PaHDR1-T*, assay conditions for both: 30 μl of fraction (enzyme), 50 μM HMBDP, 30 min, pH 6.5, 35°C

6.7 Michaelis-Menten plots

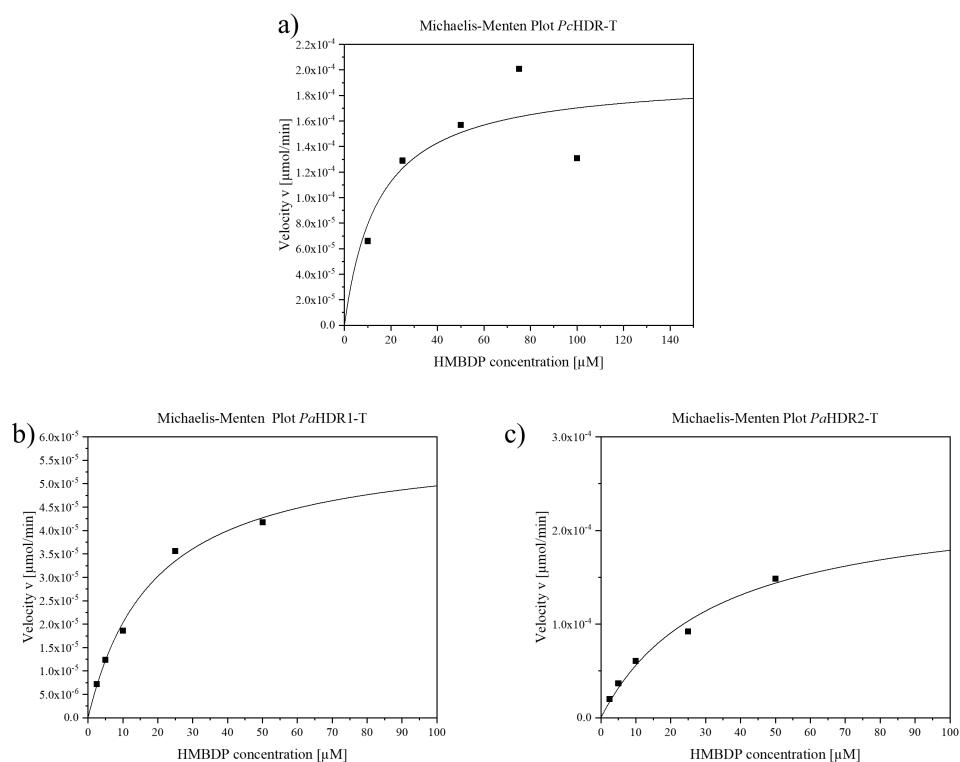


Figure 29: Michaelis-Menten Plot to determine K_M , v_{max} and k_{cat} of a) *PcHDR-T*, b) *PaHDR1-T* and c) *PaHDR2-T*